AD-781 991

MEASURING SOIL PROPERTIES IN VEHICLE MOBILITY RESEARCH. REPORT 6. RESISTANCE OF COARSE-GRAINED SOILS TO HIGH-SPEED PENETRATION

Gerald W. Turnage

Army Engineer Waterways Experiment Station
Vicksburg, Mississippi

July 1974

TECHNICAL REPORT NO. 3-652

MEASURING SOIL PROPERTIES IN VEHICLE MOBILITY RESEARCH

Report 6

RESISTANCE OF COARSE-GRAINED SOILS TO HIGH-SPEED PENETRATION

by

G. W. Turnage

July 1974

Sponsored by Assistant Secretary of the Army (R&D), Department of the Army
Project No. 4A061101A91D

Conducted by U. S. Army Engineer Waterways Experiment Station
Mobility and Environmental Systems Laboratory
Vicksburg, Mississippi

ARMY-MRC VICKSBURG MISS

APPROVED FOR PUBLIC RELEASE; DISTRIBUTION UNLIMITED

Unclassified
Security Classification

AD781991

DOCUMENT CONTROL DATA - R & D

(Security classification of title, body of abstract and indexing annotation must be entered when the overall report is classified)

1. ORIGINATING ACTIVITY (Corporate author)
U. S. Army Engineer Waterways Experiment Station
Vicksburg, Mississippi

2a. REPORT SECURITY CLASSIFICATION
Unclassified

2b. GROUP

3. REPORT TITLE
MEASURING SOIL PROPERTIES IN VEHICLE MOBILITY RESEARCH; Report 6, RESISTANCE OF COARSE-GRAINED SOILS TO HIGH-SPEED PENETRATION

4. DESCRIPTIVE NOTES (Type of report and inclusive dates)
Report 6 of a series

5. AUTHOR(S) (First name, middle initial, last name)
Gerald W. Turnage

6. REPORT DATE
July 1974

7a. TOTAL NO. OF PAGES
104

7b. NO. OF REFS
19

8a. CONTRACT OR GRANT NO.

b. PROJECT NO. 4A061101A91D

c.

d.

9a. ORIGINATOR'S REPORT NUMBER(S)
Technical Report No. 3-652
Report 6

9b. OTHER REPORT NO(S) (Any other numbers that may be assigned this report)

10. DISTRIBUTION STATEMENT
Approved for public release; distribution unlimited.

11. SUPPLEMENTARY NOTES

12. SPONSORING MILITARY ACTIVITY
Assistant Secretary of the Army (R&D)
Department of the Army
Washington, D. C.

13. ABSTRACT

For a given probe (cone or flat plate) tested vertically in air-dry sand of a given strength level, the curve of probe base pressure (sand penetration resistance force per unit probe base area, F_z/A_x) versus probe base depth departs from near-linearity as velocity V_z increases. For these conditions, values of probe base pressure at shallow depth increase with increasing velocity, but this pressure approaches a common value at substantial depth (say, 15 cm) for velocity values in the 3- to 600-cm/sec range. For a velocity near 3 cm/sec, the slope, or gradient, of the probe base pressure versus depth curve (termed penetration resistance gradient G_x) can be expressed for any of a broad range of probe sizes and shapes by $G_x = \left\{\left(G - 1\right) \times \left[0.20 + \left(0.80 \frac{\ell_s}{\ell_x}\right)\right] + 1\right\}$ where G is G_x measured under standard conditions (i.e. by a 3.23-sq-cm, 30-deg-apex-angle cone at 3.05 cm/sec), ℓ_s is A for the standard cone, and ℓ_x is the A_x for the probe of interest. Expressions were also developed to describe F_z at shallow probe depths (zero base depth for the cones, 2.5-cm depth for the plates) as a function of sand strength and probe size, shape, and velocity for a wide range of values of each of these variables. Finally, a technique is presented for estimating the F_z versus depth curve in the 0- to 15-cm depth range for cones, or the 2.5- to 15-cm depth range for plates, for V_z values less than about 100 cm/sec and any of a wide range of sand strengths and probe sizes and shapes. A second phase of this study determined expressions that describe the marked increase in sand G values caused by increases in sand unit dry weight γ_d and/or moisture content. In the third phase of this study, dimensional analysis was used to develop a description of the horizontal force acting on a given cone base as the cone moves horizontally beneath the sand F_x, as a function of probe size and velocity; depth of the cone tip relative to the undisturbed sand surface; and air-dry sand G and γ_d. A short review of major findings from two studies of horizontal cone penetration tests showed that these findings agree with and complement results of the WES study. A brief summary of another study presents related expressions that describe the horizontal and vertical components of force on plane blades operating horizontally near the sand surface.

104

DD FORM 1473, 1 NOV 65 — REPLACES DD FORM 1473, 1 JAN 64, WHICH IS OBSOLETE FOR ARMY USE.

Unclassified
Security Classification

Unclassified

Security Classification

14. KEY WORDS	LINK A		LINK B		LINK C	
	ROLE	WT	ROLE	WT	ROLE	WT
Coarse grained soils						
Mobility						
Penetration probes						
Soil penetration						
Soil properties						
Vehicles						

Unclassified

Security Classification

FOREWORD

The study reported herein was funded by Department of the Army Project 4A061101A91D, "In-House Laboratory Independent Research," sponsored by the Assistant Secretary of the Army (R&D). The major portion of the study was conducted during 1972-73, although some results are presented for the first time from tests conducted several years earlier.

The project was conceived by Mr. G. W. Turnage of the Mobility Research and Methodology Branch (MRMB), Mobility Systems Division (MSD), Mobility and Environmental Systems Laboratory (MESL), at the U. S. Army Engineer Waterways Experiment Station (WES). The test program was accomplished by personnel of the MRMB and the Mobility Investigations Branch (MIB) under the general supervision of Mr. W. G. Shockley, Chief of MESL, and Mr. A. A. Rula, Chief of MSD, and under the direct supervision of Mr. C. J. Nuttall, Jr., Chief of MRMB, and Mr. E. S. Rush, Chief of MIB. The hitherto unreported data were obtained under the direction of Mr. L. J. Lanz, formerly of WES. All other phases of the study were directed by Mr. Turnage, MRMB, who prepared this report.

BG E. D. Peixotto, CE, and COL G. H. Hilt, CE, were Directors of the WES during conduct of this study and preparation of the report. Mr. F. R. Brown was Technical Director.

CONTENTS

NOTATION *

a	Acceleration
A, A_s, A_x	Probe base area; base area of the standard WES 3.23-sq-cm cone; and base area of any given probe, respectively
c	As a subscript, refers to a circular-base-area probe of the same size base area as the probe of interest
C	Cone penetration resistance
C_D	Drag coefficient
d, d_s, d_x	Probe base diameter; diameter of the base of the standard WES cone (d_s = 2.03 cm), and diameter of the base of any circular-base-area probe, respectively
D_c	Critical depth
F, F_i, F_x, F_z	Sand penetration resistance force; inertial force; sand resistance force measured in the direction of a horizontal probe penetration; and sand resistance force measured in the direction of a vertical probe penetration, respectively
F_z/A	Probe base pressure (cone base pressure or plate base pressure, depending on which type probe is being considered)
$\dfrac{F_z/A_x}{Gh^2/d_x}$	Cone-sand pressure ratio
$\left(F_z/A^{1.3}\right)_{xs}$	Cone stress ratio

* Several other symbols that are specifically defined in context and then used no more than a few times immediately afterwards are not listed here.

$\left(F_z/A^{1.2}\right)_{xs} \times \left(R_h^{0.4}\right)_{cx}$	Plate-cone stress ratio $\left[\text{for circular-base-area plates } \left(R_h^{0.4}\right)_{cx} = 1\right]$
g	Acceleration due to gravity
G	Sand penetration resistance gradient obtained with a 3.23-sq-cm, 30-deg-apex-angle cone at $V_z = 3.05$ cm/sec
G_x	Sand penetration resistance gradient obtained with a probe of any given size and shape at any velocity small enough to cause the F_z/A_x versus probe base depth curve to be near-linear in the range of depth values sampled in obtaining G_x
h	Depth of cone tip beneath the undisturbed sand surface in horizontal penetration tests
i	Inertia
ℓ, ℓ_s, ℓ_x	$\sqrt{A}$; square root or the base area of the standard 3.23-cm^2 cone (ℓ_s = 1.80 cm); and square root of the base area of any given probe, respectively
N_R	Reynolds number
P	Perimeter of the base of a given probe
R_h	Hydraulic radius (i.e. A/P) of the base of a given probe
s	As a subscript, refers to conditions associated with a standard cone penetration to obtain G
V, V_s, V_x, V_z	Velocity; velocity in a standard penetration to obtain $G(V_s = 3.05$ cm/sec$)$; velocity in a horizontal penetration; and velocity in a vertical penetration, respectively
$V_x/\sqrt{gd_x}$	Froude number
V_z/ℓ	Velocity gradient
$\left(V_z/\ell\right)_{xs}$	Velocity gradient ratio
x	As a subscript immediately after F or V (i.e. F_x or V_x), denotes horizontal. As a subscript in any other case, indicates conditions other than those associated with a standard cone penetration to obtain G (e.g., G_x , A_x , d_x , ℓ_x , $(F_z)_x$, etc.)
z	As a subscript immediately after F or V (i.e. F_z or V_z), denotes vertical

α	Cone tip apex angle
γ_d	Sand unit dry weight
ρ	Sand dry mass density γ_d/g
$\rho\left(AV_z^2\right)_x/2$	Inertial force
ϕ	Sand angle of internal friction
ψ	Yield value

CONVERSION FACTORS, METRIC TO BRITISH UNITS OF MEASUREMENT

Metric units of measurement used in this report can be converted to British units as follows:

Multiply	By	To Obtain
meters	3.281	feet
centimeters	0.3937	inches
square centimeters	0.1550	square inches
newtons	0.2248	pounds (force)
meters per second	3.281	feet per second
centimeters per second	0.3937	inches per second
kilonewtons per cubic meter	6.366	pounds per cubic foot
kilopascals	0.1450	pounds per square inch
meganewtons per cubic meter	3.684	pounds per cubic inch (i.e. psi per inch)
kilograms	0.0685	slugs

SUMMARY

For a given probe (cone or flat plate) tested vertically in air-dry sand of a given strength level, the curve of probe base pressure (sand penetration resistance force per unit probe base area, F_z/A_x) versus probe base depth departs from near-linearity as velocity V_z increases. For these conditions, values of probe base pressure at shallow depth increase with increasing velocity, but this pressure approaches a common value at substantial depth (say, 15 cm) for velocity values in the 3- to 600-cm/sec range.

For a velocity near 3 cm/sec, the slope, or gradient, of the probe base pressure versus depth curve (termed penetration resistance gradient G_x) can be expressed for any of a broad range of probe sizes and shapes by

$$G_x = \left\{ (G - 1) \times \left[0.20 + \left(0.80 \frac{\ell_s}{\ell_x} \right) \right] + 1 \right\}$$

where G is G_x measured under standard conditions (i.e. by a 3.23-sq-cm, 30-deg-apex-angle cone at 3.05 cm/sec), ℓ_s is $\sqrt{A}$ for the standard cone, and ℓ_x is the $\sqrt{A_x}$ for the probe of interest. Expressions were also developed to describe F_z at shallow probe base depths (zero base depth for the cones, 2.5-cm depth for the plates) as a function of sand strength and probe size, shape, and velocity for a wide range of values of each of these variables. Finally, a technique is presented for estimating the F_z versus depth curve in the 0- to 15-cm depth range for cones, or the 2.5- to 15-cm depth range for plates, for V_z values less than about 100 cm/sec and any of a wide range of sand strengths and probe sizes and shapes.

A second phase of this study determined expressions that describe the marked increase in sand G values caused by increases in sand unit dry weight γ_d and/or moisture content.

In the third phase of this study, dimensional analysis was used to develop a description of the horizontal force acting on a given cone base as the cone moves horizontally beneath the sand (F_x) as a function of probe size and velocity; depth of the cone tip relative to the undisturbed sand surface; and air-dry sand G and γ_d. A short review of major findings from two studies of horizontal cone penetration tests showed that these findings agree with and complement results of the WES study. A brief summary of another study presents related expressions that describe the horizontal and vertical components of force on plane blades operating horizontally near the sand surface.

MEASURING SOIL PROPERTIES IN VEHICLE MOBILITY RESEARCH

RESISTANCE OF COARSE-GRAINED SOILS TO HIGH-SPEED PENETRATION

PART I: INTRODUCTION

Background

1. A major problem that confronts users of soil in engineering, agricultural, industrial, and military applications is forecasting how the soil will react to the force that man applies to it. Many years of study and experience have produced techniques for predicting soil behavior under static or near-static loading (dams, foundations, etc.) and under transient loading spread over a large surface area (roadbeds for paved highways, airfields, etc.). The study of soil resistance to localized, high-speed penetration has a much shorter history, and the development of quantitative descriptions of this phenomenon is relatively new.

2. Man penetrates the soil with a wide variety of implements to accomplish his objectives. The direction of movement of the penetrating element may be predominantly parallel to the soil surface (earthmoving scraper blade, tillage tools, and tires and tracks of off-road vehicles), normal to it (foundation piles, core drills, and mechanical or air-dropped penetrometers), or somewhere in between (anchors for field gun emplacements).

3. To date, nearly all studies of soil penetration by man-made probes have dealt with soil reaction to either horizontal or vertical probe movement. With attention limited to these two directions only, soil penetration resistance is still difficult to describe quantitatively because it depends on several probe variables (primarily size, shape, and velocity, along with weight in free-drop vertical tests), as well as on adequate quantitative description of the test soil's quasistatic strength characteristics.

4. The approach at the U. S. Army Engineer Waterways Experiment Station (WES) has been to concentrate attention on penetrations in classical soils, i.e. essentially purely cohesive clay and purely frictional sand. Studies of the aerial cone penetrometer in fine-grained (cohesive) soils have been documented.[1-4] The resistance of fine-grained soils to both horizontal and vertical penetrations by a variety of probe sizes and shapes was discussed in Reports 3 and 5 of this series.[5,6] This report extends the studies of Reports 3 and 5 to the behavior of coarse-grained (frictional) soils.

Purpose

5. The purpose of the study reported herein was to describe quantitatively:

a. The resistance of air-dry sand to vertical penetration by a variety of sizes and shapes of cones and flat plates over a range of penetration velocities.

b. The influence of moisture content on the resistance of sand to low-speed vertical penetrations by the standard WES cone.

c. The resistance imparted to cones and flat blades tested horizontally over a range of speeds in air-dry sand.

Scope

6. Vertical penetrations were made in soil bins of air-dry desert (Yuma) sand at speeds to over 700 cm/sec* with probes of three general shapes: 30-deg-apex-angle, right circular cones; flat, circular plates; and flat, rectangular plates. Sizes of the probe base areas ranged from 1.29 to 58.1 cm^2. The rectangular plates had width-to-length ratios of 1:1, 1:2, 1:4, and 1:8. In a second group of tests, vertical penetrations were made at speeds from 0.025 to 34.9 cm/sec with the standard WES cone (3.23-cm^2 base area) in test molds of air-dry to moist Yuma sand (moisture contents from 0.4 to 11.5 percent).

* A table of factors for converting metric units of measurements to British units is presented on page xi.

Finally, in a third group of tests, horizontal penetrations were made in test bins of air-dry Yuma sand at speeds up to 5.2 m/sec with 30-deg-apex-angle cones of circular base areas ranging from 3.23 to 23.2 cm^2.

7. The sand placement techniques used throughout this program produced a high degree of consistency within each soil test section. Within each of the three groups of penetration tests, Yuma sand test sections were used that covered a major portion of the possible range of strength values of this soil. For essentially purely frictional soils, a WES-developed concept was used herein to characterize soil strength by G, the slope of the curve of cone penetration resistance C versus depth of the cone base beneath the sand surface, where C is force per unit base area required to penetrate a soil normal to its surface at 3.05 cm/sec with a 30-deg-apex-angle, right circular cone of 3.23-cm^2 base area. This slope is usually averaged over a depth of 15 cm.

8. Complementary to relations developed from the above-mentioned horizontal penetration tests at WES, major results from pertinent studies conducted elsewhere were briefly reviewed. Particular attention was given to relations that describe horizontal and vertical forces on flat blades tested horizontally near the sand surface, and to the horizontal force on cones tested horizontally well below the sand surface.

PART II: HIGH-SPEED VERTICAL PENETRATIONS WITH CONES AND PLATES IN AIR-DRY SAND

Test Sand and Its Preparation

Test sand

9. Sand used in the high-speed vertical penetration tests was taken from active dunes near Yuma, Arizona. This sand, termed herein as Yuma sand, has a specific gravity of 2.67 and is a uniformly graded, fine sand classified SP-SM according to the Unified Soil Classification System. Gradation and soil property data are given in fig. 1.

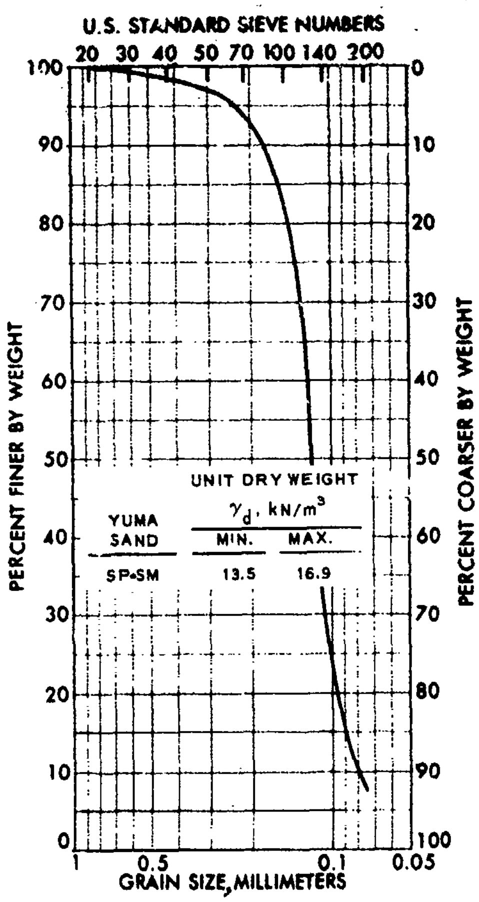

Fig. 1. Gradation and classification of Yuma sand

Sand preparation

10. To prepare each test bin, air-dry Yuma sand was deposited in uniform layers through a 6.3-mm U. S. Standard sieve to fill an 0.8- by 1.6- by 16.4-m test bin, and the top layer was screeded level to the same height as the bin sidewalls. Next, the sand was thoroughly harrowed to at least a 40-cm depth over the full width and length of the bin. Preparation of a very-low-strength test bed was completed simply by releveling the sand surface with a screed strip. All other test beds were prepared by harrowing, compacting with a given number of passes of a vibratory skid unit (comprised of an electric vibrator mounted on a steel base plate 86 cm wide), and then leveling.

11. The strength of each test bed was characterized primarily in terms of penetration resistance gradient G . Although values of cone

penetration resistance increased in near-linear fashion nearly always to at least the 25-cm depth,* reported values of G reflect measurements only in the top 15 cm to conform to general WES practice. Fig. 2 presents representative curves of cone penetration resistance versus depth

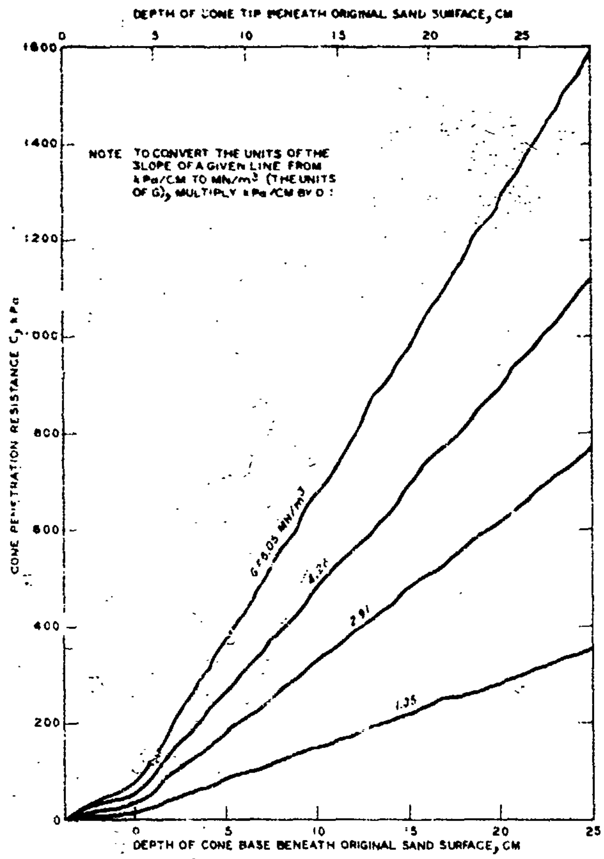

Fig. 2. Representative cone penetration versus depth curves (3.23-cm^2 cone, 3.05-cm/sec penetration speed, air-dry Yuma sand)

for several values of G . Test beds for the high-speed vertical penetration tests were prepared to three approximate strength levels--G values of about 1.3, 2.9, and 6.2 MN/m^3.

---

* Here, "depth" refers to the depth beneath the sand surface of the base of the standard WES 3.23-cm^2-base-area, 3.77-cm-height, circular cone.

Test Equipment

Cones and plates

12. The smooth steel cones and plates used in this part of the study are shown in fig. 3, and are characterized by shape and size as follows:

No.	Probe Shape	Probe Base Size: Dimensions, cm: Diameter	Width	Length	Area cm^2
1	Right circular cone	1.28	--	--	1.29
2		2.03	--	--	3.23
3		4.05	--	--	12.9
4		5.73	--	--	25.8
5		8.60	--	--	58.1
6	Flat circular plate	1.28	--	--	1.29
7		2.03	--	--	3.23
8		4.05	--	--	12.9
9		5.73	--	--	25.8
10		8.60	--	--	58.1
11	Flat rectangular plate (1:1, width to length)	--	1.27	1.27	1.61
12		--	2.54	2.54	6.45
13		--	5.08	5.08	25.8
14		--	7.62	7.62	58.1
15	Flat rectangular plate (1:2, width to length)	--	1.27	2.54	3.23
16		--	3.59	7.18	25.8
17		--	5.39	10.78	58.1
18	Flat rectangular plate (1:4, width to length)	--	1.27	5.08	6.45
19		--	2.54	10.16	25.8
20		--	3.81	15.24	58.1
21	Flat rectangular plate (1:8, width to length)	--	1.27	10.16	12.9
22		--	1.80	14.37	25.8
23		--	2.70	21.56	58.1

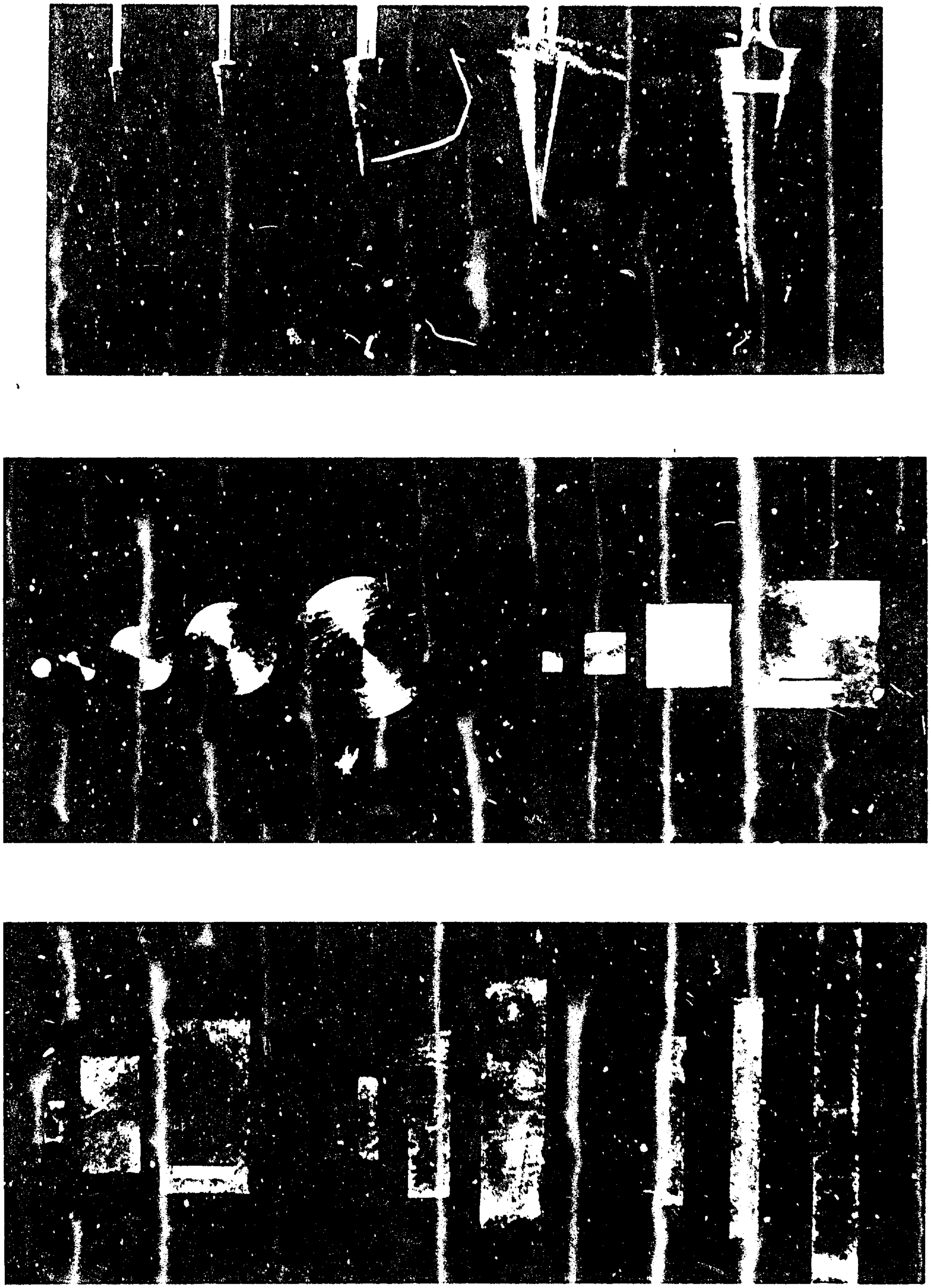

Fig. 3. Test cones and plates used in vertical penetrations of Yuma sand in test bins

The nominal penetration velocities were designated as follows:

No.	Nominal Velocity cm/sec
1	3.05
2	30
3	100
4	200
5	300
6	600

13. Each probe was of one-piece steel construction and consisted of a probe head (cone or flat plate) and a shaft. The shafts were strong enough to provide straight alignment (minimal flexure) during sand penetration, and small enough to produce negligible shaft drag compared with the sand resistance force acting on the probe head. Each probe was 41 cm long overall. The upper end of each shaft was connected to a force-measuring load cell (fig. 4).

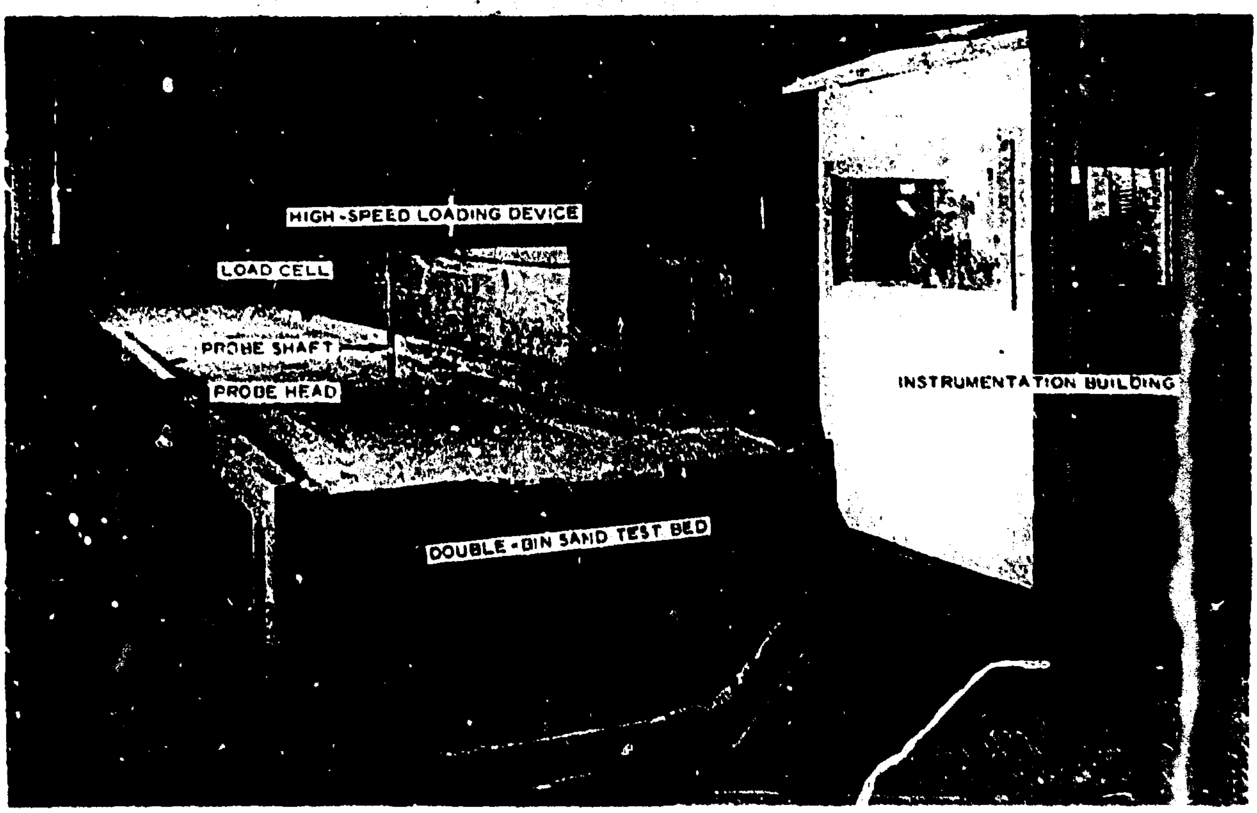

Fig. 4. General view of high-speed loading device, double-bin sand test bed, and instrumentation building

Low-speed penetrometer

14. For tests in the sand bins, a mechanized, low-speed cone penetrometer was used to obtain measurements of standard penetration resistance gradient G . An electric motor drove the 3.23-cm^2 cone vertically into the sand at a constant penetration of 3.05 cm/sec. Sand resistance force was measured by a load cell, and depth of penetration by a gear-driven circular potentiometer (fig. 5), so that a continuous record of cone penetration resistance versus depth was obtained

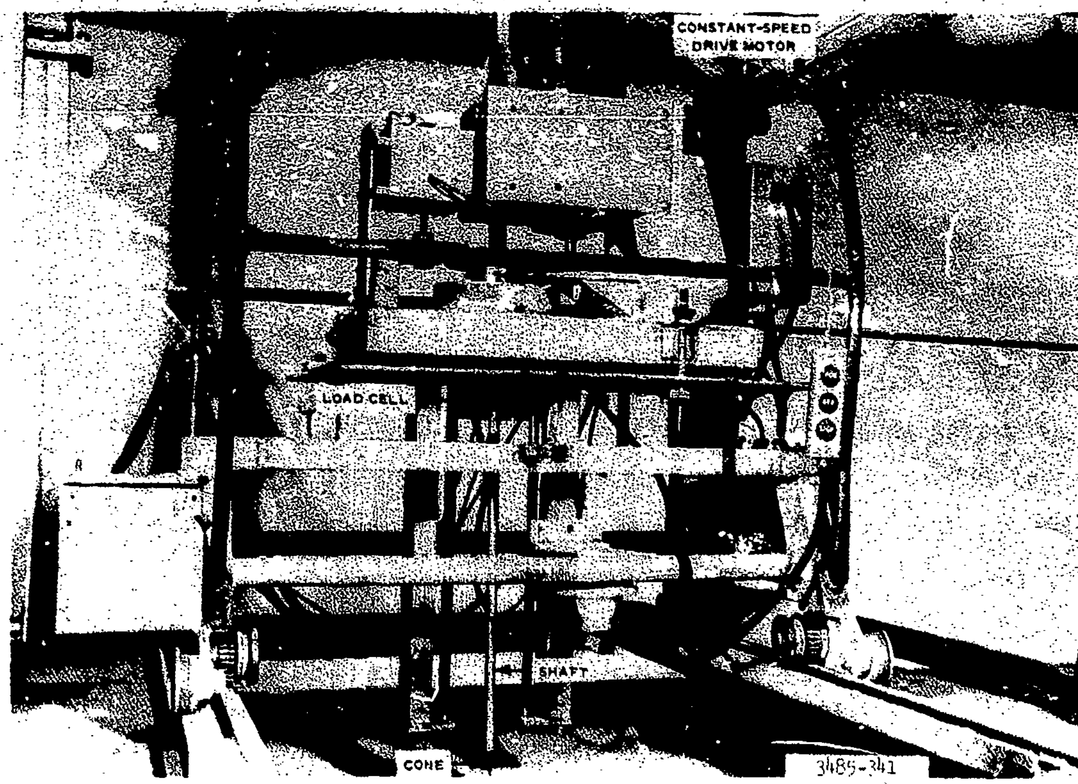

Fig. 5. Mechanized low-speed cone penetrometer

on an x-y recorder for each penetration (fig. 2). The shaft diameter used in measuring G was 0.95 cm for all tests with the standard cone in this report. (Reference 7 states, however, that essentially no influence on G values in Yuma sand is caused by using shaft diameters as different in size as 0.95 and 1.59 cm.)

High-speed loading device

15. The powerful and versatile loading device shown in fig. 4 allows loads, large or small, to be applied to test specimens (tires,

shock absorbers, soils, etc.) at controlled velocities for preset single strokes adjustable from 10 to 30 cm. Design velocities for the loading device range from near zero to about 1300 cm/sec.* During the early part of the stroke, the plunger is accelerated from rest to a preset velocity; over the middle portion of the stroke, velocity remains constant (within ±10 percent); and near the end of the stroke, the plunger is rapidly decelerated to zero velocity. When operating in air at full 30-cm stroke, the portion of the total stroke that remains within ±10 percent of constant speed is about 90 percent for speeds of the order of 10 cm/sec, but drops to about 20 percent at maximum speed.

16. For test velocities up to 200 cm/sec, conventional column-type load cells were used to measure the resistance of sand to penetration. The very large forces associated with both the acceleration and the deceleration phases of penetrations at larger velocities required that penetration resistance be measured by special low-mass, web-type load cells with mechanical restraint to prevent destructive overload. Only two of these special cells were available at the time of testing, one of 2224-N and another of 11,120-N capacity. In each test with the high-speed loading device, an accelerometer mounted just above the load cell measured acceleration during penetration.

Test Procedures

Standard measurements of G

17. After a given air-dry Yuma sand test bed was constructed, standard measurements of G were taken at six locations spaced uniformly over the length of the test bed at its transverse center line. A bed was accepted for testing only if all its standard G values were different from their average by no more than ±10 percent. After test penetrations with the various cones and plates in a given sand bed were

* The nominal upper limit of penetration velocity was taken as 600 cm/sec for this study because the available load cells were unable to withstand the acceleration and deceleration forces associated with higher velocities.

completed, standard G values were again obtained at two or three locations over the length of the test bed. The G value reported for each sand bed is the average of all before-test and after-test values measured.

Tests of cones and plates

18. At least duplicate (occasionally triplicate) penetrations were made for each combination of probe size, shape, and velocity assigned to a given sand test bed. Testing involved the measurement of sand penetration resistance force (F_z), as a function of penetration of penetration depth and velocity of penetration. Quite often, situations arose where system inertial forces were large, even during the near-constant velocity segment of the penetration stroke that was of interest. To preserve resolution in recording F_z , a special technique was used to subtract from the overall force signal a signal equivalent to those forces due to acceleration and deceleration of the probe, shaft, and load cell that passed through the load cell, thereby allowing F_z per se to be recorded directly. During each stroke, three separate signals were continuously recorded: (a) accelerometer output, (b) load cell output, and (c) force signal corrected for acceleration. Before each test or series of tests with a given probe at a given velocity, the high-speed loading device was exercised by moving the probe downward in air (i.e. with zero penetration resistance) at the test design velocity. In-air runs were repeated until, by adjusting potentiometer settings that controlled the correction signal from signal (a), the contribution of inertia to signal (c) was eliminated, and the value of signal (c) remained constant at zero throughout the in-air run. During the subsequent in-sand test, signal (c) measured sand resistance force free of the effects of acceleration and deceleration of the probe load cell assembly. Hereafter, the term sand penetration resistance force (F_z) is the force measured by signal (c). Records of the relatively low resolution signals (a) and (b) were used only for spot checks and backup.

19. Two other variables were also electrically recorded: probe vertical velocity (V_z) and depth of the probe relative to the sand surface. (Zero depth was the point where the probe base was flush with the original sand surface.) The five electrical test signals were

recorded on analog magnetic tape and later machine digitized at 1-cm penetration increments.

20. Tests were conducted by moving a sand bin beneath the high-speed loading device (fig. 4), mounting a given probe, zeroing out the effects of probe acceleration (paragraph 18), and penetrating vertically at the desired velocity. A single longitudinal lane of tests at the bin transverse center line was developed by rolling the bin along steel tracks from one specified test position to the next. Minimum spacing between adjacent penetrations was based on a zone centered on the vertical axis of the probe, the zone being circular in shape and of radius equal to six times the smaller dimension of the probe for rectangular probes and six times the diameter for circular probes.[8] Fig. 6 illustrates one such spacing. No influence of adjacent penetrations on individual F_z versus depth curves was noted in analyzing the results of this study.

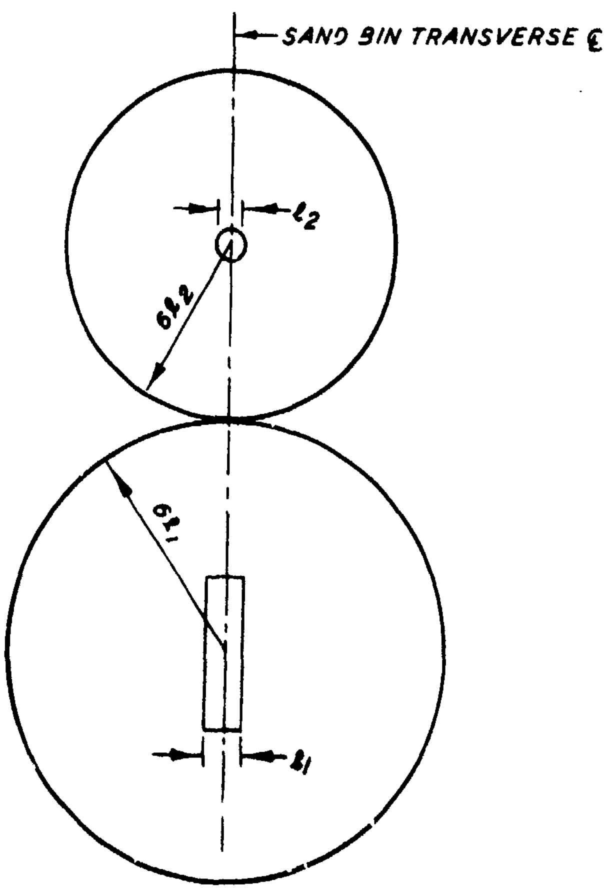

Fig. 6. Example of spacing between adjacent vertical penetrations in a Yuma sand test bin

21. For each penetration, the length of stroke required to reach near-constant velocity was noted when the effects of probe acceleration were zeroed out in air prior to testing. The pretest height of the probe above the sand was then set to a value slightly greater than this length, so that the probe was operating near the nominal test design velocity when it contacted the sand. In spite of this procedure, values of penetration velocity were found to vary considerably during the first 15 cm of penetration by the probe base for nearly all

sand penetrations at nominal velocities of 300 and 600 cm/sec, as well as for some penetrations at lower velocities.

22. This variability in vertical velocity caused no real problem. A discussion of this consideration and how the level of the velocity affects the shape of the probe base pressure versus depth curves for cones and plates, and thus affects the choice of locations along these curves to be singled out for analysis, is included in paragraphs 25-30.

23. Each of the cones and plates listed in paragraph 12 was tested at at least one penetration velocity in Yuma sand test beds of three strength levels--G values of about 1.3, 2.9, and 6.2 MN/m^3. Probes smaller than 3.23-cm^2 base area were tested only at the lowest test velocity (3.05 cm/sec) because the two special load cells designed for high-speed use had capacities too large (2224 and 11,120 N) to allow accurate measurement of the small F_z values developed by these very small probes. Neither were all of the other possible combinations of probe size, shape, and velocity and sand G value tested. Enough were tested, however, to develop a useful description of the influence of each of these variables on sand penetration resistance.

Analysis of Data

24. Results of vertical penetration tests in air-dry Yuma sand at velocities from 3 to over 600 cm/sec are presented in table 1 for five sizes of 30-deg-apex-angle cones, and table 2 for five shapes and a range of sizes of flat plates.

Curves of probe base pressure (F_z/A) versus probe depth

25. Effects of velocity on curve shape. Velocity was found to have pronounced effects on the shape of the curve of probe base pressure (sand penetration resistance force per unit probe base area, F_z/A) versus depth of probe base for each of the cones and flat plates tested. Plate 1 shows the curves obtained for the standard 3.23-cm^2 cone in the G = 2.48 MN/m^3 sand test bed for each of the six nominal penetration

velocities--3.05, 30, 100, 200, 300, and 600 cm/sec.* The progression in the shapes of these curves is representative of that obtained for each size of cone tested in a sand bed of given strength for the range of velocities considered.

26. At least three features of the curves in plate 1 are significant. First, the value of probe base pressure at zero cone base depth increases drastically as penetration velocity increases. Second, the shapes of the curves depart from near linearity as velocity increases beyond about 100 cm/sec. Third, the several curves in plate 1 tend to merge at about a cone base penetration of 10 cm. This indicates that disturbance of the sand ahead of the standard cone causes the consistency of the sand penetrated at cone depths greater than about 10 cm to correspond to the sand's critical void ratio.**

27. A family of curves similar to those in plate 1 is presented in plate 2 for the 25.8-cm^2, 1:4 rectangular plate tested over a range of velocities in Yuma sand test beds of $G \approx 2.9\ \mathrm{MN/m^3}$. The features described in paragraph 26 for plate 1 and the standard cone also apply to plate 2 if (a) the term "cone base depth" in paragraph 26 is replaced by "plate base depth," and (b) the curves in plate 2 are scrutinized only in the 2.5- to 15-cm range of plate base depths. In all considerations that follow, probe base pressure data obtained for the test plates in the 0- to 2.5-cm depth range are ignored because, in each test, penetration to some depth within this range was required before values of probe base pressure stabilized to the pattern that prevailed over the major portion of the 0- to 15-cm depth range.

28. <u>Selection of parts of curves for detailed analysis.</u> In deciding what points from, or portion of, the curves of probe base pressure versus depth to analyze under the influence of probe velocity, it is well to consider the practical implications of testing at near-constant velocity. For vertical penetrations by probes in sand, interest

* The coordinates of each curve in plates 1 and 2 were obtained by averaging the coordinates of the curves from two or more replicate tests conducted at that particular nominal test velocity.

** At the critical void ratio, the rate of application of the shearing stress has no effects on the shearing resistance of sand.

generally centers on the curve only for the low, near-constant-speed situation. It is very unusual for vertical penetration velocity in sand to be maintained near-constant at a level of, say, 200 cm/sec or above to 15 cm or more depth in real-world applications. Mechanically driven probes nearly always penetrate sand at much lower near-constant velocities, and nondriven, i.e. air-dropped or impact-propelled, probes begin deceleration immediately upon contact with the sand.

29. Accordingly, the equation of the least-squares, best-fit straight line that describes the probe base pressure versus depth curve was obtained for a given (generally low-speed) test* only if at least 90 percent of its digitized velocity readings differed from their average by no more than ±10 percent during the first 15 cm of probe base penetration. For the cones, these equations were based on probe base pressure and depth readings in the first 15 cm of base penetration; for the plates, in the first 2.5 to 15 cm of base penetration. For each near-constant-speed test, the probe base pressure versus depth relation was described by an equation of form F_z/A = (F_z/A at zero probe base depth) + G_x (depth) ,** and the coefficient of correlation for each test was equal to at least 0.9. For each of these tests, tables 1 and 2 report G_x and the average value of velocity that prevailed in the depth range described by the equation. Also, values of probe base pressure at 0- and 2.5-cm base depths are reported for the cones and plates, respectively, and at 15-cm depth for both the cones and the plates, on the basis of values indicated for these depths from their least-squares equations relating probe base pressure and depth.

30. For tests whose velocity values did not satisfy the ±10 percent criterion, table 1 reports values of probe base pressure and

---

* Here, a "test" is composed of either two or three penetrations made adjacent to one another under one set of preselected values of probe size, shape, and velocity.

** G_x is the gradient, or slope, of the probe base pressure versus depth curve for any given probe at any given velocity V_z small enough to allow the curve to be near-linear. G without a subscript denotes the gradient obtained under "standard" conditions, i.e. vertical penetration with a 3.23-cm² cone at 3.05 cm/sec in the 0- to 15-cm sand layer.

vertical velocity at 0- and 15-cm base depths for the cones, and at 2.5- and 15-cm base depths for the plates that were obtained by averaging the digital printout values from the two or more replicate tests at the particular probe base depth of interest. The 0- and 2.5-cm base depths were considered of interest for the cones and plates, respectively, because probe base pressure and vertical velocity readings at these depths should match fairly closely corresponding readings for air-dropped or impact-propelled cones and plates at the same depths. Values of probe base pressure and vertical velocity were sampled at the 15-cm depth to demonstrate that probe base pressure at substantial depth is nearly constant over the full range of velocities tested by a given probe in sand of given G value.

Penetration resistance gradient

31. Because the curve of probe base pressure versus depth generally departs more and more from linearity as velocity increases beyond the standard value of 3.05 cm/sec, a method of estimating G_x for the various test probes was developed only for this one velocity level. For a single type of sand penetrated at one speed by plates and cones of various sizes and shapes, the relation between G_x and G should be influenced only by the dimensions of the probes.

32. Effect of probe shape. Vertical penetrations were made at 3.05 cm/sec with each of the 23 test probes in sand test beds of three strength levels--standard G values of about 1.4, 3.4, and 6.6 MN/m^3. Plate 3 shows that a linear (but not 1:1) relation exists between standard G and G_x measured with one size (25.8-cm^2 base area) of each of the six probe shapes tested. No significant separation in this relation by probe shape is noted, although a very broad range of shapes is represented by the data.

33. Effect of probe size. The relation of standard G to G_x measured by probe sizes ranging from 1.29 to 58.1 cm^2 is presented in plate 4. This relation can be described by a family of straight lines, separated by probe size, that passes through coordinates (1, 1). The equation for these lines is

$$(G_x - 1) = a(G - 1) \tag{1}$$

Slope a is linearly related to the ratio ℓ_s/ℓ_x by the equation

$$a = 0.20 + \left(0.80 \frac{\ell_s}{\ell_x}\right)$$

(where ℓ_s and ℓ_x are the square roots of the base areas of the standard 3.23-cm^2 cone and of the probe used to obtain a given G_x value, respectively). Thus, equation 1 becomes

$$G_x = (G - 1)\left[0.20 + \left(0.80 \frac{\ell_s}{\ell_x}\right)\right] + 1 \tag{2}$$

34. Equation 2 indicates that if values are known for G and ℓ_s from a standard penetration ($\ell_s = \sqrt{3.23 \text{ cm}^2} = 1.80$ cm), then G_x can be estimated knowing only the value of ℓ_x for the particular cone or flat plate of interest.*

35. Equation 2 also can be expressed as

$$\frac{G_x - 1}{G - 1} = 0.20 + \left(0.80 \frac{\ell_s}{\ell_x}\right)$$

a relation of dimensionless ratios that describes G_x and its associated ℓ_x value normalized relative to G and ℓ_s, values descriptive of a standard cone penetration. In the paragraphs that follow, descriptions are developed of sand penetration resistance force (F_z) at 2.5- and 0-cm depths for the flat plates and cones, respectively. The format of these descriptions will be similar to that developed for G_x in that, in each case, F_z will be described relative to the dimensions of its associated probe base in a relation of dimensionless ratios normalized relative to the standard cone penetration.

Penetration resistance force (F_z)
<u>for flat plates at base depth = 2.5 cm</u>

36. <u>Some rheological considerations.</u> In plate 5, the relation of

---

* Equation 2 is applicable <u>only</u> if G and G_x are measured in MN/m^3.

probe base pressure to vertical velocity is shown for one plate shape (circular base area) and five plate sizes--base areas from 1.29 to 58.1 cm^2--from tests in sand beds of G values near 6.2 MN/m^3. The data separate by plate size, and the curves have the same general shape. Before dealing with the effect of plate size, it is useful to consider some basic information from rheology.

37. In rheology, the flow characteristics of a material usually are described in terms of the relation of shearing stress to rate of shear. For example, the logarithmic portion of the curve in fig. 7 illustrates the flow characteristics of a pseudoplastic, or shear-

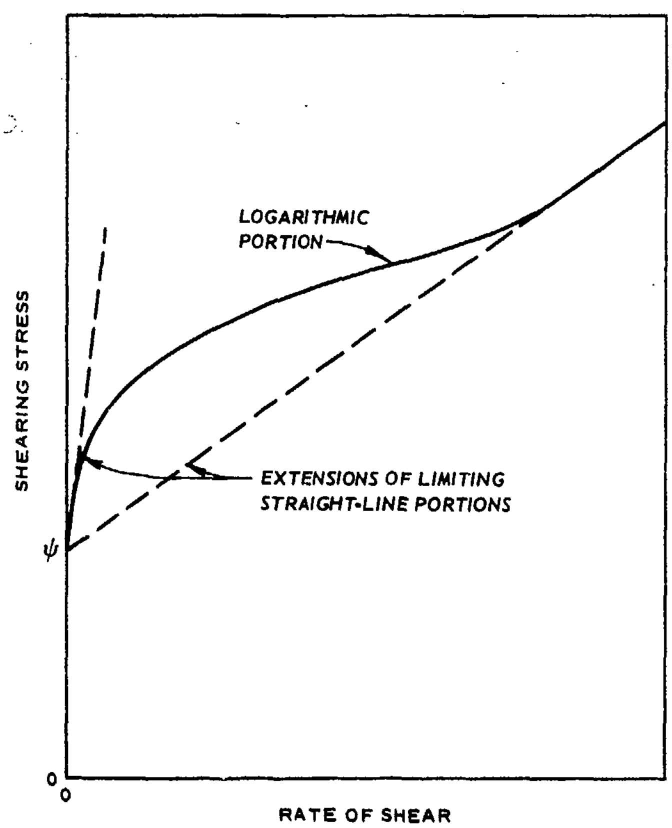

Fig. 7. Approximation of the flow curve of a pseudoplastic material with yield value ψ

thinning, fluid, i.e. a fluid whose shear stress increases less and less rapidly with increasing rate of shear. There is speculation that this relation does not remain a power function throughout an extended range of shearing stresses or rates of shear. Rather, it is thought that "the logarithmic function appears to fit that part of the curve lying between two limiting straight portions"[9] (also shown in fig. 7).

The logarithmic part of the pseudoplastic flow curve is well documented; however, the curve shape beyond the logarithmic portion is open to question because of the limited amount of data reported in the literature for shear rates outside the logarithmic zone.

38. The curve shapes in fig. 7 and in plate 5 are similar. Because the resistance of sand to penetration by a probe is a function of sand deformation and flow, it is considered reasonable to begin the description of this resistance in units common to the rheological approach. The y-axis term in fig. 7 has units of pressure, the same as the units of probe base pressure in plate 5. The x-axis term in fig. 7 has units of velocity divided by length, or units of velocity gradient. To cause the x-axis term in plate 5 to have these units, plate velocity must be divided by some characteristic linear term of the probe-sand system. The term $\ell = \sqrt{A}$ was chosen so that the velocity gradient (i.e. V_z/ℓ) for each test plate shape would be described on a common basis.

39. Effects of plate size and velocity ($V_z \leq 3$ m/sec). In examining the relation between probe base pressure and velocity gradient, attention is restricted first to data with a velocity ≤3 m/sec. An example of the reason for this is shown in plate 5, where relations are shown for the five circular-base-area plates, using data from tests in sand beds of G near 6.2 MN/m³. Each curve is convex upward (and plots straight-line on logarithmic paper) for values of velocity ≤ 3 m/sec. For velocity >3 m/sec, the curve shape is different, indicating a different type of influence of velocity on probe base pressure. A change from convex upward to another curve shape was also obtained at a velocity of about 3 m/sec for each of the other combinations of probe size and shape and sand G value tested. Thus, a velocity of 3 m/sec appears to be a meaningful upper limit to use in the next stage of analysis.

40. The logarithmic relation of probe base pressure to velocity gradient is shown in plate 6a, using those data from plate 5 with velocity ≤3 m/sec. For these circular flat plates, the relation is described by a family of parallel straight lines separated by plate base area. Plate 6b demonstrates that these data fit closely about one line if

$A^{1.2}$ is used instead of A in the y-axis variable. The ordinate term $F_z/A^{1.2}$ has units that lie almost midway between force per unit area and force per unit volume. This term is useful in that it describes on a common basis the relation of F_z to plate size under the influence of a range of values of velocity gradient for a variety of sizes of flat, circular plates.

41. Effect of sand strength. All the data in plates 5 and 6 were obtained in sand test beds with G near 6.2 MN/m^3. To describe the $F_z/A^{1.2}$ versus velocity gradient relation in plate 6b on a common basis for a range of G values, this relation was normalized relative to conditions associated with the standard cone penetration used to obtain G. In the normalized ratios used in subsequent analysis for both plate and cone penetrations, the numerator will have subscript x (to denote the numerator's value not being limited to any particular set of conditions relative to probe size, shape, or speed), and the denominator will have subscript s (to indicate that its value was obtained under conditions associated with the measurement of standard G).

42. Thus, the normalized abscissa term is $(V_z/\ell)_x/(V_z/\ell)_s$, which is further abbreviated to $(V_z/\ell)_{xs}$ and hereafter called the velocity gradient ratio. The term $(V_z/\ell)_s$ has a value of 3.09 cm/sec divided by 1.80 cm or 1.69 sec^{-1}. Similarly, the normalized ordinate term is $\left(F_z/A^{1.2}\right)_x/\left(F_z/A^{1.2}\right)_s$, or $\left(F_z/A^{1.2}\right)_{xs}$, hereafter termed the plate-cone stress ratio. In $\left(F_z/A^{1.2}\right)_s$, $\left(A^{1.2}\right)_s = (3.23\ \text{cm}^2)^{1.2} = 4.08\ \text{cm}^{2.4}$, and $(F_z)_s$ is the vertical sand resistance force acting on the 3.23-cm^2 cone at 3.05 cm/sec speed at zero (not 2.5-cm) base depth penetration. Values inside parentheses in the terms $(V_z/\ell)_x$ and $\left(F_z/A^{1.2}\right)_x$ describe the plate penetration of interest.

43. The relation of plate-cone stress ratio to velocity gradient ratio is shown in plate 7 for tests of flat circular plates of sizes from 1.29 to 58.1 cm^2 in sand test beds of G values from 1.08 to 6.91 MN/m^3, with vertical velocity ≤ 3 m/sec. The closed-symbol data points represent the same data shown in plate 6b. Clearly, the normalization technique described in paragraphs 41 and 42 can be used successfully to account for the effects of sand strength on the $F_z/A^{1.2}$

versus velocity gradient relation. The equation of the straight line used in plate 7 to describe the test results is

$$\left(\frac{F_z}{A^{1.2}}\right)_{xs} = 2.4\left(\frac{V_z}{\ell}\right)_{xs}^{0.25}$$

44. <u>Effect of plate shape.</u> A well-defined, straight-line logarithmic relation between $\left(F_z/A^{1.2}\right)_{xs}$ and velocity gradient ratio was obtained for each of the other shapes of flat plates tested (rectangular plates of 1:1, 1:2, 1:4, and 1:8 width-to-length ratios). For each plate, the slope of the line was essentially the same, 0.25; however, the value of $\left(F_z/A^{1.2}\right)_{xs}$ became progressively smaller at a given value of velocity gradient ratio as plate shape changed from circular to 1:1 to 1:2 to 1:4 to 1:8. This separation was accounted for by normalizing the ordinate variable in terms of area-perimeter ratio ($A/P = R_h$)* of a given "x" plate raised to the 0.4 power, relative to the corresponding value of a circular-base-area probe of <u>the same base area</u> as the "x" plate. That is, the ordinate term was changed from $\left(F_z/A^{1.2}\right)_{xs}$ to

$$\left(\frac{F_z}{A^{1.2}}\right)_{xs} \times \left(\frac{R_h^{0.4}{}_c}{R_h^{0.4}{}_x}\right)$$

or

$$\left(\frac{F_z}{A^{1.2}}\right)_{xs} \times \left(R_h^{0.4}\right)_{cx}$$

where $\left(R_h\right)_c$ is A/P for a circular-base-area probe of the same base area as plate "x." The term $\left(F_z/A^{1.2}\right)_{xs} \times \left(R_h^{0.4}\right)_{cx}$ takes the name "plate-cone stress ratio," the same name coined first in paragraph 42

---

* Recent literature on plate penetration in soils has designated the ratio A/P (the inverse of the perimeter-area ratio more commonly used in soil mechanics) as the "hydraulic radius,"[10] and the notation $A/P = R_h$ has been used in this report.

for $\left(F_z/A^{1.2}\right)_{xs}$ for circular-base-area plates which have a value of $\left(R_h^{0.4}\right)_{cx}$ of 1.

45. Plates 7 and 8 demonstrate that a single relation

$$\left(\frac{F_z}{A^{1.2}}\right)_{xs} \times \left(R_h^{0.4}\right)_{cx} = 2.4\left(\frac{V_z}{\ell}\right)_{xs}^{0.25} \tag{3}$$

describes quite well the response of F_z to a wide range of sand strengths (G values from 1.08 to 6.91 MN/m^3) and plates sizes and shapes.* The upper limit of vertical velocity in plates 7 and 8 is 3 m/sec. For the data shown, values of velocity-gradient ratio ranged from 0.236 to 98.0, which corresponds to a range of values of plate-cone stress ratio from equation 3 of 1.67 to 7.55.

46. Describing F_z for the full velocity range tested. To expand the description of F_z to include values of velocity larger than 3 m/sec, a relation is used similar to one often employed in fluid mechanics and aerodynamics. In this relation, drag coefficient C_D (drag force/inertial force) is plotted on logarithmic paper against Reynolds number N_R (inertial viscous/force), with a characteristic curve shape being produced like that in fig. 8. In the viscous range, the slope of the curve is -45 deg, i.e. negative 1:1, indicating that $C_D \alpha N_R^{-1}$ [drag/inertial force α (inertial force/viscous force)$^{-1}$] or drag is directly proportional to viscous force. In the dynamic range, the curve is practically flat, so (drag/inertial force) = a constant, i.e. drag is directly proportional to inertial force only. The shape of the curve in the transition range depends on both the viscous and the inertial properties of the medium penetrated.

47. Certainly, air-dry sand does not develop viscous forces in the conventional sense that these forces arise from fluid layers within a material interacting with one another. However, the increase in shear

---

* Because plate 7 represents test results for circular plates, $\left(R_h\right)_{cx} = 1$, and the ordinate variable in plate 7 has the same meaning as $\left(F_z/A^{1.2}\right)_{xs} \times \left(R_h\right)_{cx}$.

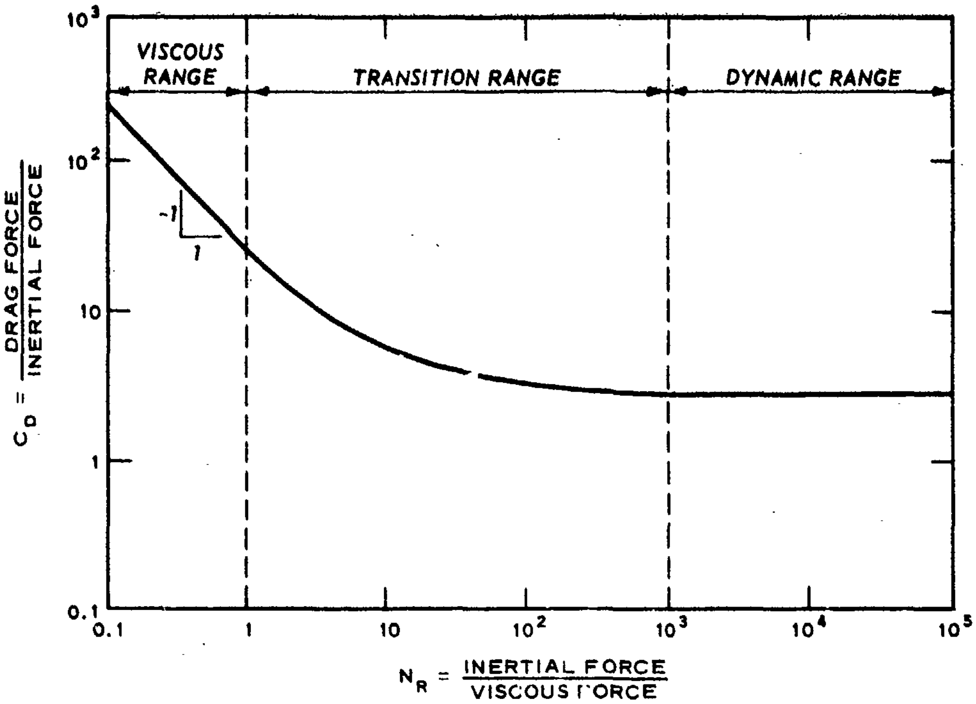

Fig. 8. Representative drag coefficient versus Reynolds number curve

resistance in the logarithmic portion of the curve in fig. 7 does result from viscosity, and equation 3 was developed to describe $\left(F_z\right)_x$ in a normalized, logarithmic format starting with variables similar to those in fig. 7 (plates 7 and 8 and paragraphs 39-45). Thus, the increase in $\left(F_z\right)_x$ for velocity ≤ 3 m/sec follows a pattern similar to the increase in viscous force of a pseudoplastic fluid. Note, also, that inertial force developed by a probe of base area A and velocity V in a fluid of density ρ* is described by

$$F_i = \frac{\rho A V^2}{2}$$

48. Taking the considerations above into account, a relation similar to that in fig. 7 was developed for flat plates in air-dry sand by (a) replacing "viscous force" in fig. 8 with

$$\left(F_z\right)_x = \left(\frac{F_z}{A^{1.2}}\right)_s \times A_x^{1.2} \times \left(K_h^{0.4}\right)_{xc} \times 2.4\left(\frac{V_z}{\ell}\right)_{xs}^{0.25} \text{ (from equation 3), (4)}$$

* For air-dry sand, ρ is mass density, defined as sand unit dry weight divided by acceleration due to gravity, γ_d/g .

(b) computing "inertial force" for sand as

$$\frac{\rho\left(AV_z^2\right)_x}{2}$$

and (c) using measured $\left(F_z\right)_x$ in place of "drag force." Plate 9 shows this relation, using all of the data from the WES tests of flat plates in air-dry Yuma sand. (Open-symbol data in plate 9 were obtained at vertical velocities ≤3 m/sec, closed-symbol data at velocities >3 m/sec.) The curve that describes this relation is linear with a slope of -1 for abscissa values up to about 0.02. Beyond 0.02, the data describe a curve that approaches the horizontal more and more as values of the abscissa term increase. This indicates that inertial forces contributed to $\left(F_z\right)_x$ for vertical velocities >3 m/sec, but no plate test was conducted at velocities large enough to cause $\left(F_z\right)_x$ to be dominated by inertial forces.

49. To estimate $\left(F_z\right)_x$ from the relation in plate 9 requires knowledge of the size, shape, and velocity of the flat plate of interest; the mass density of the sand; and information in terms of F_z, A, V_z, and ℓ_s from a cone penetration to obtain standard G. Then, the value of $\left(F_z\right)_x$ is estimated by calculating the value of the abscissa term in plate 9; determining the corresponding ordinate value from the curve; and multiplying this ordinate value by the value of $\rho AV_z^2/2$ for the plate of interest.

<u>$\left(F_z\right)_x$ for cones at base depth = 0</u>

50. The same procedure outlined in paragraphs 39-43 for the flat plates was used to obtain a description of $\left(F_z\right)_x$ at zero base depth for 30-deg-apex-angle cones of a range of sizes (base areas from 1.29 to 58.1 cm^2) in Yuma sand test beds of G values from 1.08 to 6.91 MN/m^3, with velocities ≤3 m/sec. The logarithmic relation of cone stress ratio $\left(F_z/A^{1.3}\right)_{xs}$ to velocity gradient ratio $\left(V_x/\ell\right)_{xs}$, shown in plate 10, effectively describes $\left(F_z\right)_x$ in a normalized format that includes measurements of all the major variables that influence $\left(F_z\right)_x$.

The relation is different from the corresponding one for flat circular plates (plate 7) in that (a) $A^{1.3}$ instead of $A^{1.2}$ appears in the ordinate term, and (b) the ordinate term in plate 10 increases log-linearly only after velocity gradient ratio values exceed about 2.3.

51. The curve in plate 10 must pass through coordinates (1,1) since the variables in plate 10 are normalized relative to the standard cone penetration. Accordingly, the horizontal part of the curve in plate 10 has ordinate value 1.0. For values of velocity gradient ratio greater than 2.3, the relation is described by

$$\left(\frac{F_z}{A^{1.3}}\right)_{xs} = 0.65\left(\frac{V_z}{\ell}\right)_{xs}^{0.50} \tag{5}$$

Thus, a velocity gradient ratio of 2.3 can be considered a threshold value below which cone stress ratio remains essentially constant, and above which it increases as $0.65\left(V_z/\ell\right)^{0.50}$

52. In plate 11, all the data from plate 10 (open symbols), together with all data for the cones at velocities >3 m/sec (closed symbols), are plotted logarithmically in the relation of

$$\frac{\text{measured } \left(F_z\right)_x}{\rho\left(AV_z^2/2\right)_x} \text{ versus } \frac{\rho\left(AV_z^2/2\right)_x}{\left[\left(F_z\right)_x \text{ computed from relation in plate 10}\right]}$$

No significant departure of the data from a line of slope equal to -1 is noted, indicating that the velocities of these cone tests were not large enough to develop inertial forces that were sizable in comparison with the forces expressed by the denominator of the abscissa term. This result was obtained even though values of velocity up to 6.90 m/sec are included in plate 11.

53. A comparison of plate 10 with plate 7 and plate 11 with plate 9 shows that $\left(F_z\right)_x$ for cones and flat plates is markedly different even though these probes had circular bases of the same range of sizes and operated over about the same range of velocity values in

sand beds of similar G values for the tests reported herein.

$\left(F_z\right)_x$ for plates
and cones at 15-cm depth

54. Values are listed in tables 1 and 2 for sand penetration resistance force $\left(F_z\right)_x$ and velocity $\left(V_z\right)_x$ measured at 15-cm probe base depth for each cone and plate penetration. For each combination of probe size and shape and sand G value, $\left(F_z\right)_x$ varied only slightly with velocity at the 15-cm depth (reference plates 1 and 2). If a situation arises where $\left(F_z\right)_x$ needs to be estimated at some substantial probe base depth (say, ≥10 cm) for a given flat plate or cone with velocity of >3.05 cm/sec, a reasonable approach is to estimate $\left(F_z\right)_x$ at that depth for the probe of interest with velocity equal to 3.05 cm/sec. To accomplish this, first estimate $\left(F_z\right)_x$ at 2.5-cm base depth for a given plate using equation 4 (plates 7 and 8); or estimate $\left(F_z\right)_x$ at zero base depth for a given cone using

$$\left(F_z\right)_x = A_x^{1.3} \times \left(\frac{F_z}{A^{1.3}}\right)_s$$

for $\left(V_z/\ell\right)_{xs} \leq 2.3$ and

$$\left(F_z\right)_x = A_x^{1.3} \times \left(\frac{F_z}{A^{1.3}}\right)_s \times 0.65 \left(\frac{V_z}{\ell}\right)_{xs}^{0.50}$$

for $\left(V_z/\ell\right)_{xs} > 2.3$ (plate 10). In these estimates of $\left(F_z\right)_x$, use $\left(V_z\right)_x = 3.05$ cm/sec. Next, estimate G_x for the probe of interest by using equation 2 $\left[\text{again, with } \left(V_z\right)_x = 3.05 \text{ cm/sec}\right]$. Then, $\left(F_z\right)_x$ for $\left(V_z\right)_x \geq 3.05$ cm/sec at the depth of interest (≥10 cm) can be approximated by $\left[\left(F_z\right)_x \text{ at 0 or 2.5 cm}\right] + \left[G_x \times \text{(depth of interest - 0 or 2.5 cm)}\right]$.

PART III: LOW-SPEED VERTICAL CONE PENETRATIONS IN DRY-TO-MOIST SAND

Test Sand and Its Preparation

Test sand

55. The same type of desert (Yuma) sand used in the tests described in Part II of this report (paragraph 9) was also used in the tests described in this part.

Sand preparation

56. Samples of air-dry Yuma sand (moisture content from 0.4 to 0.5 percent) were prepared in 38-cm-inside-diameter, 30-cm-high steel molds by pouring the sand from a height of 45 cm above the mold, taking care to cover the full area of a given mold uniformly as it was filled. Different sand densities (and G values) were produced by varying the rate of sand discharge into the molds. This was accomplished by use of an adjustable nozzle in the flexible hose through which the sand flowed into the molds.

57. Yuma sand test samples at moisture contents from 1.1 to 12.3 percent were produced by carefully blending prescribed amounts of sand and water to produce a homogeneous mixture at the desired moisture content. Three levels of sand unit dry weight were used for nearly all of the moist-sand samples--approximately 15.1, 15.4, and 16.0 kN/m^3. For a given sample, the sand was placed in the steel mold in shallow layers (from as little as 3.6 to as much as 5.9 cm thick) and each layer was compacted by blows of a 12.2-kg hammer falling 15 cm. The number of blows and the sand thickness per layer were varied until a combination was obtained that produced a near-linear increase of cone penetration resistance with depth for each combination of moisture content and unit dry weight tested.

58. Sand strength in the test molds was characterized primarily in terms of G , although measurements were also taken of unit dry weight and moisture content for each test sample. The cone penetration resistance versus depth curves obtained in the test molds had essentially

the same near-linear shape as those (fig. 2) obtained in the sand test bins, for both the air-dry and moist samples of Yuma sand.

Test Equipment

59. Two penetrometers with the WES standard cone (3.23-cm^2 base area) were used in the vertical penetration tests of dry-to-moist Yuma sand. The first penetrometer forced the cone into the sand at constant velocity from 0.017 to 6 cm/sec by means of a mechanical rack-and-pinion gear arrangement (fig. 9a). Cone penetration resistance versus depth of penetration was recorded by an x-y plotter (records similar to fig. 2).

60. The second penetrometer was a triaxial machine modified for this study by removing the triaxial chamber, widening the outer arms of the moving element to accept the 39.4-cm-outside-diameter test mold, and mounting a cone-shaft-load cell arrangement in the center of the moving element (fig. 9b). This machine was used for cone penetration tests at speeds from 0.3 to 35.1 cm/sec. (Values of G obtained at overlapping velocity values for the two penetrometers indicated no influence of machine type on the test results.) An oscillograph recorded F_z, depth of cone penetration, vertical velocity, acceleration, and F_z free of the effects of acceleration and deceleration of the cone-shaft-load cell assembly.*

Test Procedures

61. For both penetrometers, three cone penetrations were made in each sand mold at a given test velocity. Variables measured for each mold included sand unit dry weight and moisture content, cone vertical

---

* The influence of acceleration and deceleration of the cone-shaft-load cell assembly on measured sand penetration resistance force F_z was eliminated for tests with the modified triaxial machine by the same technique described for the high-speed loading device in paragraph 18. That is, the F_z values reported herein reflect the interaction of the cone and sand only, <u>not</u> the effects of accelerating or decelerating the cone-shaft-load cell assembly.

a. Mechanical penetrometer

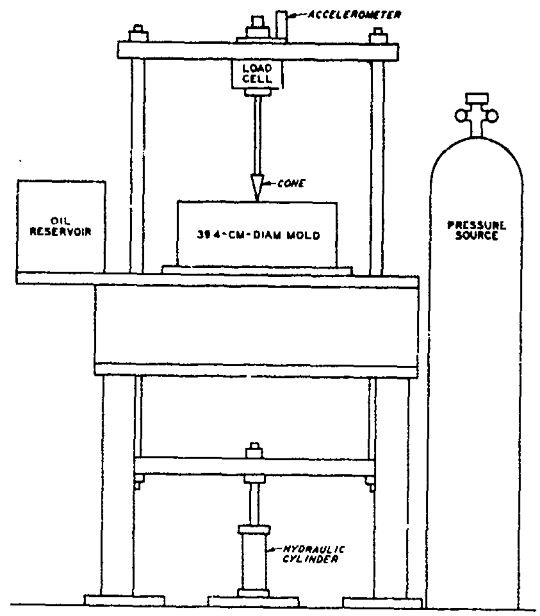

b. Modified triaxial machine

Fig. 9. Penetrometers used in vertical penetration tests of dry-to-moist Yuma sand contained in steel molds

velocity, and penetration resistance gradient G (from the curves of cone penetration resistance versus depth). Average values of each of these four variables are listed in tables 3 and 4 for each sand mold specimen tested.

Analysis of Data

62. The results of vertical penetration tests with the standard WES 3.23-cm^2 cone at $(V_z)_x$ values from 0.01 to 35.1 cm/sec in test molds of Yuma sand whose moisture contents ranged from 0.4 to 11.5 percent are presented in table 3. Table 4 presents data from a separate block of 16 tests with the standard cone at standard velocity

(3.05 cm/sec) in Yuma sand molds of 0.5 to 12.3 percent moisture content. Data in table 4 were obtained to complement relations developed from the data in table 3.

Effects of velocity

63. The relation of sand penetration resistance gradient G_x to vertical penetration velocity $(V_z)_x$ is shown in plate 12 for the 3.23-cm^2 cone tested at four levels of moisture content (approximate values of 0.5, 1.4, 2.1, and 7.0 percent) and at velocities from 0.0295 to 33.4 cm/sec. All data in plate 12 are from molds of Yuma sand tested at one level of sand unit dry weight (γ_d), approximately 15.4 kN/m^3. No significant effect of velocity on G_x is apparent, and the relation for each of the four moisture content levels is described by a horizontal line.* Clearly, G_x is strongly influenced by moisture content; more than a fourfold increase in the value of G_x resulted from increasing moisture content from 0.5 to 7.0 percent.

64. Nearly the full range of $(V_z)_x$ values in table 3 is included in plate 13. The lack of influence of $(V_z)_x$ on G_x in plate 12, together with the fact that standard velocity, 3.05 cm/sec, is included in the range of $(V_z)_x$ values in the abscissa term of this plate, allows G_x values from table 3 to be considered equivalent to standard G values. In all relations examined in the remainder of this part of the report, tables 3 and 4 are considered to contain values of G, not G_x.

Effects of unit dry weight and moisture content

65. Changes in the value of unit dry weight produce corresponding changes in the value of G, as demonstrated in plate 13 for four levels of moisture content. The semilogarithmic relation between G and unit dry weight in plate 13 is described by a family of parallel straight

---

* The insensitivity of G_x to increases in velocity up to 33.4 cm/sec (the largest velocity in plate 12) agrees with results obtained with the standard cone in Part II of this report. From page 1 of table 1, G_x values obtained with the 3.23-cm^2 cone at approximately 30 cm/sec were 1.44, 2.44, and 5.66 MN/m^3 in sand test beds of standard G values 1.40, 2.48, and 6.06 MN/m^3, respectively.

lines separated by levels of moisture content. This indicates that a given change in the value of unit dry weight produces approximately the same percentage change in the value of G for any moisture content within the range tested. Of course, the numerical change in G caused by a given change in unit dry weight increases as the value of moisture content increases.

66. The straight lines in plate 13 are described by the equation

$$\log G = \log a + \frac{\gamma_d}{3} \tag{6}$$

The algebraic value of log a in equation 6 increases with increasing values of moisture content--see fig. 10. This figure shows that the value of log a increases rapidly as moisture content increases from 0.4 to about 3 percent; beyond 3 percent, the rate of increase of log a

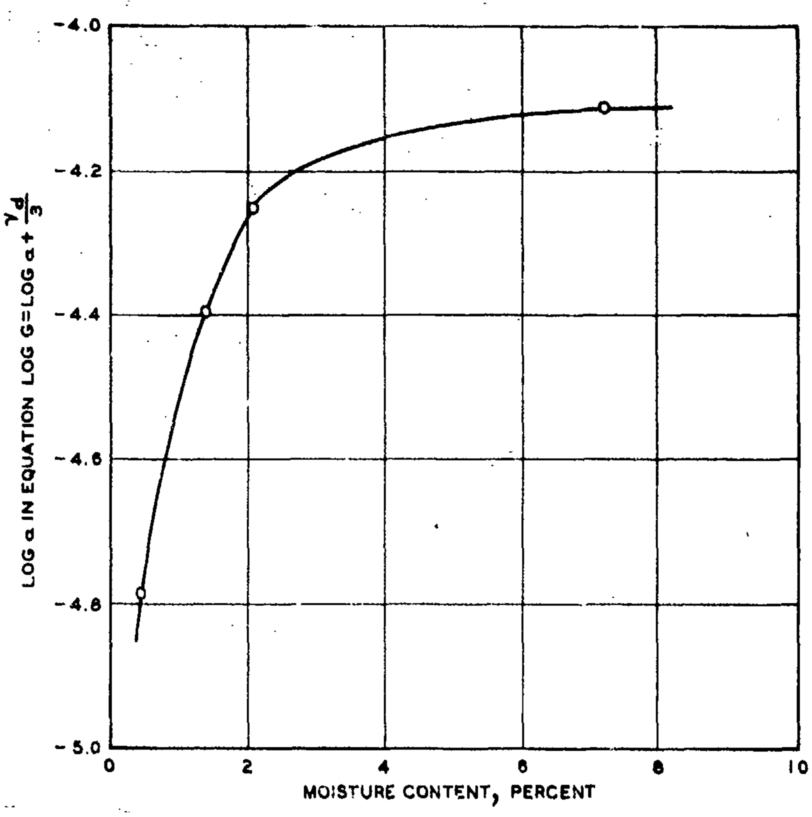

Fig. 10. Relation of log a in equation 6 to moisture content

becomes progressively much smaller. Plate 14 shows that variation in moisture content influences G in a pattern similar to its influence on log a in fig. 10. For each of the three unit dry weight levels represented in plate 14, the major portion of the increase in G occurs as moisture content increases from 0.4 to 3 percent.

67. In terms of vehicle mobility, the strong dependence of G on moisture content at small values of the latter variable carries important practical implications. All WES laboratory tests of single model wheels and tracks, as well as of prototype vehicles, have been conducted in air-dry sand. Thus, the descriptions of vehicle running gear performance based on evaluations of these tests should be conservative when a given value of sand unit dry weight is considered.* Analysis of the results of many field tests of prototype wheeled vehicles conducted in dry-to-wet sands indicated that G has the same meaning relative to running gear performance, no matter what the moisture.[11] A strong statement to this effect cannot be made at present, however, because a sizable amount of data scatter was present in the relations between running gear performance and a prediction term that included G. Controlled laboratory tests of wheels and tracks should be conducted in moist-to-wet sands to determine with improved accuracy how G at different moisture content levels is related to vehicle running gear performance.

---

* This results because vehicle running gear performance normally worsens (pull decreases, sinkage increases, motion resistance increases, tractive efficiency decreases, etc.) as the value of G decreases. Over the range of moisture contents studied herein, the smallest value of G was obtained for the air-dry condition.

PART IV: HORIZONTAL PENETRATION TESTS WITH PROBES IN AIR-DRY SAND

Test Sand and Its Preparation

68. The air-dry Yuma sand used for horizontal cone penetration tests at WES was the same type of sand described in paragraph 9. Each test was conducted in a sand bed enclosed by five 0.8- by 1.6- by 8.2-m soil bins joined end to end, with the interior bin gates removed. The sand preparation technique was the same as that described in paragraphs 10 and 11.

Test Equipment

Low-speed penetrometer

69. Measurements of standard penetration resistance gradient G were taken in a given five-bin sand test bed using the same mechanized, low-speed cone penetrometer described in paragraph 14.

Test cones and dynamometer

70. Horizontal penetrations were made with steel, 30-deg-apex-angle, right circular cones of four sizes--base areas of 3.23, 6.45, 12.90, and 23.23 cm^2--by using a special cone assembly mounted on the forward face of a dynamometer test carriage (fig. 11). In the assembly, a hollow outer shaft protected a specially machined inner shaft, which was threaded to receive the test cones and instrumented with strain gages to record only the force transmitted to its leading face by the cone, i.e. the strain gages were positioned such that forces only on the base of the cone, not on the shaft, were recorded. Calibration tests showed that axial loads over the full range subsequently encountered during testing were recorded to an accuracy of ±2 percent. Also, it was determined that forces applied perpendicularly to the shaft were not picked up by the strain gages, indicating that any nonaxial loads caused by shaft misalignment were not recorded.

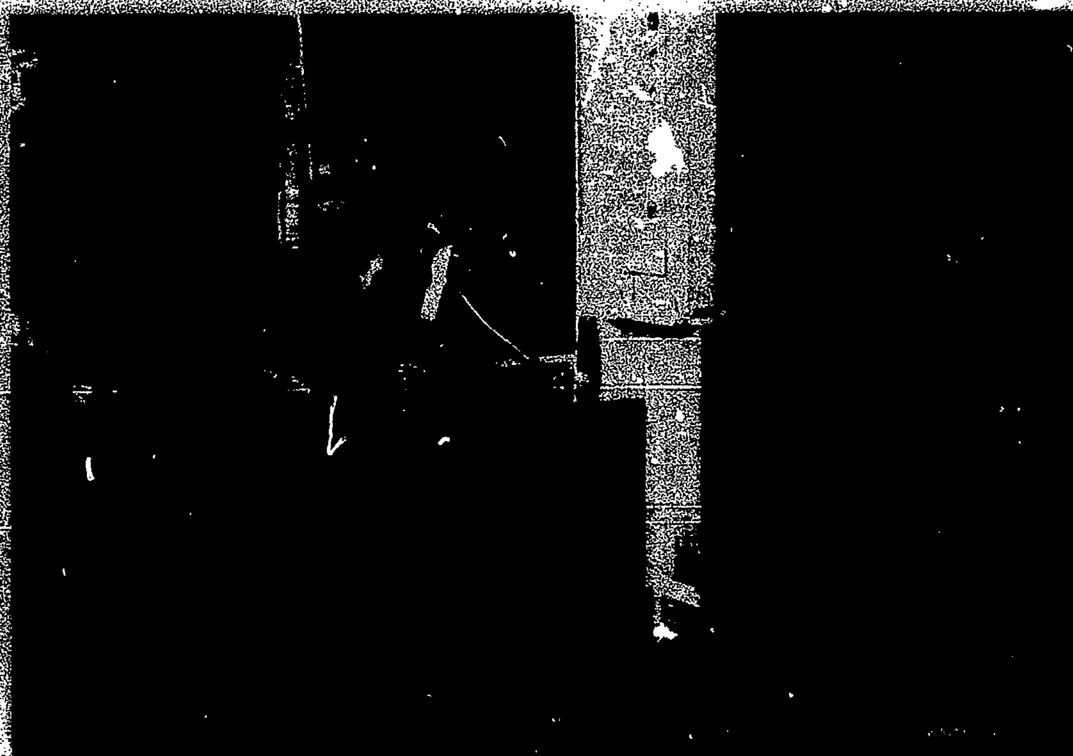

Fig. 11. Cone assembly mounted on forward face of dynamometer test carriage

Test Procedures and Data Reduction

Test procedures

71. After a given five-bin test bed of air-dry Yuma sand was prepared, measurements of G were taken at 1.5-m intervals over the length of the bed (about 18 m long for each test) at its transverse center line. Next, the test cone was screwed into the shaft of the special cone assembly, which itself was rigidly mounted on the front face and at the transverse center line of the dynamometer carriage. The tip of the cone was then set to a predetermined depth beneath the level of the sand surface, and a final check was made to assure that the cone shaft was horizontally aligned. While the cone and shaft were still in air, calibration checks were made of the cone shaft's strain-gage system and of an oscillograph system that recorded the test results.

72. To allow the penetration velocity of a test to begin at zero,

the core assembly was moved forward very slowly until the cone was several meters inside the first sand bin, at which time the carriage was stopped. The actual test was then begun by moving the assembly forward several meters at the dynamometer's lowest creep speed.* After this initial penetration period, the test velocity was programmed to increase linearly to a maximum value (about 3.8 m/sec for most tests, up to 5.2 m/sec for several), and then to decrease linearly to zero. Each horizontal penetration passed through the locations of the vertical cone penetrations that were made prior to the test to obtain standard G values. Values of horizontal force F_x acting on the base of the test cone, horizontal test cone velocity V_x, and acceleration a were recorded by the oscillograph.

Data reduction

73. Values of horizontal force were measured at corresponding values of velocity during the acceleration and deceleration phases of each test, and the average of the two force values are reported herein for each velocity level sampled. Each pair of force readings at a common velocity had nearly equal values, indicating that the increasing-, then decreasing-speed technique affected the force negligibly. Using the average of two force values measured at locations a considerable distance apart also had the advantage of "balancing out" the effects of slight nonuniformities in sand strength over the length of the test bed.

Performance of Cones and Plane Blades in Sand

Some general considerations

74. Soil cutting by tillage tools is a practice many centuries old. Earth moving by machines with scraper blades has become a common practice since the turn of the century. In both cases, the penetrating implement moves generally parallel to the soil surface. Also in both

---

* Even this procedure failed to produce usable data below about 0.3 m/sec, since F_x (horizontal force imparted by the sand to the cone base) stabilized to a given pattern only after a velocity of about 0.3 m/sec was reached.

cases, a quantitative description of the influence on soil penetration resistance of the pertinent soil and implement variables would lead to better, more rational design of the penetrating implement.

75. Two types of horizontal penetrations in sand may be considered: (a) those made well below the sand surface and (b) those made near the surface. Only penetrations of the second type were conducted at WES for this study. Analysis of the results of these cone penetration tests, together with a summary of major findings from two similar non-WES studies, is presented below. This analysis is followed by a discussion of some major points from a comprehensive study[12] of plane cutting blades tested near the sand surface.

Cones tested beneath the sand surface at WES

76. Data from 22 horizontal penetration tests conducted beneath the surface of air-dry Yuma sand with four sizes of 30-deg-apex-angle, right circular cones are presented in table 5.

77. Dimensionless description of the cone-sand system. To describe the physical characteristics of the system in which the horizontal cone penetration tests were conducted, the sketch in fig. 12 was prepared. The following variables and their associated units of force,

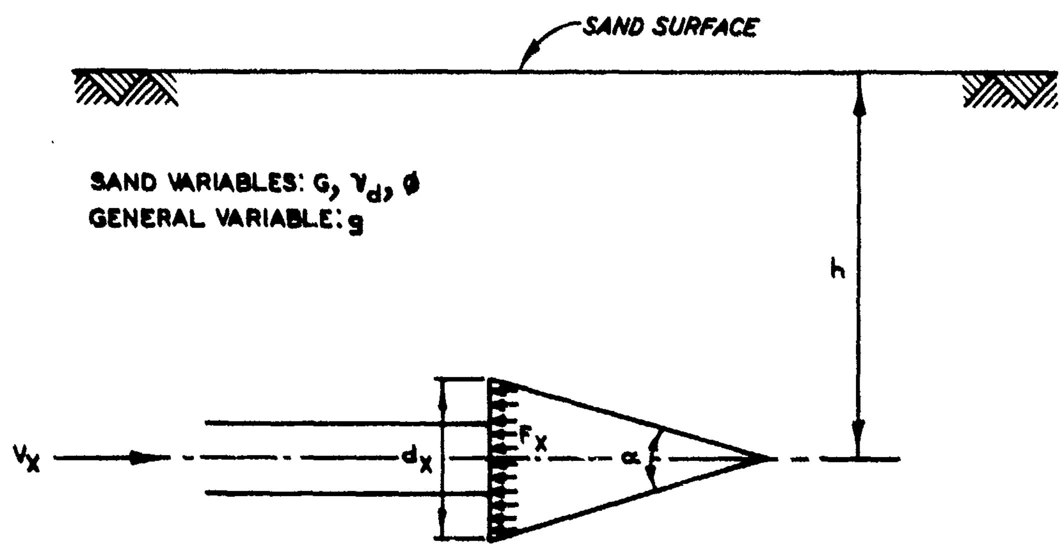

Fig. 12. Sketch of cone-sand system for a cone penetrating horizontally beneath the sand surface

length, and time (FLT units) describe the system:

a. Dependent variable.

F_x , sand resistance force measured in the direction of horizontal cone penetration (F)

b. Independent variables.

(1) Cone.

α , cone tip apex angle (deg)

d_x , diameter of cone base* (L)

h , depth of cone tip in its test position beneath the undisturbed sand surface (L)

V_x , horizontal cone velocity (LT^{-1})

(2) Sand.

G , sand standard penetration resistance gradient (FL^{-3})

γ_d , sand unit dry weight (FL^{-3})

ϕ , angle of internal friction of the sand (deg)

(3) General.

g , acceleration due to gravity (LT^{-2})

78. From dimensional analysis, the Buckingham Pi Theorem states that the number of dimensionless terms needed to express a relation among the variables is equal to the number of pertinent variables minus the number of dimensions (i.e. force, length, and time units) among these variables. Assuming all the variables in paragraph 77 are pertinent , six (9 - 3) dimensionless terms are needed in the general relation that describes force F_x . Formal techniques have been developed for forming the terms, but they can be derived easily by inspection for this analysis. The general form of the relation between F_x and the independent variables in paragraph 77 can be expressed as

$$\frac{F_x}{Gd_x^3} = f\left(\alpha, \frac{h}{d_x}, \frac{V_x}{\sqrt{gd_x}}, \frac{\gamma_d}{G}, \phi\right) \tag{7}$$

79. Only four of the dimensionless terms in equation 7 were needed to describe the WES cone-sand system since (a) cone tip apex

---

* Because all of the test cones had the same shape, any given linear dimension of the cone can be used to characterize cone size.

angle α was 30 deg for all the test cones, and (b) angle of internal friction ϕ varied by only about 2 deg for the full range of G values tested and, therefore, could be considered constant. Thus, equation 7 was reduced to

$$\frac{F_x}{Gd_x^3} = f\left(\frac{h}{d_x}, \frac{V_x}{\sqrt{gd_x}}, \frac{\gamma_d}{G}\right) \tag{8}$$

It is emphasized that variables of the same dimensions in equation 8 can be interchanged, the dimensionless terms can be inverted, and different dimensionless terms can be formed by multiplying or dividing dimensionless terms by one another and/or by performing the same mathematical operation on the numerator and denominator of a given dimensionless term.

80. Test results at 30 cm/sec. A logical representation of the term F_x/Gd_x^3 in equation 8 is $\left(F_x/d_x^2\right)/Gd_x$, or $\left(F_x/A_x\right)/Gd_x$ where A_x is the base area of the cone. The numerator in the latter term describes cone base pressure, and the denominator can be considered an indicator of sand pressure at some unspecified depth. This term can be altered to another dimensionless term by multiplying it by $\left(d_x/h\right)^2$, i.e.

$$\frac{F_x/A_x}{Gd_x} \times \frac{d_x^2}{h^2} = \frac{F_x/A_x}{Gh^2/d_x} \tag{9}$$

This last dimensionless term has been produced by manipulation of the first two terms in equation 8, and is hereafter called the "cone-sand pressure ratio."

81. To determine whether the cone-sand pressure ratio is a meaningful, stable term, its numerator was plotted versus its denominator in plate 15, using data thought to be affected very little by the last two dimensionless terms in equation 8. Relative to the Froude number $(V_x/\sqrt{gd_x})$, velocity V_x was held constant at 30 cm/sec, the lowest velocity in the programmed-velocity tests that was judged adequate to produce reliable measurements of F_x. Concerning the term γ_d/G, values of G for the horizontal cone penetration tests ranged from

1.05 to 4.33 MN/m^3 (table 5). From plate 13, corresponding values of γ_d are 14.4 and 16.3 kN/m^3, respectively, which define a very small range. Thus, it was anticipated that the Froude number and γ_d/G would have only slight influence on the relation of F_x/A_x to Gh^2/d_x .

82. The data in plate 15 fit closely about the straight line described by

$$\frac{F_x}{A_x} = 70 + \left(0.050 \frac{Gh^2}{d_x}\right)$$

All but two of the 22 tests represented in plate 15 were conducted at $h = 17.8$ cm (open-symbol data points). The other two tests (closed symbols) were conducted at $h = 10.2$ cm and at $h = 25.4$ cm . The data point for $h = 10.2$ cm lies very close to the straight line. The one for $h = 25.4$ cm is within a reasonable distance from the line, but lies noticeably to the right side. This separation is considered to result primarily from the fact that 25 cm is approximately the maximum depth that could be maintained near-linear in the Yuma sand test beds (paragraph 11). For $G = 1.05$ MN/m^3 and the standard 3.23-cm^2 cone, this depth also corresponds closely to the "critical depth" D_c described in Report 4 of this series.[7] Below the critical depth, sand resistance "increases only slightly, and the rate of increase remains constant." Because horizontal performance of a cone at a given depth is influenced by sand strength both above and to some depth below the height of the cone tip, the <u>effective</u> value of G for the test at $h = 25.4$ cm likely is slightly less than 1.05 MN/m^3. A smaller value of G for the data point at $h = 25.4$ cm would shift its location leftward, and therefore closer to the curve in plate 15.

83. The major point is that cone base pressure F_x/A is closely related to the sand pressure term Gh^2/d_x . However, this relation holds true only for data obtained well within that depth of sand wherein cone penetration resistance increases in near-linear fashion.

84. <u>Relation of the cone-sand pressure ratio to the Froude number.</u> To introduce the effects of velocity of F_x , the cone-sand pressure ratio was plotted against the Froude number for each of the four test cones, as shown in plate 16. The left side of plate 16 shows that, for each

penetration test, a log-linear relations exists for values of the Froude number up to about 5. The slope n of these lines can be described by

$$n = \frac{1.037 - \log\left[\frac{\gamma_d}{G} \times \left(\frac{d_x}{d_s}\right)^{0.5}\right]}{3} , \quad \frac{V_x}{\sqrt{gd_x}} \le 5 \qquad (10)$$

where

d_x = diameter of the cone of interest

d_s = 2.03 cm, the diameter of the standard 3.23-cm^2 cone.*

Note that n may be positive or negative. The tests represented in plate 16 had values of $\left[\left(\gamma_d/G\right)\left(d_x/d_s\right)^{0.5}\right]$ from 2.66 to 23.2, and corresponding n values from equation 10 of 0.20 to -0.11.

85. To develop a means of estimating the cone-sand pressure ratio from an equation of the form

$$\frac{F_x/A_x}{Gh^2/d_x} = k\left(\frac{V_x}{\sqrt{gd_x}}\right)^n \qquad (11)$$

with $V_x/\sqrt{gd_x} \le 5$, it was necessary next to determine a relation for k, the value of $(F_x/A_x)/\left(Gh^2/d_x\right)$ at $V_x/\sqrt{gd_x} = 1$. Cone base pressure F_x/A_x was plotted versus the sand pressure ratio Gh^2/d_x for the condition $V_x/gd_x = 1$, and the well-defined linear relation

$$\frac{F_x}{A_x} = 55 + \left(0.060\,\frac{Gh^2}{d_x}\right)$$

was produced, so that

$$k = \frac{F_z/A_x}{Gh^2/d_x} = \frac{55}{Gh^2/d_x} + 0.060 , \quad \frac{V_x}{\sqrt{gd_x}} = 1 \qquad (12)$$

86. The right side of plate 16 shows that, at about $V_x/\sqrt{gd_x} = 5$, the relation of $\left(F_x/A_x\right)/\left(Gh^2/d_x\right)$ to $V_x/\sqrt{gd_x}$ becomes linear on an arithmetic basis. The slope m of the lines in the right side of plate 16 can be described by

---

* In equations 10 and 13, the units of γ_d are kN/M^3 and those of G are MN/m3. d_x/d_s and $V_x/\sqrt{gd_x}$ are dimensionless ratios.

$$m = \frac{\log\left(\frac{\gamma_d}{G} \times \frac{d_x}{d_s}\right) - 0.57}{115}, \quad \frac{V_x}{\sqrt{gd_x}} > 5^* \tag{13}$$

87. Overall, then the relation of the cone-sand pressure ratio to the Froude number can be described by equation 11, with k defined by equation 12 and n by equation 10 for $V_x/\sqrt{gd_x} \leq 5$. For $V_x/\sqrt{gd_x} > 5$,

$$\frac{F_x/A_x}{Gh^2/d_x} = \left(\frac{F_x/A_x}{Gh^2/d_x} \text{ at } \frac{V_x}{\sqrt{gd_x}} = 5\right) + m\left(\frac{V_x}{\sqrt{gd_x}} - 5\right)$$

The curves describing force F_x versus velocity V_x in plate 17 were defined on the basis of the relations just cited in this paragraph, using inputs of known A_x, G, h, and d_x for five horizontal cone penetration tests in table 5. The patterns of F_x versus V_x described by the data points of these tests are traced reasonably well by the curves thus developed.

88. Other cone studies. Results from two other studies[13,14] involving horizontal cone penetration tests well below the sand surface provide information complementary to the WES results described in paragraphs 76-87. In both studies, the test material was an air-dry sand with a specific gravity of 2.67, an angle of internal friction ϕ by triaxial test of 30.5 deg, and grain-size distribution such that 95 percent, by weight, lies between 0.015 and 0.06 mm. Three levels of unit dry weight were used--14.3, 15.2, and 16.0 kN/m^3. Twelve circular-base-area cones were tested whose base areas ranged from 20.3 to 81.1 cm^2, and whose apex angles ranged from 15 to 90 deg. Some of the steel cones were tested smooth, others with sandpaper glued to the outer surface. Maximum horizontal cone test velocity V_x in the two studies was 2.4 m/sec, and cone tip depths at which penetrations were made ranged from 7.6 to 61.0 cm.

89. The principal aim of the two studies was to investigate the effect on horizontal force F_x caused by variations in depth of penetration, model variation (i.e. cone size, apex angle, and surface roughness), cone speed, and the "state of packing" of the sand. The following are among the most important findings from the two studies:

<u>a</u>. For a given value of sand unit dry weight and a cone of given size tested horizontally at low speed, sand penetration resistance force increases roughly as the square of depth for tests near the sand surface [because the cone "is effectively pushing a block of sand of depth (h) ahead of it and so suffering a passive pressure proportional to depth squared"[14]], and roughly linearly with depth for tests substantially below the surface.* This first result agrees with that developed herein from the WES cone tests, in that h^2 was determined to be the depth term appropriate in a description of F_x .

<u>b</u>. At a given depth well below the sand surface, and at low penetration velocity, F_x increases linearly with cone base area. For the WES test results, plate 18b demonstrates that curves based on equations 10, 11, and 12 describe the relation of F_x to cone base area slightly better than would straight-line approximations. The data points in plate 18b were obtained from a cross-plot of the F_x versus G relation shown in plate 18a, using data at velocity $V_x = 30.5$ cm/sec from the 20 tests in table 5 that had $h = 17.8$ cm .

<u>c</u>. Slight reductions in F_x resulted from reducing the cone apex angle (in the 90- to 15-deg range) and from using polished steel, rather than sandpaper-covered, cones. However, the magnitudes of these effects on F_x are quite small compared with those of the other variables considered.

<u>d</u>. Values of F_x change with cone speed in different patterns for loose and dense sand, with larger increase in F_x (both on a percentage and on a numerical basis) being obtained in the dense state (for V_x values up to 2.4 m/sec). In the loose state, a general reduction in F_x with increasing V_x occurred up to 1.2 m/sec, with F_x increasing with V_x beyond 1.2 m/sec. Roughly, this pattern was obtained in the WES tests, except that the transition point for different F_x values was taken as occurring at Froude number $(V_x/\sqrt{gd_x}) = 5$. (See plates 16 and 17 and paragraphs 84-87.)

---

* Depths at which the horizontal cone penetrations were conducted in tests in references 13 and 14 ranged from 7.6 to 61 cm.

e. For the range of values used, the "state of packing." i.e. sand unit dry weight, affected F_x more than any other variable studied. In the WES tests, both cone size (area) and state of packing (G) had great influence on F_x for the low-speed condition--see plate 18, for example. For velocity values up to 5.2 m/sec, F_x was strongly influenced by cone size (expressed in terms of A_x and d_x), state of packing (G), and cone depth (h)--see paragraphs 84-87.

Plane cutting blades operating near the surface in sand

90. The primary object of the study described in reference 12* was to develop equations capable of predicting the force response of air-dry sand of three unit weights to plane cutting blades of various sizes, inclination angles, and depths of cut over a range of penetration velocities. Values of sand penetration resistance gradient G and unit dry weight γ_d of the test sand were:

	Low	Medium	High
G , MN/m^3	1.44	3.23	5.97
γ_d , kN/m^3	15.7	16.3	16.7

91. A schematic of the cutting blade is shown in fig. 13. The blade variables considered in this study were:

b , blade width, cm

ℓ , blade length, cm

z , blade operating depth,** cm

α , blade angle, radians

V_x , operating velocity, cm/sec

Test values of b ranged from 2.54 to 25.4 cm, of ℓ from 11.7 to 39.2 cm, of z from 2 to 34 cm, and of $z/(\ell \sin \alpha)$† from 0.25 to 2.0. Each of 10 plane blades was tested at α = 30, 45, 60, 90, and 105 deg,

* The authors of reference 12 have also conducted a similar study using clay as the test soil (reference 15).

** z is the vertical distance from the bottom of the blade to the original sand surface.

† $z/\ell \sin \alpha$ is the proportion of blade height in sand at the start of a given test. For a blade whose top edge is at the height of the original sand surface, $z/(\ell \sin \alpha) = 1$.

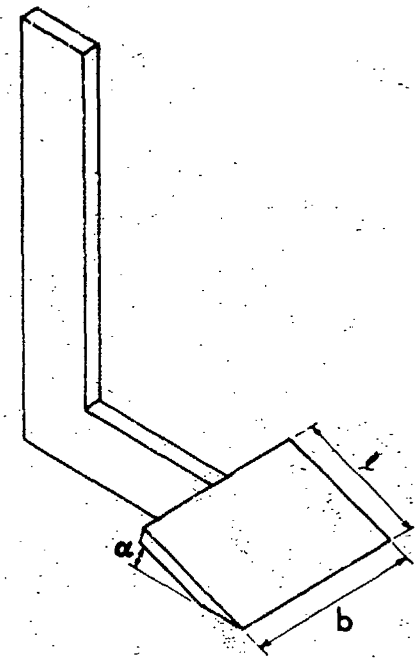

Fig. 13. Plane cutting blade
(from reference 12)

and values of V_x ranged from 25 to 255 cm/sec. The only sand variable that appeared ultimately in the prediction equations was γ_d, unit dry weight. Test response was measured by f_x, horizontal component of blade reaction force, and f_z, vertical component of blade reaction force.

92. The nondimensional relations developed to predict f_x and f_z for the range of conditions tested were

$$\frac{f_x}{\gamma_d b z^{0.5} \ell^{1.5}} = \alpha^{1.73} \left(\frac{z}{\ell \sin \alpha}\right)^{0.770} \left[1.05 \left(\frac{z}{b}\right)^{1.10} + 1.26 \left(\frac{V_x^2}{g\ell}\right) + 3.91\right] \quad (14)$$

and

$$\frac{f_z}{\gamma_d b z^{0.5} \ell^{1.5}} = \left[1.93 - (\alpha - 0.714)^2\right] \left(\frac{z}{\ell \sin \alpha}\right)^{0.770}$$

$$\left[1.31\left(\frac{z}{b}\right)^{0.966} + 1.43\left(\frac{V_x^2}{g\ell}\right) + 5.60\right] \quad (15)$$

where g is acceleration due to gravity, 9.805 m/sec^2. Four independent (controlled) dimensionless terms--α, $z/(\ell \sin \alpha)$, z/b, and

$V_x^2/g\ell$--appear in the right side of equations 14 and 15. Fig. 14 presents some representative relations of these variables, in turn, to $f_x/\gamma_d bz^{0.5}\ell^{1.5}$ (figs. 14a-14d), and to $f_z/\gamma_d bz^{0.5}\ell^{1.5}$ (figs. 14e-14h). The relations described by equations 14 and 15 are quite complex, particularly those by equation 15, which shows both positive and negative values of $f_z/\gamma_d bd^{0.5}\ell^{1.5}$ (each of figs. 14e-14h), as well as a nonmonotonic influence on $f_z/\gamma_d bz^{0.5}\ell^{1.5}$ of variable α (fig. 14e). In each of figs. 14a-14h, the curves (which represent equations 14 and 15) trace the pattern of behavior of the test data reasonably well.

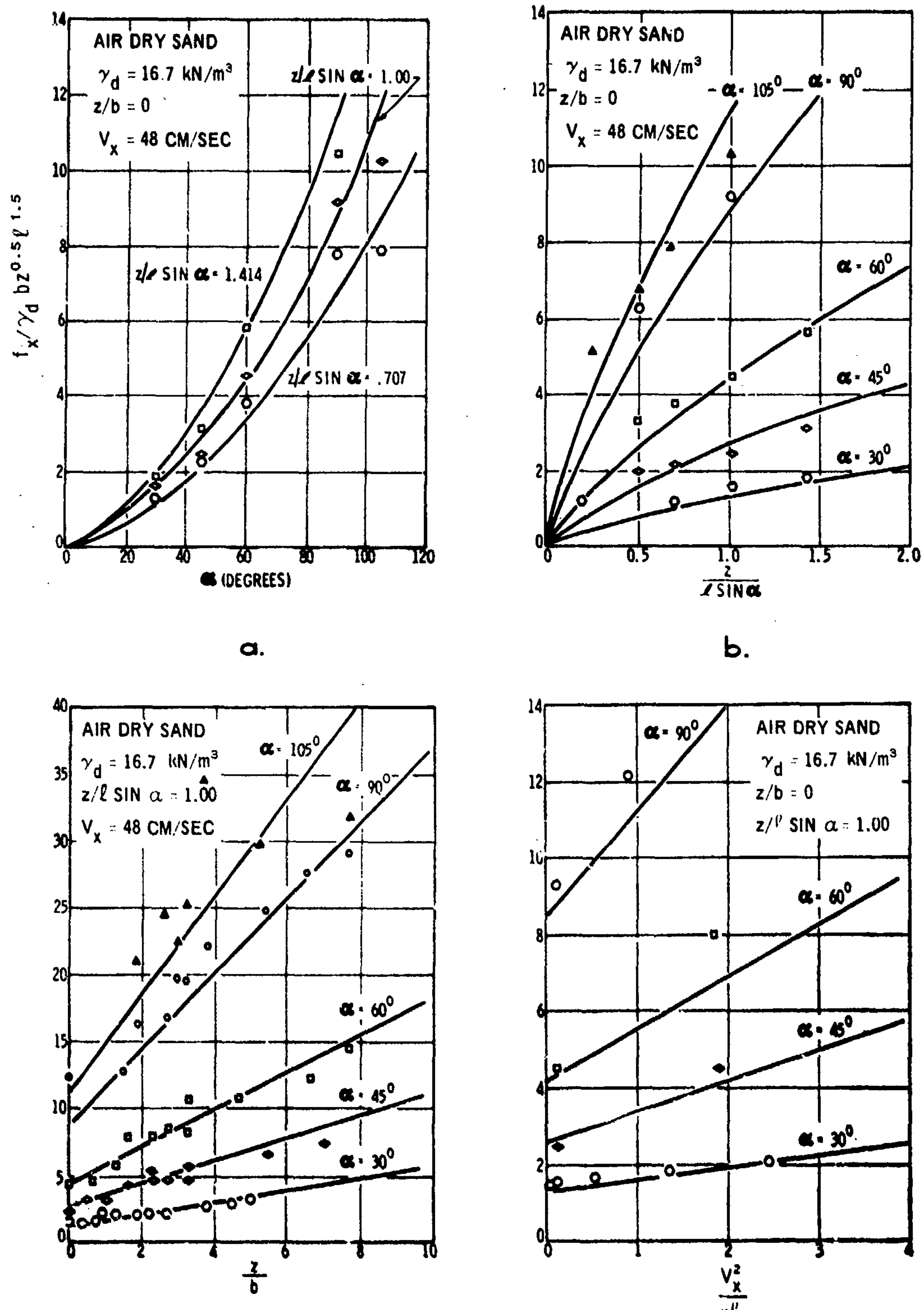

Fig. 14. Representative relations of $f_x/\gamma_d bz^{0.5}\ell^{1.5}$ and $f_z/\gamma_d bz^{0.5}\ell^{1.5}$ to γ , $z/\ell \sin \alpha$, z/b , and $V_x^2/g\ell$ (from reference 12) (sheet 1 of 2)

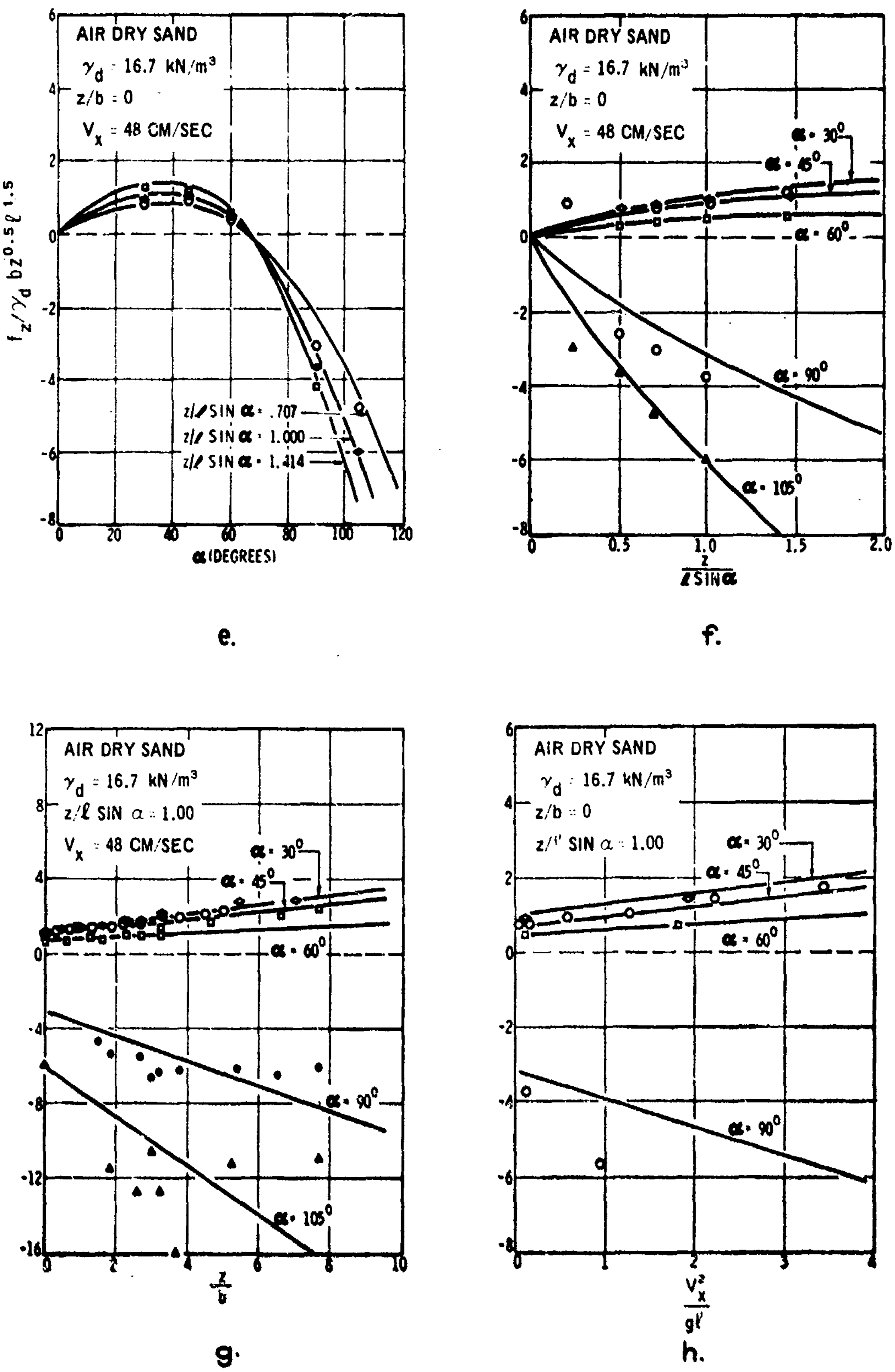

Fig. 14. (sheet 2 of 2)

PART V: CONCLUSIONS AND RECOMMENDATIONS

Conclusions

93. The foregoing analysis is considered adequate basis for the following conclusions:

- a. For a given cone or flat plate tested vertically in air-dry sand of given strength, the curve of sand penetration resistance force per unit probe base area F_z/A_x versus probe base depth departs from near linearity as velocity V_z increases. Values of F_z/A_x at shallow depths increase with increases in V_z, but F_z/A_x approaches a common value at substantial depth (say, 15 cm) for V_z values in the 3- to 600-cm/sec range (plates 1 and 2 and paragraphs 25-27).

- b. Penetration resistance gradient G_x for any of a broad range of cone sizes and plate sizes and shapes can be estimated if values are known for the gradient obtained under "standard" conditions with the 3.23-cm^2 cone at 3.05 cm/sec (G) and the probe base area A_x, for V_z = 3.05 cm/sec (equation 2 and paragraphs 31-35). Because of the factors cited in a above, G_x should be estimated by equation 2 only for V_z near 3 cm/sec.

- c. Values of F_z at probe base penetration depths of 2.5 and 0 cm for flat plates and cones, respectively, can be estimated from relations of dimensionless terms that describe F_z as a function of sand strength and probe size, shape, and velocity normalized relative to conditions of a standard cone penetration (paragraphs 36-53 and plates 7-9 for plates, 10 and 11 for cones). Data used in the development of these relations included values of G from 1.08 to 6.91 MN/m^3; A_x from 1.29 to 58.1 cm^2; one cone shape and five flat plate shapes; and V_z values from 3 to well over 600 cm/sec.

- d. Values of G increase markedly with increases in sand unit dry weight and/or moisture content (plates 12-14 and paragraphs 63-66).

- e. For a given probe tested horizontally in sand, force F_x on the probe base depends on probe size, shape, and velocity; depth of the probe relative to the undisturbed sand surface; and sand strength. A description of such a system, obtained by using dimensional analysis and data from cone penetration tests in air-dry sand, allows F_x for cones to be estimated from relations of dimensionless terms that include descriptions of the variables mentioned above (plates 15-17 and paragraphs 76-87).

f. A brief review of major findings from two studies[13,14] of horizontal cone penetration tests shows that these findings agree with and complement results of the WES tests (from e above). Some major conclusions from these studies are: Increase in F_x changes from a squared function of depth for small depths to a linear function for large depths; F_x increases with cone base area; cone apex angle and surface roughness influence F_x only slightly; F_x changes with velocity in complex patterns influenced by probe size, probe depth, and the sand's state of packing (paragraphs 88-89).

g. A brief summary of results from another study[12] shows that the horizontal and vertical components (f_x and f_z, respectively) of forces on plane blades operating horizontally near the sand surface can be estimated by equations that incorporate functions of the variables mentioned in e above (paragraphs 90-92).

Recommendations

94. It is recommended that:

a. Model tests of plane blades and bulldozer blades be conducted in another type sand than that used in developing equations 14 and 15 to determine what modifications should be made to these equations to account for the effects on f_x and f_z of sand type (plane blade performance) and of bulldozer blade curvature.

b. A study like that in a above be conducted in clay to verify the relations from reference 15 and to extrapolate them to bulldozer blade performance.

c. Free-fall or impact-driven vertical penetration tests be conducted with cones in dry-to-moist sand to complement similar studies conducted by WES in fine-grained soils (references 1-4).

d. Laboratory tests of wheels and tracks be conducted in moist-to-wet sands to improve present knowledge of how G at different moisture content levels is related to vehicle running gear performance.

e. A study be made to apply the descriptions presented herein of the influence of probe shape and velocity on sand penetration resistance force to the sand-vehicle running gear situation.

LITERATURE CITED

1. Knight, S. J., "Studies of Aerial Cone Penetrometer; Laboratory Study of Mechanical Principles," Technical Report No. 3-462, Report 1, Jul 1957, U. S. Army Engineer Waterways Experiment Station, CE, Vicksburg, Miss.

2. _________, "Studies of Aerial Cone Penetrometer; Field Tests," Technical Report No. 3-462, Report 2, Apr 1958, U. S. Army Engineer Waterways Experiment Station, CE, Vicksburg, Miss.

3. Blackmon, C. A., Knight, S. J., and Rone, C. L., "Studies of Aerial Cone Penetrometer; Field Tests in Fine-Grained Soils, 1960," Technical Report No. 3-462, Report 3, Aug 1963, U. S. Army Engineer Waterways Experiment Station, CE, Vicksburg, Miss.

4. Kennedy, J. G., "Studies of Aerial Cone Penetrometer; Impact Velocity - Impact Force Investigation, 1968," Technical Report No. 3-462, Report 4, Jun 1970, U. S. Army Engineer Waterways Experiment Station, CE, Vicksburg, Miss.

5. Turnage, G. W., "Measuring Soil Properties in Vehicle Mobility Research; Effects of Velocity, Size, and Shape of Probes on Penetration Resistance of Fine-Grained Soils," Technical Report No. 3-652, Report 3, Nov 1970, U. S. Army Engineer Waterways Experiment Station, CE, Vicksburg, Miss.

6. _________, "Measuring Soil Properties in Vehicle Mobility Research; Resistance of Fine-Grained Soils to High-Speed Penetration," Technical Report No. 3-652, Report 5, Jun 1973, U. S. Army Engineer Waterways Experiment Station, CE, Vicksburg, Miss.

7. Melzer, K.-J., "Measuring Soil Properties in Vehicle Mobility Research; Relative Density and Cone Penetration Resistance," Technical Report No. 3-652, Report 4, Jul 1971, U. S. Army Engineer Waterways Experiment Station, CE, Vicksburg, Miss.

8. _________, "Penetrometer Investigations in Sand," Dissertation, 1968 (in German). Technical University of Aachen, Aachen, West Germany.

9. Van Wazer, J. R., et al., "Viscosity and Flow Measurement; A Laboratory Handbook of Rheology," Interscience Publishers, New York, 1963, pp 12-19.

10. Sela, A. D. and Ehrlich, I. R., "Load Support Capability of Flat Plates of Various Shapes in Soils," Journal of Terramechanics, Vol 8, No. 3, 1972, pp 39-69.

11. Turnage, G. W., "Performance of Soils Under Tire Loads; Application of Test Results to Tire Selection for Off-Road Vehicles," Technical Report No. 3-666, Report 8, Sep 1972, U. S. Army Engineer Waterways Experiment Station, CE, Vicksburg, Miss.

12. Luth, H. J. and Wismer, R. D., "Performance of Plane Soil Cutting Blades in Sand," Transactions of the ASAE, Vol 14, No. 2, Mar-Apr 1971, pp 255-259 and 262.

13. Saperstein, L. W. and Franklin, R. N., "An Investigation into the Forces on Bodies Dragged Through Sand," Journal of Terramechanics, Vol 8, No. 2, 1971, pp 29-37.

14. Wilson, J. and Franklin, R. N., "Further Measurements of Drag on Bodies Moving Through Sand," Journal of Terramechanics, Vol 8, No. 2, 1971, pp 39-48.

15. Wismer, R. D. and Luth, H. J., "Performance of Plane Soil Cutting Blades in Clay," Paper No. 70-120, 1970, American Society of Agricultural Engineers, St. Joseph, Mich.

Table 1

Vertical Penetration Tests with Cones in Bins of Yuma Sand

(1) Test No.	(2) Cone Base Area A_x cm^2	(3) Standard Penetration Resistance Gradient G MN/m^3	(4) Sand Unit Dry Weight γ_d kN/m^3	(5) Sand Dry Mass Density ρ $kN\text{-}sec^2/m^4$	(6) Penetration Resistance Gradient G_x* MN/m^3	(7) Penetration Velocity $(V_z)_x$ cm/sec	(8) Velocity Gradient $(V_z/t)_x$ sec^{-1}	(9) Velocity Gradient Ratio $(V_z/t)_{xs}$	(10) Cone Base Pressure $(F_z/A)_x$ kPa	(11) Standard Cone Base Pressure $(F_z/A)_s$ kPa	(12) Cone Stress Ratio $(F_z/A^{1.3})_{xs}$	(13) Inertial Force $\rho(AV_z^2)_x/2$ N	(14) Computed Viscous-Type Force for $(V_z/t)_{xs} < 2.3$** N	(15) Computed Viscous-Type Force for $(V_z/t)_{xs} \geq 2.3$† N	(16) Modified Drag Coefficient C_D††	(17) Modified Reynolds Number N_R‡	(18) Cone Base Pressure (See note 1) $(F_z/A)_x$ kPa	(19) Penetration Velocity (See note 1) $(V_z)_x$ cm/sec
21-169-3-1	1.79	1.35	14.74	1.503	1.18	3.05	2.68	1.58	11.2	16.1	0.917	0.0000902	1.58	--	16,000	0.0000571	218	3.05
19-167-3-1		3.50	15.98	1.630	4.50	3.05	2.68	1.58	34.6	41.8	1.09	0.0000978	4.10	--	45,600	0.0000239	710	3.05
17-124-1-1		6.91	16.87	1.720	6.73	3.05	2.68	1.58	51.0	82.5	0.815	0.000103	8.08	--	63,900	0.0000127	1360	3.05
23-191-2-1	3.23	1.40	14.79	1.508	1.40	3.05	1.70	1.00	16.7	16.7	1.00	0.000227	5.39	--	23,800	0.0000421	227	3.05
23-192-2-2		1.40	14.79	1.508	1.44	36.3	20.2	11.9	36.2	16.7	2.17	0.0321	--	12.1	364	0.00266	252	36.3
10-75-2-1		2.48	15.53	1.584	2.48	8.05	1.70	1.00	29.6	29.6	1.00	0.000238	9.56	--	40,200	0.0000249	402	3.05
10-84-2-2		2.48	15.53	1.584	2.44	24.2	13.5	7.93	55.5	29.6	1.88	0.0150	--	17.5	1,200	0.000956	422	24.2
10-83-2-3		2.48	15.53	1.584	1.68	105	58.4	34.4	126	29.6	4.26	0.282	--	36.5	144	0.00773	378	105
10-80-2-4		2.48	15.53	1.584	--	277	154	90.8	205	29.6	6.93	1.96	--	59.0	33.7	0.0332	395	215
10-79-2-5		2.48	15.53	1.584	--	404	225	132	245	29.6	8.28	4.17	--	71.4	19.0	0.0584	380	286
10-76-2-6		2.48	15.53	1.584	--	698	388	229	407	29.6	13.8	12.5	--	94.0	10.5	0.133	443	572
17-129-2-1		6.91	16.87	1.720	6.91	3.05	1.70	1.00	82.5	82.5	1.00	0.000258	26.6	--	103,000	0.00000970	1170	3.05
29-230-2-2		6.06	16.70	1.703	5.66	37.8	21.0	12.4	129	72.3	1.78	0.0394	--	53.3	1,060	0.000739	978	37.8
30-241-2-3		6.15	16.72	1.705	5.07	114	63.4	37.4	318	73.4	4.33	0.359	--	94.5	286	0.00380	1079	114
31-254-2-4		6.30	16.75	1.708	--	209	116	68.5	425	75.2	5.65	1.20	--	130	114	0.00921	1042	213
32-263-2-5		6.00	16.68	1.702	--	389	216	128	435	71.6	6.08	4.17	--	170	33.7	0.0245	1125	303
33-274-2-6		5.63	16.55	1.688	--	669	372	219	774	64.8	11.9	12.2	--	201	20.5	0.0607	1180	570
21-176-3-1	12.9	1.35	14.74	1.503	1.26	3.05	0.849	0.500	22.0	16.1	0.904	0.000901	31.5	--	31,500	0.0000286	211	3.05
23-196-3-2		1.40	14.79	1.508	0.99	39.8	11.1	6.53	33.3	16.7	1.31	0.154	--	54.4	280	0.00283	182	39.8
27-222-3-6		1.16	14.54	1.483	--	694	193	114	149	13.8	7.12	46.1	--	187	4.17	0.247	202	618

(Continued)

* G_x values are listed in column 6 only for those tests that (a) had velocity $(V_z)_x$ values in the 0 - to 15-cm depth range at least 90 percent of which differed from their average value by no more than ± 10 percent, and (b) had a coefficient of correlation of at least 0.90 for the least-squares linear relation between $(F_z/A)_x$ and cone base depth in the 0- to 15-cm depth range.

** $(F_z/A^{1.3})_s \cdot A_x^{1.3}$

† $(F_z/A^{1.3})_s \cdot A_x^{1.3} \cdot 0.65\ (V_z/t)_{xs}^{0.50}$

†† $(F_z)_x : \rho(AV_z^2)_x/2$

‡ $\rho(AV_z^2)_x/2 : \left[(F_z/A^{1.3})_s \cdot A_x^{1.3}\right]$ or $\rho(AV_z^2)_x/2 : \left[(F_z/A^{1.3})_s \cdot A_x^{1.3} \cdot 0.65\ (V_z/t)_{xs}^{0.50}\right]$, i.e. column (13) : column (14) or column (13) : column (15).

NOTES:

1. Variables in columns 7-10 and 12-17 describe the condition of a given test cone at base depth = 0 ; those in columns 18 and 19 at base depth = 15 cm
2. In columns 7 and 19, the values listed for $(V_z)_x$ are (a) the average velocity in the 0- to 15-cm range of cone base depths for a given test that has a listed value of G_x, or (b) the values of velocity that prevailed at the 0- and the 15-cm base depths, respectively, for a test without a listed value of G_x.

(Sheet 1 of 2)

Table 1 (Concluded)

(1) Test No.	(2) Cone Face Area A_s cm^2	(3) Standard Penetration Resistance Gradient G MN/m^3	(4) Sand Unit Dry Weight γ_d kN/m^3	(5) Sand Dry Mass Density ρ $kN\text{-}sec^2/m^4$	(6) Penetration Resistance Gradient G_x* MN/m^3	(7) Penetration Velocity $(V_z)_x$ cm/sec	(8) Velocity Gradient $(V_z/\ell)_x$ sec^{-1}	(9) Velocity Gradient Ratio $(V_z/\ell)_{xs}$	(10) Cone Base Pressure $(F_z/A)_x$ kPa	(11) Standard Cone Base Pressure $(F_z/A)_s$ kPa	(12) Cone Stress Ratio $(F_z/A^{1.3})_{xs}$	(13) Inertial Force $\rho(AV_z^2)_x/2$ N	(14) Computed Viscous-Type Force for $(V_z/\ell)_{xs}<2.3$** N	(15) Computed Viscous-Type Force for $(V_z/\ell)_{xs}\geq 2.3$ N	(16) Modified Drag Coefficient C_D'	(17) Modified Reynolds Number N_R‡	(18) Cone Base Pressure (See note 1) $(F_z/A)_x$ kPa	(19) Penetration Velocity (See note 1) $(V_z)_x$ cm/sec
19-154-3-1	12.9	3.50	15.98	1.630	2.55	3.05	0.949	0.500	58.8	41.8	0.930	0.000978	81.7	--	77,600	0.0000120	446	3.05
4-24-3-2		2.55	15.57	1.588	2.35	24.2	6.74	1.97	59.8	30.4	1.30	0.0600	--	76.9	1,290	0.000780	412	24.2
4-29-3-3		2.55	15.57	1.588	1.37	101	28.1	16.6	171	30.4	3.71	1.04	--	157	211	0.00663	377	101
3-39-3-4		2.91	15.74	1.605	1.43	227	63.2	37.3	210	34.7	3.99	5.34	--	270	50.7	0.0198	425	227
5-60-3-5		2.93	15.74	1.605	1.38	282	78.5	46.3	267	34.7	5.07	8.23	--	299	41.8	0.0275	474	282
6-50-3-6		2.35	15.46	1.577	--	686	192	113	359	18.1	8.44	48.1	--	379	9.62	0.127	506	547
17-132-3-1		6.91	16.87	1.720	4.61	3.05	0.849	0.500	138	82.5	1.10	0.00103	161	--	173,000	0.00000640	830	3.05
29-234-3-2		6.06	16.70	1.703	3.29	37.0	10.3	6.07	219	72.3	1.99	0.151	--	226	1,860	0.000669	712	37.0
30-247-3-3		6.15	16.72	1.705	3.07	113	31.5	18.5	402	73.4	3.61	1.41	--	403	369	0.00350	862	113
31-256-3-4		6.30	16.75	1.708	3.78	208	57.9	34.1	380	75.2	3.33	4.76	--	557	103	0.00854	947	208
21-179-4-1	25.8	1.35	14.74	1.503	1.16	3.05	0.600	0.354	25.0	16.1	0.831	0.00180	77.5	--	35,800	0.0000232	199	3.05
23-201-4-2		1.40	14.79	1.508	0.83	39.2	7.72	4.55	41.5	16.7	1.33	0.299	--	111	358	0.00269	166	39.2
24-206-4-3		1.28	14.67	1.496	0.95	112	22.0	13.0	54.9	15.3	1.92	2.42	--	173	58.4	0.0140	198	112
26-218-4-5		1.25	14.64	1.493	--	309	60.8	35.9	88.8	14.9	3.19	19.4	--	279	12.6	0.0660	211	268
[illegible]-157-4-1		3.50	15.98	1.630	2.25	3.05	0.600	0.354	78.8	41.8	1.01	0.00196	201	--	184,000	0.00000975	431	3.05
1-1-4-2		2.64	15.41	1.592	1.69	29.5	5.81	3.42	89.5	31.5	1.52	0.179	--	182	1,297	0.000982	343	29.5
2-7-4-3		2.92	15.75	1.606	1.38	105	20.7	12.2	202	34.9	3.10	2.28	--	381	228	0.00598	409	105
2-12-4-4		2.92	15.75	1.606	1.32	205	40.4	23.8	244	34.9	3.75	8.69	--	530	72.4	0.0164	442	205
3-18-4-6		2.42	15.50	1.581	--	414	121	71.5	374	28.9	6.00	77.4	--	766	10.8	0.101	432	541
17-135-4-1		6.91	16.87	1.720	1.61	3.05	0.600	0.354	147	92.5	0.954	0.00206	397	--	184,000	0.00000519	689	3.05
14-10[illegible]-4-2		4.48	16.78	1.711	3.21	35.0	6.80	4.06	231	77.4	1.60	0.271	--	487	2,200	0.000556	713	35.0
15-111-4-3		4.08	16.7	1.703	2.67	106	20.9	12.3	386	72.6	2.85	2.47	--	797	403	0.00310	787	106
[illegible]-112-4-4		4.08	16.70	1.703	--	197	38.8	22.9	426	72.6	3.15	8.51	--	1090	129	0.00784	715	167
16-115-4-5		5.75	16.63	1.696	--	327	64.4	38.0	531	69.6	4.15	23.4	--	1320	58.5	0.0177	762	272
14-124-4-6		5.75	16.63	[illegible]	--	614	121	71.3	665	68.6	5.19	92.6	--	1810	20.8	0.0456	671	556
22-[illegible]5-5-1	58.1	1.27	14.66	1.495	1.38	3.05	0.600	0.236	36.4	15.2	1.00	0.00404	210	--	52,300	0.0000192	243	3.05
11-5[illegible]-5-2		1.27	14.66	1.495	0.96	26.9	3.53	2.08	38.2	15.2	1.05	0.314	210	--	706	0.00150	182	26.9
12-60-5-3		1.17	14.55	1.484	0.92	101	13.3	7.81	46.9	14.0	1.41	4.40	--	352	62.0	0.0125	185	101
13-95-5-4		1.08	14.45	1.474	0.89	196	25.7	15.2	56.7	12.9	1.84	16.4	--	451	20.0	0.0364	190	196
[illegible]-1[illegible]5-5-1		3.27	15.89	1.621	2.31	3.05	0.400	0.236	[illegible]	39.0	0.934	0.00428	539	--	115,000	0.00000813	433	3.05
2-54-5-2		2.26	15.41	1.572	1.93	30.0	3.94	2.32	73.5	27.0	1.14	[illegible]	--	369	1,040	0.00111	363	30.0
7-63-5-3		2.26	15.41	1.572	[illegible]	98.2	12.9	7.60	125	27.0	1.95	4.40	--	668	165	0.00659	317	98.2
8-67-5-4		2.65	15.71	1.603	1.72	191	25.1	14.8	175	34.0	2.16	17.0	--	1170	59.9	0.0145	433	191
9-68-5-5		2.76	15.47	1.598	--	266	34.9	20.6	206	37.9	2.63	32.8	--	1340	36.5	0.0245	375	237
14-144-5-1		6.30	16.75	1.709	3.49	3.05	0.400	0.236	179	75.2	1.00	0.00461	1040		224,000	0.00000443	702	3.05
29-250-5-2		6.06	16.70	1.703	2.65	38.2	5.01	2.96	227	72.3	1.32	0.720	--	11[illegible]	1,830	0.000646	625	38.2
3-253-5-3		6.15	16.72	1.705	2.84	110	14.4	8.51	353	73.4	2.02	5.98	--	1[illegible]	343	0.00311	779	110
31-262-5-4		6.30	16.75	1.708	--	210	27.6	16.2	402	75.2	2.25	21.9	--	27[illegible]	107	0.00806	682	192
32-273-5-5		6.00	16.68	1.702	--	263	34.5	20.3	455	71.6	2.67	34.2	--	2900	77.2	0.0118	717	241
33-286-5-6		5.43	16.55	1.688	--	529	69.4	40.9	633	64.8	4.11	137	--	3720	26.8	0.0368	753	501

(Sheet 2 of 2)

Table 2

Vertical Penetration Tests with Plates in Bins of Yuma Sand

(1) Test No.	(2) Plate Base Area A_x cm^2	(3) Standard Penetration Resistance Gradient G MN/m^3	(4) Sand Unit Dry Weight γ_d kN/m^3	(5) Sand Dry Mass Density ρ $kN\text{-}sec^2/m^4$	(6) Penetration Resistance Gradient G_x* MN/m^3	(7) Penetration Velocity $(V_z)_x$ cm/sec	(8) Velocity Gradient $(V_z/l)_x$ sec^{-1}	(9) Velocity Gradient Ratio $(V_z/l)_{xs}$	(10) Plate Base Pressure $(F_z/A)_x$ kPa	(11) Standard Cone Base Pressure $(F_z/A)_s$ kPa	(12) Plate-Cone Stress Ratio**	(13) Inertial Force $\rho(AV_z^2)_x/2$ N	(14) Computed Viscous-Type Force† N	(15) Modified Drag Coefficient C_D††	(16) Modified Reynolds Number N_R‡	(17) Plate Base Pressure (See note 1) $(F_z/A)_x$ kPa	(18) Penetration Velocity (See note 1) $(V_z)_x$ cm/sec
Flat Circular Plates																	
21-170-6-1	1.29	1.35	14.74	1.503	1.23	3.05	2.68	1.58	38.7	16.1	2.85	0.0000902	4.65	54,600	0.0000194	192	3.05
19-148-6-1		3.50	15.98	1.630	4.45	3.05	2.68	1.58	118	41.8	3.39	0.0000978	12.1	156,000	0.00000811	699	3.05
17-126-6-1		6.91	16.87	1.720	10.01	3.05	2.68	1.58	159	82.5	2.31	0.000103	23.8	198,000	0.00000432	1660	3.05
21-173-7-1	3.23	1.35	14.74	1.503	1.27	3.05	1.70	1.00	41.8	16.1	2.60	0.000226	12.5	59,800	0.0000161	201	3.05
23-193-7-2		1.40	14.79	1.508	1.04	38.8	21.6	12.7	81.7	16.7	4.89	0.0368	24.4	717	0.00151	212	38.8
26-202-7-3		1.28	14.67	1.496	—	134	74.6	43.9	85.4	15.3	5.58	0.425	30.5	64.8	0.0139	223	111
19-151-7-1		3.50	15.98	1.630	3.40	3.05	1.70	1.00	119	41.8	2.85	0.000245	32.3	156,000	0.00000758	569	3.05
10-85-7-2		2.48	15.53	1.584	2.36	25.4	14.1	8.32	138	29.6	4.66	0.0165	39.1	2,700	0.000422	433	25.4
10-82-7-3		2.48	15.53	1.584	1.88	106	59.0	37.9	207	29.6	6.99	0.287	56.7	233	0.00506	442	106
10-81-7-4		2.48	15.53	1.584	--	272	151	89.2	251	29.6	8.48	1.89	70.3	47.8	0.0269	453	216
10-78-7-5		2.48	15.53	1.584	--	423	235	139	336	29.6	11.4	4.59	78.9	23.7	0.0582	410	347
10-77-7-6		2.48	15.53	1.584	--	652	363	214	536	29.6	18.1	10.9	87.9	15.9	0.124	445	583
17-129-7-1		6.91	16.87	1.720	7.14	3.05	1.70	1.00	177	82.5	2.15	0.000258	6.39	22,100	0.0000404	1070	3.05
30-242-7-3		6.15	16.72	1.705	6.05	111	61.8	36.4	364	73.4	4.96	0.339	140	347	0.00242	1120	111
31-255-7-4		6.30	16.75	1.708	--	299	166	98.0	596	75.2	7.92	2.46	184	78.1	0.0134	1090	231
32-264-7-5		6.00	16.68	1.702	--	446	248	146	605	71.6	8.45	5.46	193	35.8	0.0283	1390	364
33-275-7-6		5.43	16.55	1.688	--	715	398	234	886	64.8	13.6	13.9	196	20.6	0.0709	1050	630
21-177-8-1	12.9	1.35	14.74	1.503	1.27	3.05	0.849	0.501	47.5	16.1	2.23	0.000902	55.3	68,000	0.0000163	238	3.05
23-195-8-2		1.40	14.79	1.508	1.06	40.0	11.1	6.57	104	16.7	4.73	0.156	109	860	0.00143	237	40.0
26-205-8-3		1.28	14.67	1.496	1.12	116	32.3	19.0	88.2	15.3	4.36	1.30	130	87.5	0.0100	228	116
25-212-8-4		1.48	14.86	1.516	--	207	57.6	34.0	147	17.7	6.30	4.19	174	45.2	0.0241	254	221
27-221-8-6		1.16	14.54	1.483	—	691	192	113	264	13.8	14.5	45.7	139	7.46	0.328	231	537

(Continued)

* G_x values are listed in column 6 only for those tests that (a) had velocity $(V_z)_x$ values in the 0- to 15-cm depth range at least 90 percent of which differed from their average value by no more than ±10 percent, and (b) had a coefficient of correlation of at least 0.90 for the least-squares linear relation between $(V_z/A)_x$ and plate base depth in the 2.5- to 15-cm depth range.

** $(F_z/A^{1.2})_{xs} \cdot (R_h^{0.4})_{cx}$ For circular-base-area plates, $(R_h^{0.4})_{cx} = 1$ and the plate-cone stress ratio is $(F_z/A^{1.2})_{xs}$.

† $(F_z/A^{1.2})_s \cdot A_x^{1.2} \cdot (R_h^{0.4})_{xc} \cdot 2.4\ (V_z/l)_{xs}^{0.25}$

†† $(F_z)_x : \rho(AV_z^2)_x/2$

‡ $\left[\rho(AV_z^2)_x/2\right] : \left[(F_z/A^{1.2})_s \cdot A_x^{1.2} \cdot (R_h^{0.4})_{xc} \cdot 2.4\ (V_z/l)_{xs}^{0.25}\right]$, i.e. column (13) column (14)

NOTES:

1. Variables in columns 7-10 and 12-16 describe the condition of a given test plate at base depth = 2.5 cm; those in columns 17 and 18 at base depth = 15 cm.
2. In columns 7 and 18, the values listed for $(V_z)_x$ are (a) the average velocity in the 0- to 15-cm range of plate base depths for a given test that has a listed value of G_x , or (b) the values of velocity that prevailed at the 2.5-cm and the 15-cm plate base depths, respectively, for a test without a listed value of G_x .

Table 2 (Continued)

(1) Test No.	(2) Plate Base Area A_x cm^2	(3) Standard Penetration Resistance Gradient G MN/m^3	(4) Sand Unit Dry Weight γ_d kN/m^3	(5) Sand Dry Mass Density ρ $kN\text{-}sec^2/m^4$	(6) Penetration Resistance Gradient G_x MN/m^3	(7) Penetration Velocity $(V_z)_x$ cm/sec	(8) Velocity Gradient $(V_z/t)_x$ sec^{-1}	(9) Velocity Gradient Ratio $(V_z/t)_{xs}$	(10) Plate Base Pressure $(F_z/A)_x$ kPa	(11) Standard Cone Base Pressure $(F_z/A)_s$ kPa	(12) Plate-Cone Stress Ratio**	(13) Inertial Force $\rho(AV_z^2)_x/2$ N	(14) Computed Viscous-Type Force N	(15) Modified Drag Coefficient C_D**	(16) Modified Reynolds Number N_R*	(17) Plate Base Pressure (See note 1) $(F_z/A)_x$ kPa	(18) Penetration Velocity (See note 1) $(V_z)_x$ cm/sec
Flat Circular Plates (Continued)																	
19-155-8-1	[illegible]	3.50	15.98	1.630	2.58	3.05	0.849	[illegible]	132	41.8	2.39	0.000978	143	174,000	0.00000683	454	3.05
4-27-8-2		2.55	15.57	1.588	1.47	26.4	7.35	4.33	173	30.4	4.31	0.0712	180	3,130	0.000397	356	26.4
4-30-8-3		2.55	15.57	1.588	1.04	104	29.0	17.1	246	30.4	6.13	1.11	254	286	0.00438	376	104
5-38-8-4		2.91	15.74	1.605	--	213	59.3	35.0	258	34.7	5.64	4.70	346	70.9	0.0136	450	194
5-41-8-5		2.91	15.74	1.605	--	409	114	67.1	343	34.7	7.48	17.3	405	25.6	0.0427	516	325
6-49-8-6		2.35	15.46	1.577	--	667	196	109	456	28.1	12.3	45.3	371	13.0	0.122	457	573
17-133-8-1		6.41	16.87	1.720	4.16	3.05	0.849	0.501	185	82.5	1.70	0.00103	283	23,100	0.00000364	705	3.05
29-213-8-2		6.06	16.70	1.703	3.03	37.6	10.5	6.17	307	72.3	3.22	0.155	467	2,550	0.000332	696	37.6
30-246-8-3		6.15	16.72	1.705	--	114	37.3	22.0	490	73.4	5.06	1.97	570	321	0.00346	850	113
33-280-8-4		5.63	16.55	1.688	--	714	199	117	1031	64.8	12.0	55.5	871	24.0	0.0637	840	582
21-180-9-1	25.8	1.35	14.74	1.503	1.27	3.05	0.601	0.354	47.9	16.1	1.97	0.00180	116	68,500	0.0000155	207	3.05
19-158-9-1		3.50	15.98	1.630	2.48	3.05	0.601	0.354	104	41.8	1.64	0.00196	302	137,000	0.00000648	364	3.05
1-2-9-2		2.64	15.61	1.592	1.37	33.1	6.52	3.84	178	31.5	3.73	0.225	413	2,040	0.000545	349	33.1
2-6-9-3		2.92	15.75	1.606	1.03	105	20.7	12.2	242	34.9	4.57	2.28	611	273	0.00373	371	105
3-15-9-5		2.62	15.50	1.581	--	407	80.1	47.2	327	28.9	7.45	33.8	710	25.0	0.0476	418	268
3-14-9-6		2.62	15.50	1.581	--	535	105	62.1	467	29.9	10.7	58.3	761	20.7	0.0766	393	524
17-136-9-1		6.91	16.87	1.720	3.63	3.05	0.600	0.354	189	82.5	1.51	0.00206	59.5	236,000	0.00000346	643	3.05
14-102-9-2		6.48	16.78	1.712	2.11	36.4	7.17	4.22	410	77.4	3.50	0.292	1040	3,630	0.000281	674	36.4
15-115-9-3		6.08	16.70	1.703	--	133	26.2	15.4	531	72.6	4.83	3.89	1260	352	0.00309	803	105
16-116-9-5		5.75	16.63	1.696	--	415	81.7	48.2	642	68.6	6.33	37.7	1700	44.0	0.0222	882	268
16-123-9-6		5.75	16.63	1.696	--	702	138	81.5	1036	68.6	9.96	108	1940	24.8	0.0557	690	584
22-186-10-1	56.1	1.27	14.46	1.495	1.47	3.05	0.400	0.236	48.6	15.2	1.79	0.00404	264	69,900	0.0000153	232	3.05
11-87-10-2		1.27	16.66	1.495	1.41	31.0	4.07	2.40	71.3	15.2	2.63	0.417	470	993	0.000888	248	31.0
12-91-10-3		1.17	14.55	1.484	1.28	112	14.7	8.70	79.5	14.0	3.19	5.41	598	85.3	0.00905	240	112
13-96-10-4		1.08	14.45	1.474	--	261	34.2	20.2	134	12.9	5.83	29.2	681	26.7	0.0429	234	199
26-226-10-5		1.38	14.77	1.506	--	596	78.2	46.1	240	16.5	8.13	155	1070	8.99	0.145	282	539
20-164-10-1		3.27	15.89	1.621	2.18	3.05	0.400	0.236	121	39.0	1.74	0.00438	675	99,200	0.0000105	394	3.05
6-55-10-2		2.75	15.46	1.577	1.74	26.3	3.45	2.03	172	28.1	3.43	0.317	832	3,160	0.000381	390	26.3
7-58-10-3		2.26	15.41	1.572	1.81	104	13.6	8.05	220	27.0	4.57	4.94	1130	259	0.00436	446	104
8-66-10-4		2.85	15.71	1.603	--	262	34.4	20.3	326	34.0	5.38	32.0	[illegible]	59.3	0.0178	436	194
9-59-10-5		2.76	15.67	1.598	--	400	52.5	31.0	366	32.9	6.23	74.4	[illegible]	28.6	0.0386	424	[illegible]
9-76-10-6		2.76	15.67	1.598	--	561	73.6	43.4	553	32.9	9.42	146	[illegible]	22.0	0.0695	465	523
18-142-10-1		6.30	16.75	1.708	2.63	3.05	0.400	0.236	385	75.2	1.76	0.00461	1300	296,000	0.00000354	714	3.05
29-239-10-2		6.06	16.70	1.703	2.00	38.9	5.10	3.01	427	72.3	3.31	0.749	2360	3,310	0.000317	727	38.9
30-252-10-3		6.15	16.72	1.705	2.16	115	15.1	8.90	572	73.4	4.37	6.57	3160	506	0.00208	842	115
31-261-10-4		6.30	16.75	1.708	--	254	34.0	20.0	621	75.2	4.63	33.2	3940	108	0.00843	908	198
32-272-10-5		6.00	16.68	1.702	--	382	50.1	29.6	824	71.6	6.45	72.0	4140	66.5	0.0174	870	265
33-285-10-6		5.47	16.55	[illegible]	--	[illegible]	[illegible]	49.5	1032	64.8	8.92	201	4270	29.8	0.0471	893	531
Flat Rectangular (1:1) Plates																	
21-171-11-1	1.61	1.35	14.74	1.503	1.14	3.05	2.40	1.42	31.6	16.1	2.36	0.000113	5.65	45,200	0.0000200	174	3.05

(Continued)

56

Table 2 (Continued)

(1) Test No.	(2) Plate Base Area A_x cm^2	(3) Standard Penetration Resistance Gradient G MN/m^3	(4) Sand Unit Dry Weight γ_d kN/m^3	(5) Sand Dry Mass Density ρ $kN\text{-}sec^2/m^4$	(6) Penetration Resistance Gradient G_x^* MN/m^3	(7) Penetration Velocity $(V_z)_x$ cm/sec	(8) Velocity Gradient $(V_z/l)_x$ sec^{-1}	(9) Velocity Gradient Ratio $(V_z/l)_{xs}$	(10) Plate Base Pressure $(F_z/A)_x$ kPa	(11) Standard Cone Base Pressure $(F_z/A)_s$ kPa	(12) Plate-Cone Stress Ratio**	(13) Inertial Force $\rho(AV_z^2)_x/2$ N	(14) Computed Viscous-Type Force N	(15) Modified Drag Coefficient C_D	(16) Modified Reynolds Number N_R	(17) Plate Base Pressure (See note 1) $(F_z/A)_x$ kPa	(18) Penetration Velocity (See note 1) $(V_z)_x$ cm/sec
Flat Rectangular (1:1) Plates (Continued)																	
19-149-11-1	1.61	3.50	15.98	1.630	4.54	3.05	2.40	1.42	79.5	41.8	2.29	0.000122	14.6	105,000	0.00000835	647	3.05
17-127-11-1		6.91	16.87	1.720	9.36	3.05	2.40	1.42	173	82.5	2.52	0.000129	28.9	216,000	0.00000447	1340	3.05
21-174-12-1	6.45	1.35	14.74	1.503	1.32	3.05	1.20	0.708	54.9	16.1	3.12	0.000451	25.1	78,500	0.0000180	220	3.05
19-152-12-1		3.50	15.98	1.630	2.95	3.05	1.20	0.708	115	41.8	2.51	0.000489	65.2	152,000	0.00000750	484	3.05
4-25-12-2		2.55	15.57	1.588	2.06	25.8	10.2	5.99	141	30.4	4.24	0.0341	80.6	2,670	0.000423	399	25.8
4-32-12-3		2.55	15.57	1.588	1.82	105	41.3	24.4	231	30.4	6.94	0.564	114	264	0.00494	459	105
5-36-12-4		2.21	15.74	1.605	1.71	173	68.1	40.2	261	34.7	6.86	1.55	149	109	0.0104	475	173
5-43-12-5		2.41	15.74	1.605	--	432	170	100	313	34.7	8.24	9.68	186	20.9	0.0521	482	365
6-48-12-6		2.35	15.66	1.577	--	676	266	157	506	28.1	16.5	23.2	168	14.1	0.138	487	534
17-130-12-1		6.91	16.87	1.720	5.54	3.05	1.20	0.708	184	82.5	2.04	0.000516	128	230,000	0.00000402	877	3.05
29-232-12-2		6.04	16.70	1.703	4.37	38.7	15.2	8.98	238	77.3	3.00	0.0826	212	1,860	0.000389	784	38.7
30-245-12-3		6.15	16.72	1.705	--	166	65.4	38.5	532	73.4	6.62	1.52	310	226	0.00490	899	133
32-267-12-5		6.00	16.68	1.702	--	437	172	101	584	71.6	7.45	10.5	385	35.8	0.0273	1010	365
33-278-12-6		5.43	16.55	1.688	--	725	285	168	962	64.8	13.5	28.6	395	21.7	0.0724	1020	534
21-181-13-1	25.8	1.35	14.74	1.503	1.27	3.05	0.601	0.354	46.9	16.1	2.02	0.00180	110	67,100	0.0000163	206	3.05
23-200-13-2		1.40	14.79	1.508	1.11	39.6	7.80	4.60	77.4	16.7	3.20	0.304	219	6,560	0.00139	216	39.6
19-159-13-1		3.50	15.98	1.630	2.17	3.05	0.601	0.354	130	41.8	2.15	0.00196	290	172,000	0.00000677	401	3.05
1-3-13-2		2.64	15.61	1.592	1.83	32.5	6.40	3.77	189	31.5	4.16	0.217	392	2,250	0.000553	418	32.5
2-9-13-3		2.92	15.75	1.606	--	109	21.5	12.7	268	34.9	5.32	2.46	589	281	0.00418	406	99.3
3-16-13-5		2.42	15.50	1.581	--	424	83.5	49.2	308	28.9	7.41	36.6	683	21.7	0.0536	418	323
3-20-13-6		2.42	15.50	1.581	--	546	108	63.4	471	28.9	11.3	60.9	730	20.0	0.0834	392	533
17-137-13-1		6.91	16.87	1.720	3.49	3.05	0.601	0.354	186	82.5	1.55	0.00206	569	233,000	0.00000362	622	3.05
14-103-13-2		6.48	16.78	1.712	1.85	35.8	7.05	4.16	404	77.4	3.61	0.284	990	3,670	0.000287	635	35.8
15-109-13-3		6.08	16.70	1.703	--	135	26.5	15.7	606	72.6	5.78	4.00	1290	390	0.00310	788	108
15-113-13-4		6.08	16.70	1.703	--	184	36.2	21.4	530	72.6	5.06	7.43	1400	184	0.00532	825	197
16-117-13-5		5.75	16.63	1.696	--	412	81.8	47.8	726	68.6	7.34	37.2	1620	50.4	0.0230	834	263
16-122-13-6		5.75	16.63	1.696	--	681	134	79.0	1022	68.6	10.3	101	1820	26.0	0.0554	676	522
22-187-16-1	58.1	1.27	14.66	1.495	1.43	3.05	0.400	0.236	49.5	15.2	1.92	0.00404	251	71,200	0.0000161	228	3.05
12-92-16-3		1.17	14.55	1.484	1.46	108	14.2	8.36	76.3	14.0	3.21	5.03	564	88.2	0.00892	259	108
13-97-16-4		1.08	14.45	1.474	1.20	264	34.6	20.4	108	12.9	4.92	29.9	651	21.0	0.0459	258	264
28-227-16-6		1.38	14.77	1.506	--	732	82.9	48.9	232	16.5	8.30	175	1040	7.71	0.169	291	539
20-165-16-1		3.27	15.89	1.621	2.19	3.05	0.400	0.236	136	30.0	2.06	0.00438	645	180,000	0.00000679	410	3.05
6-54-16-2		2.35	15.46	1.577	1.69	27.6	3.62	2.14	178	28.1	3.73	0.349	808	2,960	0.000432	389	27.6
7-59-16-3		2.26	15.41	1.572	1.76	103	13.5	7.97	204	27.0	4.45	4.85	1080	245	0.00451	424	103
8-65-16-4		2.85	15.71	1.603	--	238	31.2	18.4	327	34.0	5.67	26.4	1670	72.0	0.0158	573	190
9-70-16-5		2.76	15.67	1.702	--	397	52.1	30.7	338	32.9	6.07	77.0	1840	25.2	0.0424	608	264
9-73-16-6		2.76	15.67	1.702	--	642	84.2	49.7	579	32.9	10.4	204	2070	16.5	0.0986	554	529
18-143-16-1		6.30	16.75	1.708	2.77	3.05	0.400	0.236	250	75.2	1.95	0.00461	1240	315,000	0.00000371	596	3.05
29-238-16-2		6.06	16.70	1.703	2.28	37.9	4.97	2.93	365	72.3	2.97	0.709	2240	2,990	0.000316	650	37.9

(Continued)

Table 2 (Continued)

(1) Test No.	(2) Plate Base Area A_x cm^2	(3) Standard Penetration Resistance Gradient C MN/m^3	(4) Sand Unit Dry Weight γ_d kN/m^3	(5) Sand Dry Mass Density ρ $kN\text{-}sec^2/m^4$	(6) Penetration Resistance Gradient C_x* MN/m^3	(7) Penetration Velocity $(V_z)_x$ cm/sec	(8) Velocity Gradient $(V_z/\ell)_x$ sec^{-1}	(9) Velocity Gradient Ratio $(V_z/\ell)_{xs}$	(10) Plate Base Pressure $(F_z/A)_x$ kPa	(11) Standard Cone Base Pressure $(F_z/A)_s$ kPa	(12) Plate-Cone Stress Ratio**	(13) Inertial Force $\rho(AV_z^2)_x/2$ N	(14) Computed Viscous-Type Force N	(15) Modified Drag Coefficient C_D	(16) Modified Reynolds Number N_R	(17) Plate Base Pressure (See note 1) $(F_z/A)_x$ kPa	(18) Penetration Velocity (See note 1) $(V_z)_x$ cm/sec
Flat Rectangular (1:1) Plates (Continued)																	
30-251-14-3	58.1	6.15	14.77	1.705	2.23	115	15.1	8.90	521	73.4	4.18	6.57	3000	461	0.00219	800	115
31-260-14-4		6.30	16. [illegible]	1.708	--	267	35.0	20.7	598	75.2	4.68	35.4	3800	98.2	0.00931	897	221
33-284-14-6		5.43	16. [illegible]5	1.688	--	635	83.3	49.1	1028	64.8	9.36	198	4070	30.2	0.0486	875	533
Flat Rectangular (1:2) Plates																	
21-172-15-1	3.23	1.35	14.74	1.503	1.24	3.05	1.70	1.00	37.0	16.1	2.47	0.000226	11.6	52,900	0.0000194	192	3.05
19-150-15-1		3.50	15.96	1.630	3.64	3.05	1.70	1.00	125	41.8	3.21	0.000245	30.2	165,000	0.00000812	580	3.05
4-23-15-2		2.55	15.57	1.588	2.63	24.7	13.7	8.10	129	30.4	5.46	0.0156	36.7	2,670	0.000425	458	24.7
4-34-15-3		2.55	15.57	1.588	2.64	104	57.9	34.1	196	30.4	6.93	0.277	52.9	298	0.00524	526	104
5-45-15-5		2.91	15.74	1.605	--	415	231	136	279	34.7	8.64	4.46	85.6	26.2	0.0521	513	269
6-45-15-6		2.35	15.46	1.577	--	627	349	206	412	28.1	15.8	10.0	76.9	13.3	0.130	480	539
17-128-15-1		6.91	16.87	1.720	7.32	3.05	1.70	1.00	179	92.5	2.33	0.000259	59.3	224,000	0.00000435	1090	3.05
29-231-15-2		6.96	16.70	1.703	6.80	38.2	21.[illegible]	12.5	247	72.3	3.66	0.0401	98.3	1,990	0.000408	1100	38.2
30-243-15-3		6.15	16.72	1.705	--	116	64.6	38.0	475	73.4	6.95	0.371	131	413	0.00283	1160	113
32-265-15-5		6.[illegible]	16.68	1.702	--	445	248	146	542	71.6	8.13	5.46	180	32.1	0.0304	1300	270
33-276-15-6		5.43	16.55	1.688	--	718	400	235	862	64.8	14.3	14.1	184	19.8	0.0767	1090	525
21-182-16-1	25.8	1.35	14.74	1.503	1.24	3.05	0.601	0.354	41.3	16.1	1.83	0.00180	108	59,100	0.0000166	196	3.05
23-199-16-2		1.40	14.79	1.508	1.12	39.2	7.72	4.55	94.9	16.7	3.60	0.299	214	732	0.00140	225	39.2
24-208-16-3		1.28	14.67	1.496	1.11	121	23.8	14.0	85.3	15.3	3.95	2.84	258	77.5	0.0110	224	121
26-217-16-5		1.25	14.64	1.493	--	323	63.6	37.5	136	14.9	6.47	20.1	343	17.5	0.0577	184	309
27-225-16-6		1.16	14.54	1.483	--	612	120	710	255	13.8	1.31	71.7	351	9.17	0.204	219	530
20-160-16-1		3.27	15.89	1.621	2.10	3.05	0.601	[illegible]	119	39.0	2.16	0.00195	264	158,000	0.00000739	382	3.05
1-4-16-2		2.64	15.61	1.592	1.40	31.4	6.18	[illegible]	136	31.5	3.06	0.202	378	1,735	0.000533	311	31.4
2-10-16-3		2.92	15.75	1.606	1.31	99.2	19.5	[illegible]	281	34.9	5.71	2.04	564	356	0.00362	307	99.2
2-13-16-4		2.92	15.75	1.606	--	291	57.3	[illegible]	343	34.9	6.96	17.5	732	50.4	0.0239	449	244
3-21-16-6		2.42	15.59	1.591	--	580	114	67.[illegible]	480	28.9	11.7	68.6	722	18.0	0.0950	386	528
17-138-16-1		6.91	16.87	1.720	[illegible]	3.05	0.601	0.354	170	82.5	1.46	0.00206	557	213,000	0.00000370	660	3.05
16-104-16-2		6.48	16.78	1.712	[illegible]	36.0	7.00	4.18	404	77.4	3.70	0.286	966	3,640	0.000296	680	36.0
15-108-16-3		6.08	16.70	1.703	--	134	26.4	15.6	591	72.6	5.77	3.95	1260	386	0.00313	753	107
15-114-16-4		6.08	16.70	1.703	--	185	36.4	21.5	563	72.6	5.49	7.51	1370	193	0.00550	809	193
16-118-16-5		5.75	16.63	1.696	--	410	80.7	47.6	666	68.6	6.89	36.9	1580	46.6	0.0234	890	265
16-121-16-6		5.75	16.63	1.696	--	696	137	80.8	984	68.6	10.1	106	1800	25.1	0.0590	722	519
22-188-17-1	58.1	1.27	14.66	1.495	1.37	3.05	0.400	0.236	48.7	15.2	1.92	0.00404	245	70,100	0.0000165	220	3.05
13-98-17-4		1.08	14.45	1.474	--	294	38.6	22.7	111	12.9	5.20	57.0	650	17.4	0.0569	231	232
21-228-17-6		1.38	14.77	1.506	--	639	83.8	49.4	240	16.5	8.73	178	1010	7.82	0.176	276	536
20-166-17-1		3.27	15.89	1.621	2.09	3.05	0.400	0.236	122	39.0	1.89	0.00638	628	162,000	0.00000698	383	3.05
6-53-17-2		2.35	15.46	1.577	1.75	24.9	3.27	1.93	149	28.1	3.19	0.284	768	3,050	[illegible]	362	24.9
3-60-17-3		2.26	15.41	1.572	1.81	107	14.0	8.28	171	27.0	3.81	5.23	1060	190	0.00495	397	107
6-66-17-4		2.85	15.71	1.603	--	261	34.2	20.2	257	34.0	4.56	31.7	1670	47.1	0.0190	502	196
9-71-17-5		2.76	15.67	1.598	--	403	52.9	31.2	324	32.9	5.93	75.5	1800	24.9	0.0419	559	260
9-72-17-6		2.76	15.67	1.598	--	643	84.4	49.8	523	32.9	9.58	192	2030	15.8	0.0948	540	528

(Continued)

Table 2 (Continued)

(1) Test No.	(2) Plate Base Area A_x cm^2	(3) Standard Penetration Resistance Gradient G MN/m^3	(4) Sand Unit Dry Weight γ_d kN/m^3	(5) Sand Dry Mass Density ρ $kN\text{-}sec^2/m^4$	(6) Penetration Resistance Gradient, G_x MN/m^3	(7) Penetration Velocity $(V_z)_x$ cm/sec	(8) Velocity Gradient $(V_z/\ell)_x$ sec^{-1}	(9) Velocity Gradient Ratio $(V_z/\ell)_{xs}$	(10) Plate Base Pressure $(F_z/A)_x$ kPa	(11) Standard Cone Base Pressure $(F_z/A)_s$ kPa	(12) Plate-Cone Stress Ratio**	(13) Inertial Force $\rho(AV_z^2)_x/2$ N	(14) Computed Viscous-Type Force N	(15) Modified Drag Coefficient C_D**	(16) Modified Reynolds Number N_R*	(17) Plate Base Pressure (See note 1) $(F_z/A)_x$ kPa	(18) Penetration Velocity (See note 1) $(V_z)_x$ cm/sec
Flat Rectangular (1:2) Plates (Continued)																	
18-144-17-1	58.1	6.30	16.75	1.708	3.08	3.05	0.400	0.236	195	75.2	1.56	0.00461	1210	246,000	0.00000380	580	3.05
29-237-17-2		6.06	16.70	1.703	2.37	38.5	5.05	2.99	382	72.3	3.18	0.732	2200	3,050	0.000333	678	38.5
30-250-17-3		6.15	16.72	1.705	2.80	118	15.5	9.13	465	73.4	3.82	6.91	2950	391	0.00234	815	118
31-259-17-4		6.30	16.75	1.708	--	246	32.3	19.0	494	75.2	3.95	30.0	3630	95.6	0.00827	800	200
32-27.-17-5		6.00	16.68	1.702	--	393	51.6	30.4	655	71.6	5.51	76.1	1880	50.0	0.0196	832	264
33-283-17-6		5.43	16.55	1.688	--	616	80.8	47.7	981	64.8	9.10	186	4110	30.7	0.0453	807	536
Flat Rectangular (1:4) Plates																	
21-175-18-1	6.45	1.35	14.74	1.503	1.34	3.05	1.20	0.708	41.6	16.1	2.58	0.000451	22.9	59,500	0.0000197	209	3.05
23-194-18-2		1.40	14.79	1.508	1.21	39.9	15.7	9.26	96.1	16.7	5.74	0.0774	45.3	801	0.00171	247	39.9
27-219-18-6		1.16	14.54	1.483	--	665	262	154	274	13.8	19.9	21.2	75.7	8.35	0.280	200	530
19-153-18-1		3.50	15.98	1.629	2.08	3.05	1.20	0.708	98.5	41.8	2.35	0.000489	59.4	129,000	0.00000823	484	3.05
4-24-18-2		2.55	15.57	1.588	2.26	24.9	9.80	5.78	123	30.4	4.04	0.0217	72.9	2,500	0.000435	406	24.9
4-32-18-3		2.55	15.57	1.588	1.45	104	40.9	24.1	224	30.4	7.36	0.554	105	261	0.00530	405	104
5-35-18-4		2.91	15.74	1.605	1.93	253	99.6	58.7	197	34.7	5.67	3.32	149	38.3	0.0223	445	253
5-44-18-5		2.91	15.74	1.605	--	434	171	101	342	34.7	9.85	9.74	170	22.6	0.0572	458	295
6-47-18-6		2.35	15.46	1.577	--	692	272	161	483	28.1	17.2	24.4	155	12.8	0.157	425	529
17-131-18-1		6.91	16.87	1.720	5.75	3.05	1.20	0.708	139	82.5	1.68	0.000516	117	174,000	0.00000440	858	3.05
30-244-18-3		6.15	16.72	1.705	4.62	111	43.7	25.8	393	73.4	5.35	0.677	256	374	0.00264	971	111
32-266-18-5		6.00	16.68	1.702	--	444	175	103	511	71.6	7.13	10.8	352	30.4	0.0307	1090	261
33-277-18-6		5.43	16.55	1.688	--	690	272	160	904	64.8	14.0	25.9	357	22.5	0.0726	940	534
22-183-19-1	25.8	1.27	14.66	1.495	1.05	3.05	0.601	0.354	43.8	15.2	2.18	0.00179	95.5	63,100	0.0000187	175	3.05
23-198-19-2		1.40	14.79	1.508	1.03	40.0	7.88	4.64	86.0	16.7	3.90	0.312	200	711	0.00156	215	40.0
24-207-19-3		1.28	14.67	1.496	0.84	109	21.5	12.7	97.1	15.3	4.81	2.29	236	109	0.00971	202	109
25-211-19-4		1.48	14.86	1.516	--	220	43.3	25.5	95.0	17.7	4.06	9.47	325	25.9	0.0291	169	225
26-216-19-5		1.25	14.64	1.493	--	460	90.6	53.4	152	14.9	7.72	40.8	332	9.62	0.123	175	318
27-224-19-6		1.16	14.54	1.483	--	650	128	75.4	276	13.8	15.1	80.8	333	8.92	0.243	218	547
20-161-19-1		3.27	15.89	1.621	1.96	3.05	0.601	0.354	90.8	39.0	1.77	0.00195	247	120,000	0.00000790	336	3.05
1-5-19-2		2.64	15.61	1.592	1.62	31.5	6.21	3.66	156	31.5	3.75	0.204	357	1,970	0.000572	359	31.5
2-11-19-3		2.92	15.75	1.606	--	94.5	18.6	11.0	242	34.9	5.24	1.85	521	338	0.00355	403	101
2-14-19-4		2.92	15.75	1.606	--	303	59.7	35.2	325	34.9	7.05	19.0	696	44.1	0.0273	388	223
3-17-19-5		2.42	15.50	1.581	--	412	81.1	47.8	358	28.9	9.39	34.6	622	26.7	0.0556	363	265
3-22-19-6		2.42	15.50	1.581	--	529	104	61.4	488	28.9	12.7	57.0	663	22.1	0.0860	329	509
18-139-9-1		6.30	16.75	1.708	3.63	3.05	0.601	0.354	156	75.2	1.56	0.00205	476	195,000	0.00000431	610	3.05
14-105-19-2		6.48	16.78	1.712	2.37	36.1	7.11	4.19	318	77.4	3.11	0.289	906	2,840	0.00319	614	36.1
14-107-19-3		6.48	16.78	1.712	--	136	26.8	15.8	467	77.4	4.57	4.08	1260	296	0.00324	672	112
16-119-19-5		5.75	16.63	1.696	--	412	81.1	47.8	639	69.6	7.03	37.2	1480	44.3	0.0252	796	264
16-120-19-6		5.75	16.63	1.696	--	672	132	78.0	1112	68.6	12.3	98.8	1670	29.0	0.0593	750	572
22-189-20-1	58.1	1.27	14.66	1.495	1.21	3.05	0.400	0.236	42.7	15.2	1.81	0.00404	230	61,400	0.0000176	194	3.05
11-88-20-2		1.27	14.66	1.495	0.98	34.1	4.47	2.64	77.6	15.2	3.29	0.505	421	893	0.00120	200	34.1
12-93-20-3		1.17	14.55	1.484	0.86	120	15.7	9.29	85.0	14.0	3.90	6.22	532	79.4	0.0117	193	120

(Continued)

Table 2 (Continued)

(1) Test No.	(2) Plate Base Area A_x cm²	(3) Standard Penetration Resistance Gradient G MN/m³	(4) Sand Unit Dry Weight γ_d kN/m³	(5) Sand Dry Mass Density kN-sec²/m⁴	(6) Penetration Resistance Gradient G_x* MN/m³	(7) Penetration Velocity $(V_z)_x$ cm/sec	(8) Velocity Gradient $(V_z/\ell)_x$ sec⁻¹	(9) Velocity Gradient Ratio $(V_z/\ell)_{xs}$	(10) Plate Base Pressure $(F_z/A)_x$ kPa	(11) Standard Cone Base Pressure $(F_z/A)_s$ kPa	(12) Plate-Cone Stress Ratio**	(13) Inertial Force $\rho(AV_z^2)_x/2$ N	(14) Computed Viscous-Type Force N†	(15) Modified Drag Coefficient C_D††	(16) Modified Reynolds Number N_R‡	(17) Plate Base Pressure (See note 1) $(F_z/A)_x$ kPa	(18) Penetration Velocity (See note 1) $(V_z)_x$ cm/sec
Flat Rectangular (1:4) Plates (Continued)																	
13-99-20-4		1.98	14.45	1.474	--	213	27.9	16.5	74.1	12.9	3.69	19.4	562	22.2	0.0345	164	202
20-167-20-1		3.27	15.89	1.621	1.87	3.05	0.400	0.236	98.4	39.0	1.62	0.00709	586	80,700	0.0000121	332	3.05
6-52-20-2		2.35	15.46	1.577	1.34	31.0	4.07	2.40	115	28.1	2.63	0.440	755	1,520	0.000583	283	31.0
7-[illegible]-20-3		2.26	15.41	1.572	1.30	104	13.6	8.05	168	27.0	4.00	4.94	988	198	0.00500	331	104
8-63-20-4		2.85	15.71	1.603	--	266	34.9	20.6	212	34.0	4.02	32.9	1570	37.4	0.0210	342	201
18-145-20-1		6.30	16.75	1.708	2.87	3.05	0.400	0.239	149	75.2	1.27	0.00461	1130	188,000	0.00000407	508	3.05
29-236-20-2		6.06	16.70	1.703	2.39	38.3	5.02	2.96	340	72.3	3.03	0.726	2060	2,720	0.00353	658	38.3
30-249-20-3		6.15	16.72	1.705	2.60	115	15.1	8.90	403	73.4	3.53	6.55	2750	357	0.00238	728	115
31-258-20-4		6.30	16.75	1.708	--	252	33.1	19.5	514	75.2	4.41	21.5	3420	94.8	0.00920	719	202
32-270-20-5		6.00	16.68	1.702	--	397	52.1	30.7	671	71.6	6.04	77.9	3660	50.1	0.0213	690	261
33-282-20-6		5.43	16.55	1.688	--	648	85.0	50.1	[illegible]	64.8	8.95	206	3740	25.4	0.0551	783	537
Flat Rectangular (1:8) Plates																	
21-178-21-1	12.9	1.35	14.74	1.503	1.31	3.05	0.849	0.501	41.5	16.1	2.49	0.000502	43.6	59,700	0.0000206	206	3.05
24-204-21-3		1.28	14.67	1.496	1.05	95.1	26.5	15.6	90.5	15.3	5.66	0.872	98.3	134	0.00887	222	95.1
25-210-21-4		1.48	14.86	1.516	--	288	80.2	47.3	112	17.7	6.07	8.11	150	17.8	0.0542	191	246
26-214-21-5		1.25	14.64	1.493	--	462	129	75.8	139	14.9	8.93	20.5	141	8.74	0.145	177	374
27-220-21-6		1.16	14.54	1.483	--	677	188	111	220	13.8	20.1	43.9	144	8.53	0.304	190	525
19-154-21-1		3.50	15.99	1.630	2.37	3.05	0.849	0.501	78.9	41.8	1.81	0.000978	114	104,000	0.00000860	375	3.05
4-26-21-2		2.55	15.57	1.588	1.49	26.5	7.38	4.35	128	30.4	4.03	0.0720	142	2,290	0.000507	377	26.5
4-31-21-3		2.55	15.57	1.588	2.01	104	29.0	17.1	169	30.4	5.39	1.11	200	197	0.00554	420	104
5-37-21-4		2.91	15.74	1.605	--	225	62.6	36.9	185	34.7	5.10	5.24	276	45.6	0.0190	412	199
5-42-21-5		2.91	15.74	1.605	--	414	115	68.0	280	34.7	7.72	17.8	322	20.3	0.0552	441	267
17-134-21-1		6.91	16.87	1.720	4.78	3.05	0.849	0.501	184	82.5	2.14	0.00103	224	230,000	0.00000460	781	3.05
14-106-21-3		6.48	16.78	1.712	4.56	107	29.8	17.6	304	77.4	3.77	1.26	510	310	0.00247	874	107
32-268-21-5		5.43	16.55	1.688	--	442	123	72.6	522	64.8	7.72	21.3	612	31.6	0.0348	872	266
35-279-21-6		6.06	16.70	1.703	--	717	200	118	841	72.3	11.1	56.5	770	19.2	0.0734	754	524
22-184-22-1	25.8	1.27	14.66	1.495	1.26	3.05	0.601	0.354	44.3	15.2	2.43	0.00179	86.9	63,700	0.0000206	202	3.05
23-197-22-2		1.40	14.79	1.508	0.87	40.2	7.91	4.67	75.1	16.7	3.75	0.315	182	615	0.00173	184	40.2
24-206-22-3		1.28	14.67	1.496	0.75	105	20.7	12.2	67.9	15.3	3.70	2.13	213	82.3	0.0100	162	105
26-215-22-4		1.25	14.64	1.493	--	453	89.2	52.6	142	14.9	7.95	39.5	299	9.28	0.132	162	341
27-223-22-5		1.16	14.54	1.483	--	644	127	74.7	251	13.8	15.2	79.5	302	8.15	0.263	184	538
6-162-22-1		3.27	15.89	1.621	1.48	3.05	0.601	0.354	71.5	39.0	1.53	0.00194	223	9,500	0.00000870	319	3.05
1-6-22-2		2.64	15.61	1.592	1.20	31.7	6.24	3.68	164	31.5	4.35	0.206	324	2,050	0.000635	325	31.7
18-140-22-1		6.30	16.75	1.708	3.67	3.05	0.601	0.354	187	75.2	2.07	0.00205	432	226,000	0.00000475	646	3.05
22-190-23-1	58.1	1.27	[illegible]	1.495	[illegible]	3.05	0.400	0.236	35.5	15.2	1.66	0.00404	208	51,100	0.0000194	167	3.05
11-89-23-2		1.27	14.66	1.495	1.13	32.4	4.25	2.51	63.5	15.2	2.96	0.456	377	809	0.00121	205	32.4
12-94-23-3		1.17	[illegible]	1.484	0.71	123	16.1	9.52	71.9	14.0	3.64	6.51	486	64.2	0.0134	161	123

(Continued)

Table 2 (Concluded)

(1) Test No.	(2) Plate Base Area A_x cm^2	(3) Standard Penetration Resistance Gradient G MN/m^3	(4) Sand Unit Dry Weight γ_d kN/m^3	(5) Sand Dry Mass Density $kN\text{-}sec^2/m^4$	(6) Penetration Resistance Gradient G_x^* MN/m^3	(7) Penetration Velocity $(V_z)_x$ cm/sec	(8) Velocity Gradient $(V_z/l)_x$ sec^{-1}	(9) Velocity Gradient Ratio $(V_z/l)_{xs}$	(10) Plate Base Pressure $(F_z/A)_x$ kPa	(11) Standard Cone Base Pressure $(F_z/A)_s$ kPa	(12) Plate-Cone Stress Ratio**	(13) Inertial Force $\rho(AV_z^2)_x/2$ N	(14) Computed Viscous-Type Force N	(15) Modified Drag Coefficient C_D**	(16) Modified Reynolds Number N_R†	(17) Plate Base Pressure (See note 1) $(F_z/A)_x$ kPa	(18) Penetration Velocity (See note 1) $(V_z)_x$ cm/sec
								Flat Rectangular (1:8) Plates (Continued)									
13-1[illegible]-23-4	58.1	1.0[illegible]	14.45	1.474	--	269	35.3	20.8	96.6	17.9	5.31	31.0	543	18.1	0.0571	239	225
28-22[illegible]-23-6		1.38	14.77	1.506	--	654	85.8	50.6	261	16.5	11.2	187	866	8.11	0.216	229	538
20-1[illegible]-23-1		3.27	15.89	1.621	1.73	3.05	0.400	0.236	79.4	39.0	1.44	0.00438	534	105,000	0.00000820	296	3.05
6-51-23-2		2.35	15.46	1.577	1.47	29.4	3.86	2.[illegible]	87.8	29.1	2.21	0.396	679	1,290	0.000583	272	29.4
7-62-23-3		2.26	15.41	1.572	1.22	107	14.0	8.26	153	27.0	4.02	5.23	900	170	0.00581	306	107
18-146-23-1		6.30	16.75	1.718	3.15	3.05	0.400	0.236	216	75.2	2.04	0.00461	1030	272,000	0.00000448	610	3.05
24-235-23-2		6.96	16.70	1.703	2.64	38.2	5.01	2.96	269	72.7	2.64	0.720	1870	2,170	0.000386	599	38.2
30-246-23-3		6.15	16.72	1.705	1.60	115	15.1	8.90	389	73.4	3.75	6.57	2500	344	0.00263	589	115
31-257-23-4		6.40	16.75	1.706	--	291	38.2	22.5	468	75.2	4.41	42.0	3210	64.7	0.0131	666	226
32-264-23-5		6.00	16.68	1.702	--	400	52.5	31.0	575	71.6	5.69	79.0	3320	42.3	0.0238	702	269
33-2[illegible]1-23-6		5.43	16.55	1.698	--	649	95.1	50.2	670	64.9	10.6	206	3390	27.3	0.0608	688	536

60<

Table 3

Vertical Penetration Tests with 3.23-cm^2 Cone in Molds of Yuma Sand

Penetration Velocity, 0.017 to 35.1 cm/sec

Test No.	Moisture Content %	Unit Dry Weight γ_d kN/m^3	Penetration Velocity v_z cm/sec	Penetration Resistance Gradient G_x* MN/m^3
1	0.5	15.42	2.50	1.99
2		15.14	2.50	1.92
3		15.58	2.50	2.57
4		15.01	2.50	1.77
5	0.4	15.37	8.97	2.25
6		15.37	17.4	2.23
7		15.37	3.26	2.12
8	0.5	15.36	34.5	2.60
9	0.4	15.39	3.34	2.31
10	0.5	15.50	33.5	2.77
11		15.45	3.13	2.42
12		15.39	0.381	2.33
13		15.45	0.381	2.51
14		14.92	3.34	1.43
15		15.34	8.64	2.12
16		15.36	32.9	2.38
17		15.40	17.1	2.45
18		15.40	0.381	2.27
19		15.50	34.1	2.68
20		15.43	12.7	2.57
21		15.50	3.47	2.21
22		15.45	0.423	2.16
23		15.48	33.0	2.79
24	0.4	15.51	12.2	2.64
25		15.47	12.5	2.66
26		15.45	3.73	2.53
27		14.98	3.64	1.47
28		14.84	3.56	1.59

(Continued)

* Values of G_x listed in this table can be considered equivalent to standard G values because G_x was found to be influenced negligibly by the full range of V_z values in this table (which values bound standard velocity V_s = 3.05 cm/sec).

(Sheet 1 of 3)

Table 3 (Continued)

Test No.	Moisture Content %	Unit Dry Weight γ_d kN/m^3	Penetration Velocity V_z cm/sec	Penetration Resistance Gradient G_x MN/m^3
29	0.4	15.94	3.60	3.38
30	↓	16.11	3.56	3.38
31		15.78	3.60	2.90
32		15.61	3.56	2.57
33		14.85	3.51	1.68
34		14.81	3.47	1.53
35	1.5	15.32	32.3	5.00
36	1.6	15.33	13.9	5.49
37	1.2	15.28	0.423	5.86
38	1.1	15.41	3.01	5.27
39	1.5	15.36	33.4	5.10
40	1.5	15.47	0.423	5.88
41	1.3	15.38	3.64	5.50
42	1.3	15.36	12.8	4.65
43	2.2	15.44	3.30	7.97
44	2.2	15.35	6.39	7.44
45	2.2	15.32	0.0423	6.93
46	2.1	15.39	0.0295	7.65
47	2.0	15.41	6.35	7.68
48	2.2	15.35	0.127	7.63
49	2.1	15.39	3.05	7.47
50	2.1	15.33	0.381	7.65
51	2.0	15.41	34.6	8.19
52	2.1	15.33	3.39	7.66
53	2.1	15.35	12.8	7.43
54	2.2	15.33	33.5	7.64
55	2.1	15.39	13.5	7.57
56	2.2	15.39	0.423	8.43
57	2.0	15.58	3.51	7.81
58	2.0	15.52	3.05	7.22
59	2.8	15.50	3.05	9.33
60	4.3	15.50	3.05	9.62
61	5.2	15.46	3.05	11.23
62	5.3	15.47	3.05	10.76
63	5.7	15.50	3.05	11.93
64	5.9	15.54	3.05	10.54
65	6.1	15.49	3.05	10.52

(Continued) (Sheet 2 of 3)

Table 3 (Concluded)

Test No.	Moisture Content %	Unit Dry Weight γ_d kN/m^3	Penetration Velocity V_z cm/sec	Penetration Resistance Gradient G_x MN/m^3
66	6.8	15.39	0.423	10.42
67	7.8	15.22	33.5	9.50
68	7.5	15.13	0.423	8.14
69	7.7	15.11	35.1	8.53
70	6.9	15.49	3.98	11.09
71	7.0	15.14	13.0	8.93
72	7.1	15.50	3.26	11.03
73	7.1	15.47	2.96	11.21
74	7.1	15.46	33.4	10.66
75	7.1	15.43	13.5	10.58
76	6.9	15.44	0.381	11.51
77	7.0	15.55	13.0	11.26
78	7.2	15.57	0.466	11.56
79	6.9	15.74	3.51	13.94
80	7.4	15.88	3.81	15.72
81	7.5	15.91	3.68	16.45
82	7.7	15.90	0.423	15.52
83	6.8	15.94	34.9	16.19
84	7.3	15.93	0.0254	14.61
85	7.3	16.04	0.127	15.54
86	7.3	15.87	0.0339	15.41
87	7.3	15.99	0.127	15.24
88	7.2	16.04	0.0169	16.84
89	7.3	15.90	0.127	16.53
90	11.3	15.57	3.05	10.59
91	11.5	15.65	3.05	10.81

(Sheet 3 of 3)

Table 4

Vertical Penetration Tests with 3.23-cm^2 Cone in Molds of Yuma Sand

Penetration Velocity, 3.05 cm/sec

Test No.	Moisture Content %	Unit Dry Weight γ_d kN/m^3	Penetration Velocity v_z cm/sec	Penetration Resistance Gradient G MN/m^3
1	2.1	15.32	3.05	7.50
2	2.0	15.93		10.90
3	2.0	15.03		5.60
4	1.6	15.03		4.32
5	1.6	15.99		8.24
6	6.2	14.94		7.31
7	6.1	15.99		14.58
8	0.5	16.35		4.22
9	3.5	15.93		14.37
10	4.8	16.05		15.08
11	12.3	16.23		16.36
12	0.5	16.23		4.10
13	11.9	16.16		16.44
14	3.2	15.08		7.14
15	4.8	15.00		7.98
16	11.8	14.75		6.38

Table 5

Horizontal Penetration Tests with 30-Deg-Apex-Angle, Circular Cones in Air-Dry Yuma Sand

Test No.	Cone Base Area A_x cm^2	Penetration Resistance Gradient G MN/m^3	Sand Unit Dry Weight γ_d kN/m^3	Depth of Cone Tip h cm	Horizontal Velocity V_x m/sec	Horizontal Force F_x N	Froude Number $\frac{V_x}{\sqrt{gd_x}}$	Cone-Sand Pressure Ratio $\frac{F_x/A_x}{Gh^2/d_x}$
1	3.23	1.32	14.71	17.8	0.305	57.5	0.683	0.0864
					0.610	57.8	1.37	0.0869
					0.914	57.5	2.05	0.0864
					1.22	59.4	2.73	0.0893
					1.52	59.4	3.42	0.0893
					1.83	59.4	4.10	0.0893
					2.13	59.8	4.79	0.0899
					2.44	61.0	5.47	0.0917
					2.74	62.0	6.15	0.0932
					3.05	64.6	6.84	0.0971
					3.35	68.2	7.52	0.102
					3.66	70.7	8.20	0.106
2	3.23	1.28	14.67	17.8	0.305	54.6	0.683	0.0846
					0.610	55.6	1.37	0.0862
					0.914	55.9	2.05	0.0866
					1.22	57.2	2.73	0.0887
					1.52	56.2	3.42	0.0871
					1.83	56.8	4.10	0.0880
					2.13	57.2	4.79	0.0887
					2.44	56.8	5.47	0.0880
					2.74	56.8	6.15	0.0880
					3.05	58.5	6.84	0.0907
					3.35	60.4	7.52	0.0936
					3.66	62.7	8.20	0.0972
3	3.23	2.47	15.53	17.8	0.305	83.0	0.683	0.0667
					0.610	88.8	1.37	0.0713
					0.914	90.1	2.05	0.0724
					1.22	91.7	2.73	0.0737
					1.52	94.0	3.42	0.0755
					1.83	95.9	4.10	0.0770
					2.13	96.9	4.79	0.0778

(Continued)

(Sheet 1 of 9)

Table 5 (Continued)

Test No.	Cone Base Area A_x cm^2	Penetration Resistance Gradient G MN/m^3	Sand Unit Dry Weight γ_d kN/m^3	Depth of Cone Tip h cm	Horizontal Velocity V_x m/sec	Horizontal Force F_x N	Froude Number $\frac{V_x}{\sqrt{g d_x}}$	Cone-Sand Pressure Ratio $\frac{F_x/A_x}{Gh^2/d_x}$
3	3.23	2.47	15.53	17.8	2.44	97.9	5.47	0.0786
					2.74	99.2	6.15	0.0797
					3.05	102	6.84	0.0819
					3.35	104	7.52	0.0835
					3.66	103	8.20	0.0827
					3.96	108	8.89	0.0867
4	3.23	1.70	15.04	17.8	0.305	61.7	0.683	0.0720
					0.610	63.3	1.37	0.0739
					0.914	64.0	2.05	0.0747
					1.22	65.6	2.73	0.0765
					1.52	67.8	3.42	0.0791
					1.83	67.8	4.10	0.0791
					2.13	68.5	4.79	0.0799
					2.44	70.1	5.47	0.0818
					2.74	72.0	6.15	0.0840
					3.05	73.0	6.84	0.0852
					3.35	73.0	7.52	0.0852
					3.66	74.3	8.20	0.0867
					3.96	75.9	8.89	0.0886
					4.27	79.5	9.57	0.0927
					4.57	81.1	10.3	0.0[illegible]6
					4.88	84.0	10.9	0.0980
					5.18	84.6	11.6	0.0988
5	3.23	0.59	13.66	17.8	0.305	38.4	0.683	0.129
					0.610	38.1	1.37	0.128
					0.914	37.5	2.05	0.126
					1.22	35.2	2.73	0.118
					1.52	33.6	3.42	0.113
					1.83	32.3	4.10	0.109
					2.13	32.9	4.79	0.111
					2.44	31.3	5.47	0.105
					2.74	32.0	6.15	0.108
					3.05	33.3	6.84	0.112
					3.35	33.3	7.52	0.112
					3.66	36.5	8.20	0.123

(Continued)

(Sheet 2 of 9)

Table 5 (Continued)

Test No.	Cone Base Area A_x cm^2	Penetration Resistance Gradient G MN/m^3	Sand Unit Dry Weight γ_d kN/m^3	Depth of Cone Tip h cm	Horizontal Velocity V_x m/sec	Horizontal Force F_x N	Froude Number $\frac{V_x}{\sqrt{gd_x}}$	Cone-Sand Pressure Ratio $\frac{F_x/A_x}{Gh^2/d_x}$
5	3.23	0.59	13.66	17.8	3.96	35.9	8.89	0.121
					4.27	36.5	9.57	0.123
					4.57	37.1	10.3	0.125
					4.88	38.1	10.9	0.128
					5.18	39.4	11.6	0.132
6	3.23	3.81	16.09	17.8	0.305	117	0.683	0.0609
					0.610	122	1.37	0.0635
					0.914	126	2.05	0.0656
					1.22	133	2.73	0.0692
					1.52	132	3.42	0.0687
					1.83	131	4.10	0.0682
					2.13	132	4.79	0.0687
					2.44	134	5.47	0.0698
					2.74	135	6.15	0.0703
					3.05	134	6.84	0.0698
					3.35	136	7.52	0.0708
					3.66	139	8.20	0.0724
					3.96	141	8.89	0.0734
7	3.23	3.05	15.80	17.8	0.305	92.1	0.683	0.0590
					0.610	95.6	1.37	0.0622
					0.914	98.2	2.05	0.0638
					1.22	102	2.73	0.0663
					1.52	105	3.42	0.0683
					1.83	106	4.10	0.0689
					2.13	107	4.79	0.0696
					2.44	109	5.47	0.0709
					2.74	110	6.15	0.0715
					3.05	112	6.84	0.0728
					3.35	113	7.52	0.0735
8	3.23	4.04	16.17	17.8	0.305	121	0.683	0.0594
					0.610	125	1.37	0.0614
					0.914	128	2.05	0.0628
					1.22	130	2.73	0.0638
					1.52	131	3.42	0.0643

(Continued) (Sheet 3 of 9)

Table 5 (Continued)

Test No.	Cone Base Area A_x cm^2	Penetration Resistance Gradient G MN/m^3	Sand Unit Dry Weight γ_d kN/m^3	Depth of Cone Tip h cm	Horizontal Velocity V_x m/sec	Horizontal Force F_x N	Froude Number $\frac{V_x}{\sqrt{gd_x}}$	Cone-Sand Pressure Ratio $\frac{F_x/A_x}{Gh^2/d_x}$
8	3.23	4.04	16.17	17.8	1.83	132	4.10	0.0648
					2.13	134	4.79	0.0658
					2.44	135	5.47	0.0663
					2.74	136	6.15	0.0668
					3.05	137	6.84	0.0672
					3.35	139	7.52	0.0682
					3.66	139	8.20	0.0682
9	6.45	1.92	15.20	17.8	0.305	108	0.575	0.0790
					0.610	108	1.15	0.0790
					0.914	110	1.72	0.0805
					1.22	113	2.30	0.0827
					1.52	117	2.87	0.0856
					1.83	119	3.45	0.0871
					2.13	122	4.02	0.0892
					2.44	124	4.60	0.0907
					2.74	124	5.17	0.0907
					3.05	126	5.75	0.0922
					3.35	130	6.32	0.0951
					3.66	132	6.90	0.0966
10	6.45	1.25	14.64	17.8	0.305	78.0	0.575	0.0879
					0.610	77.4	1.15	0.0873
					0.914	78.7	1.72	0.0887
					1.22	79.3	2.30	0.0894
					1.52	78.7	2.87	0.0887
					1.83	79.3	3.45	0.0894
					2.13	82.6	4.02	0.0931
					2.44	81.9	4.60	0.0923
					2.74	83.9	5.17	0.0946
					3.05	89.7	5.75	0.101
					3.35	91.6	6.32	0.103
					3.66	95.5	6.90	0.108
					3.96	96.8	7.47	0.109
					4.27	98.7	8.05	0.111
					4.57	102	8.62	0.115

(Continued) (Sheet 4 of 9)

Table 5 (Continued)

Test No.	Cone Base Area A_x cm^2	Penetration Resistance Gradient G MN/m^3	Sand Unit Dry Weight γ_d kN/m^3	Depth of Cone Tip h cm	Horizontal Velocity V_x m/sec	Horizontal Force F_x N	Froude Number $\frac{V_x}{\sqrt{gd_x}}$	Cone-Sand Pressure Ratio $\frac{F_x/A_x}{Gh^2/d_x}$
10	6.45	1.25	14.64	17.8	4.88	111	9.20	0.125
					5.18	114	9.77	0.129
11	6.45	3.54	16.00	17.8	0.305	168	0.575	0.0670
					0.610	181	1.15	0.0721
					0.914	188	1.72	0.0749
					1.22	194	2.30	0.0773
					1.52	199	2.87	0.0793
					1.83	202	3.45	0.0805
					2.13	205	4.02	0.0817
					2.44	208	4.60	0.0829
					2.74	210	5.17	0.0837
					3.05	212	5.75	0.0845
					3.35	213	6.32	0.0849
					3.66	215	6.90	0.0857
12	6.45	0.93	14.26	17.8	0.305	73.5	0.575	0.111
					0.610	73.5	1.15	0.111
					0.914	71.0	1.72	0.107
					1.22	69.7	2.30	0.105
					1.52	69.0	2.87	0.104
					1.83	70.3	3.45	0.106
					2.13	71.0	4.02	0.107
					2.44	71.0	4.60	0.107
					2.74	71.6	5.17	0.108
					3.05	73.5	5.75	0.111
					3.35	75.5	6.32	0.114
					3.66	77.4	6.90	0.117
					3.96	80.0	7.47	0.121
					4.27	83.2	8.05	0.126
					4.57	85.1	8.62	0.129
					4.88	90.3	9.20	0.136
13	6.45	4.26	16.24	17.8	0.305	215	0.575	0.0708
					0.610	226	1.15	0.0745
					0.914	235	1.72	0.0775

(Continued) (Sheet 5 of 9)

Table 5 (Continued)

Test No.	Cone Base Area A_x cm^2	Penetration Resistance Gradient G MN/m^3	Sand Unit Dry Weight γ_d kN/m^3	Depth of Cone Tip h cm	Horizontal Velocity V_x m/sec	Horizontal Force F_x N	Froude Number $\frac{V_x}{\sqrt{gd_x}}$	Cone-Sand Pressure Ratio $\frac{F_x/A_x}{Gh^2/d_x}$
13	6.45	4.26	16.24	17.8	1.22	244	2.30	0.0804
					1.52	250	2.87	0.0824
					1.83	253	3.45	0.0834
					2.13	256	4.02	0.0844
					2.44	259	4.60	0.0854
					2.74	261	5.17	0.0860
					3.05	263	5.75	0.0867
					3.35	264	6.32	0.0870
					3.66	265	6.90	0.0873
					3.96	267	7.47	0.0880
14	12.90	0.85	14.14	17.8	0.305	129	0.483	0.150
					0.610	129	0.967	0.150
					0.914	125	1.45	0.146
					1.22	123	1.93	0.143
					1.52	123	2.42	0.143
					1.83	124	2.90	0.145
					2.13	126	3.38	0.147
					2.44	128	3.87	0.149
					2.74	129	4.35	0.150
					3.05	132	4.83	0.154
					3.35	133	5.32	0.155
					3.66	139	5.80	0.162
15	12.90	1.95	15.22	17.8	0.305	190	0.483	0.0965
					0.610	199	0.967	0.101
					0.914	208	1.45	0.106
					1.22	215	1.93	0.109
					1.52	224	2.42	0.114
					1.83	227	2.90	0.115
					2.13	232	3.38	0.118
					2.44	236	3.87	0.120
					2.74	239	4.35	0.121
					3.05	248	4.83	0.126
					3.35	253	5.32	0.129
					3.66	261	5.80	0.133

(Continued) (Sheet 6 of 9)

Table 5 (Continued)

Test No.	Cone Base Area A_x cm^2	Penetration Resistance Gradient G MN/m^3	Sand Unit Dry Weight γ_d kN/m^3	Depth of Cone Tip h cm	Horizontal Velocity V_x m/sec	Horizontal Force F_x N	Froude Number $\frac{V_x}{\sqrt{gd_x}}$	Cone-Sand Pressure Ratio $\frac{F_x/A_x}{Gh^2/d_x}$
16	12.90	3.37	15.93	17.8	0.305	271	0.483	0.0797
					0.610	290	0.967	0.0853
					0.914	312	1.45	0.0918
					1.22	333	1.93	0.0979
					1.52	353	2.42	0.104
					1.83	369	2.90	0.109
					2.13	382	3.38	0.112
					2.44	390	3.87	0.115
					2.74	395	4.35	0.116
					3.05	400	4.83	0.118
					3.35	406	5.32	0.119
					3.66	412	5.80	0.121
					3.96	415	6.28	0.122
17	12.90	4.33	16.26	17.8	0.305	316	0.483	0.0725
					0.610	342	0.967	0.0784
					0.914	377	1.45	0.0865
					1.22	399	1.93	0.0915
					1.52	414	2.42	0.0950
					1.83	419	2.90	0.0961
					2.13	432	3.38	0.0991
					2.44	437	3.87	0.100
					2.74	449	4.35	0.103
					3.05	454	4.83	0.104
					3.35	470	5.32	0.108
					3.66	470	5.80	0.108
					3.96	473	6.28	0.109
18	23.23	0.62	13.64	17.8	0.305	181	0.417	0.231
					0.610	184	0.834	0.234
					0.914	186	1.25	0.237
					1.22	186	1.67	0.237
					1.52	186	2.09	0.237
					1.83	186	2.50	0.237
					2.13	188	2.92	0.240
					2.44	188	3.34	0.240

(Continued)

(Sheet 7 of 9)

Table 5 (Continued)

Test No.	Cone Base Area A_x cm^2	Penetration Resistance Gradient G MN/m^3	Sand Unit Dry Weight γ_d kN/m^3	Depth of Cone Tip h cm	Horizontal Velocity V_x m/sec	Horizontal Force F_x N	Froude Number $\frac{V_x}{\sqrt{gd_x}}$	Cone-Sand Pressure Ratio $\frac{F_x/A_x}{Gh^2/d_x}$
18	23.23	0.62	13.64	17.8	2.74	188	3.75	0.240
					3.05	188	4.17	0.240
					3.35	188	4.59	0.240
					3.66	188	5.01	0.240
					3.96	190	5.42	0.242
19	23.23	3.49	15.93	17.8	0.305	409	0.417	0.0868
					0.610	441	0.834	0.0936
					0.914	458	1.25	0.0972
					1.22	492	1.67	0.104
					1.52	518	2.09	0.110
					1.83	548	2.50	0.116
					2.13	578	2.92	0.123
					2.44	585	3.34	0.124
					2.74	595	3.75	0.126
					3.05	602	4.17	0.128
					3.35	609	4.59	0.129
					3.66	611	5.01	0.130
					3.96	595	5.42	0.126
20	23.23	2.73	15.66	17.8	0.305	358	0.417	0.0969
					0.610	402	0.834	0.109
					0.914	432	1.25	0.117
					1.22	455	1.67	0.123
					1.52	497	2.09	0.135
					1.83	525	2.50	0.142
					2.13	541	2.92	0.146
					2.44	551	3.34	0.149
					2.74	560	3.75	0.152
					3.05	571	4.17	0.155
					3.35	583	4.59	0.158
					3.66	595	5.01	0.161
					3.96	602	5.42	0.163
21	3.23	1.05	14.41	25.4	0.305	63.6	0.683	0.0589
					0.610	61.7	1.37	0.0571
					0.914	61.0	2.05	0.0565

(Continued) (Sheet 8 of 9)

Table 5 (Concluded)

Test No.	Cone Base Area A_x cm^2	Penetration Resistance Gradient G MN/m^3	Sand Unit Dry Weight γ_d kN/m^3	Depth of Cone Tip h cm	Horizontal Velocity V_x m/sec	Horizontal Force F_x N	Froude Number $\frac{V_x}{\sqrt{gd_x}}$	Cone-Sand Pressure Ratio $\frac{F_x/A_x}{Gh^2/d_x}$
21	3.23	1.05	14.41	25.4	1.22	57.8	2.73	0.0535
					1.52	56.5	3.42	0.0523
					1.83	57.2	4.10	0.0530
					2.13	56.2	4.79	0.0520
					2.44	55.9	5.47	0.0518
					2.74	55.9	6.15	0.0518
					3.05	58.5	6.84	0.0542
					3.35	59.8	7.52	0.0554
					3.66	63.0	8.20	0.0583
22	3.23	3.10	15.82	10.2	0.305	53.6	0.683	0.104
					0.610	62.3	1.37	0.121
					0.914	67.5	2.05	0.132
					1.22	73.3	2.73	0.143
					1.52	79.5	3.42	0.155
					1.83	81.1	4.10	0.158
					2.13	84.3	4.79	0.164
					2.44	86.9	5.47	0.169
					2.74	90.1	6.15	0.176
					3.05	94.0	6.84	0.183
					3.35	96.9	7.52	0.189
					3.66	101	8.20	0.197
					3.96	102	8.89	0.199

(Sheet 9 of 9)

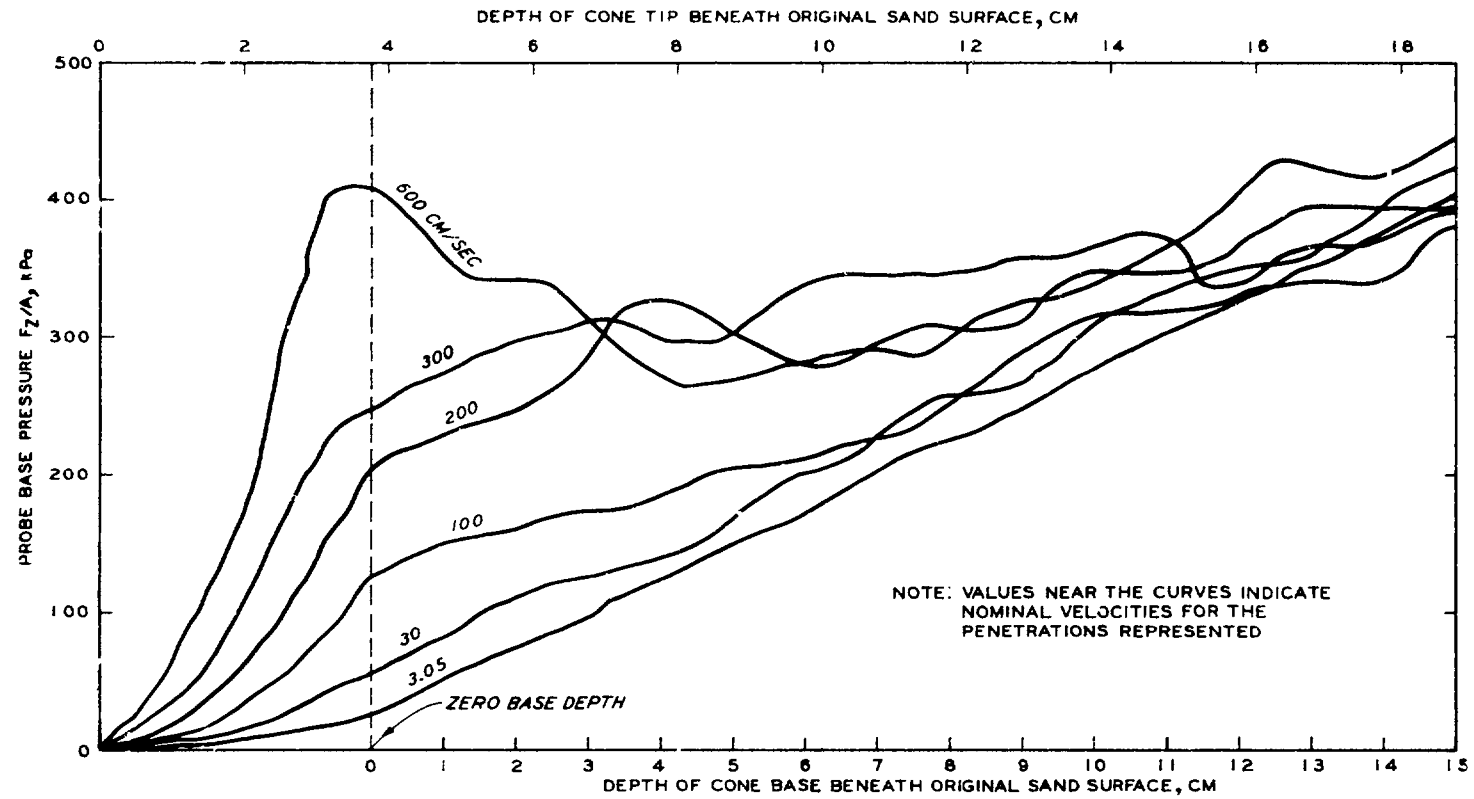

PROBE BASE PRESSURE VERSUS DEPTH CURVES FOR THE 3.23-CM^2 CONE AT NOMINAL VELOCITIES FROM 3 TO 600 CM/SEC

VERTICAL PENETRATIONS
AIR-DRY YUMA SAND
$G = 2.48\ MN/m^3$

74<

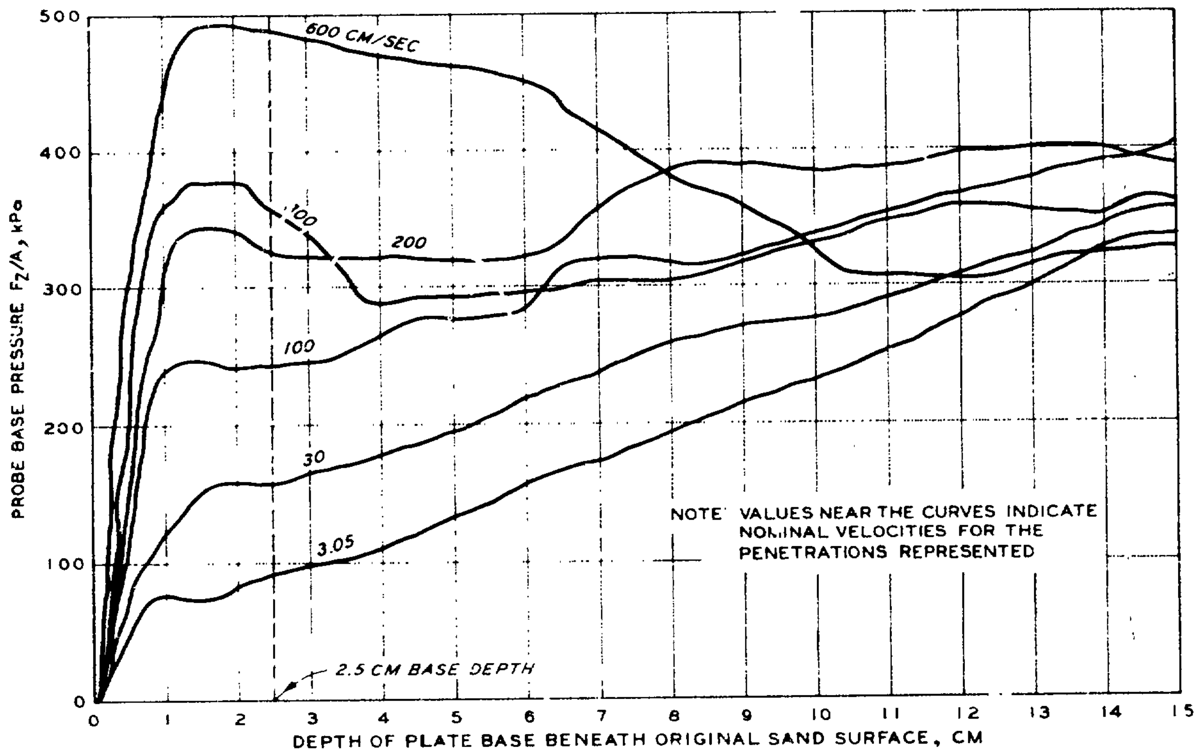

PROBE BASE PRESSURE VERSUS DEPTH CURVES FOR THE 25.8-CM^2, 1:4 PLATE AT NOMINAL VELOCITIES FROM 3 TO 600 CM/SEC

VERTICAL PENETRATIONS
AIR-DRY YUMA SAND
$G \approx 2.9$ MN/m^3

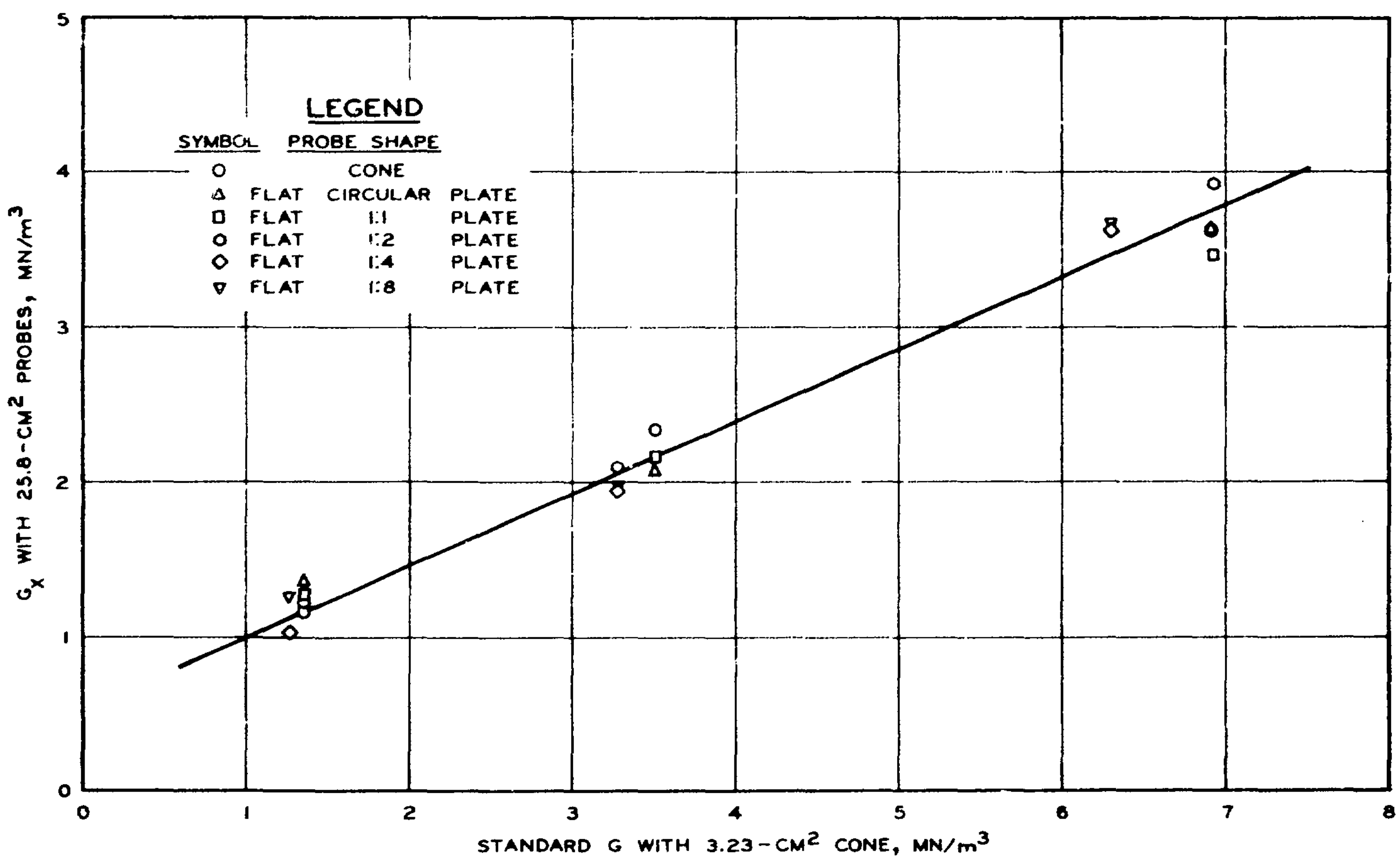

INFLUENCE OF PROBE SHAPE ON PENETRATION RESISTANCE GRADIENT AT LOW VELOCITY

VERTICAL PENETRATIONS
25.8-CM^2-BASE-AREA PROBES
3.05 CM/SEC PENETRATION SPEED
AIR-DRY YUMA SAND

76<

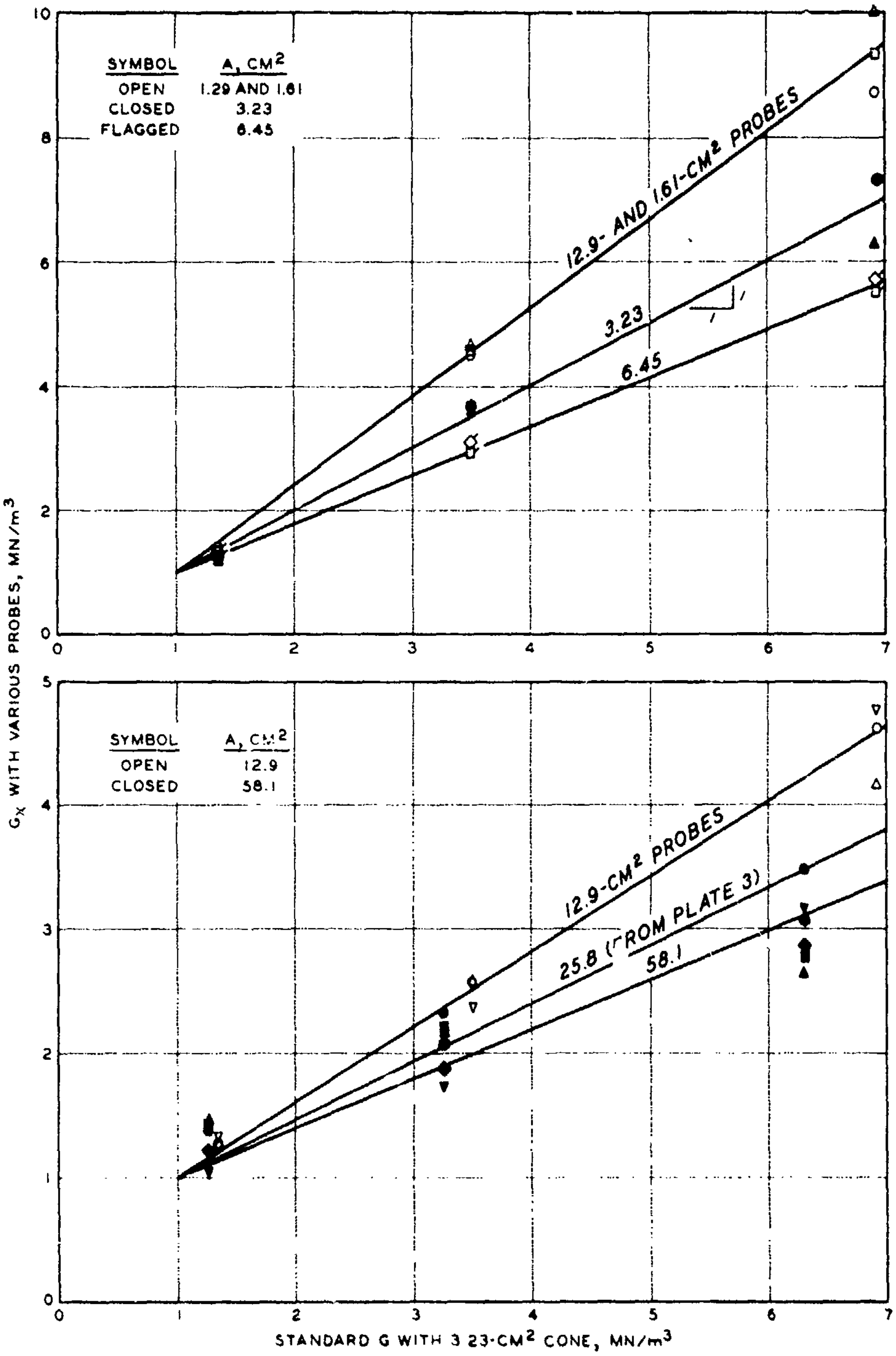

LEGEND

SYMBOL	PROBE SHAPE
○	CONE
△	FLAT CIRCULAR PLATE
□	FLAT 1:1 PLATE
○	FLAT 1:2 PLATE
◇	FLAT 1:4 PLATE
▽	FLAT 1:8 PLATE

INFLUENCE OF PROBE SIZE ON PENETRATION RESISTANCE GRADIENT AT LOW VELOCITY

VERTICAL PENETRATIONS
23 PROBE SIZES AND SHAPES
3.05 CM/SEC PENETRATION SPEED
AIR-DRY YUMA SAND

77

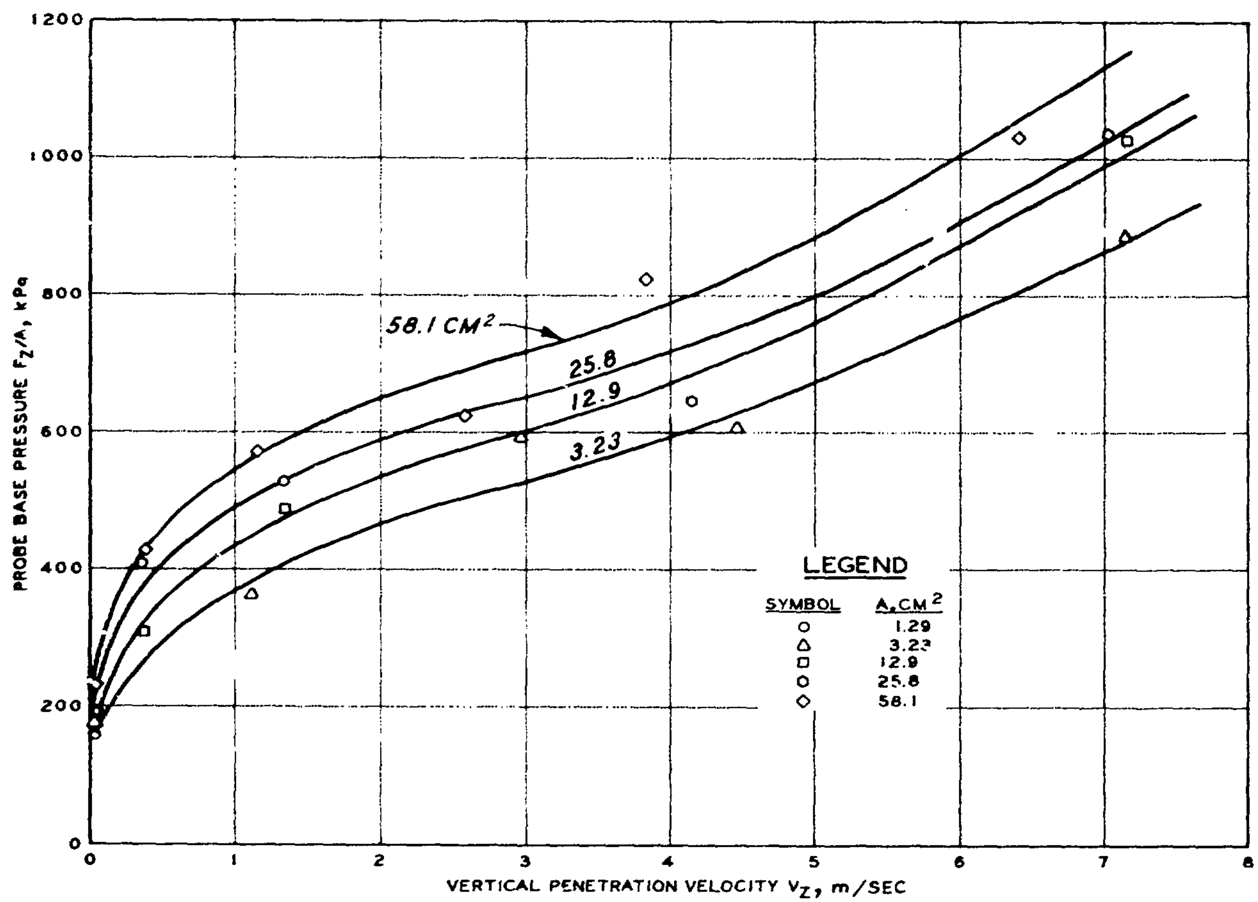

RELATION OF PROBE BASE PRESSURE
TO VELOCITY FOR CIRCULAR-BASE-AREA PLATES
IN SAND OF G VALUES NEAR 6.2 MN/m³
VERTICAL PENETRATIONS
AIR-DRY YUMA SAND

PLATE 5

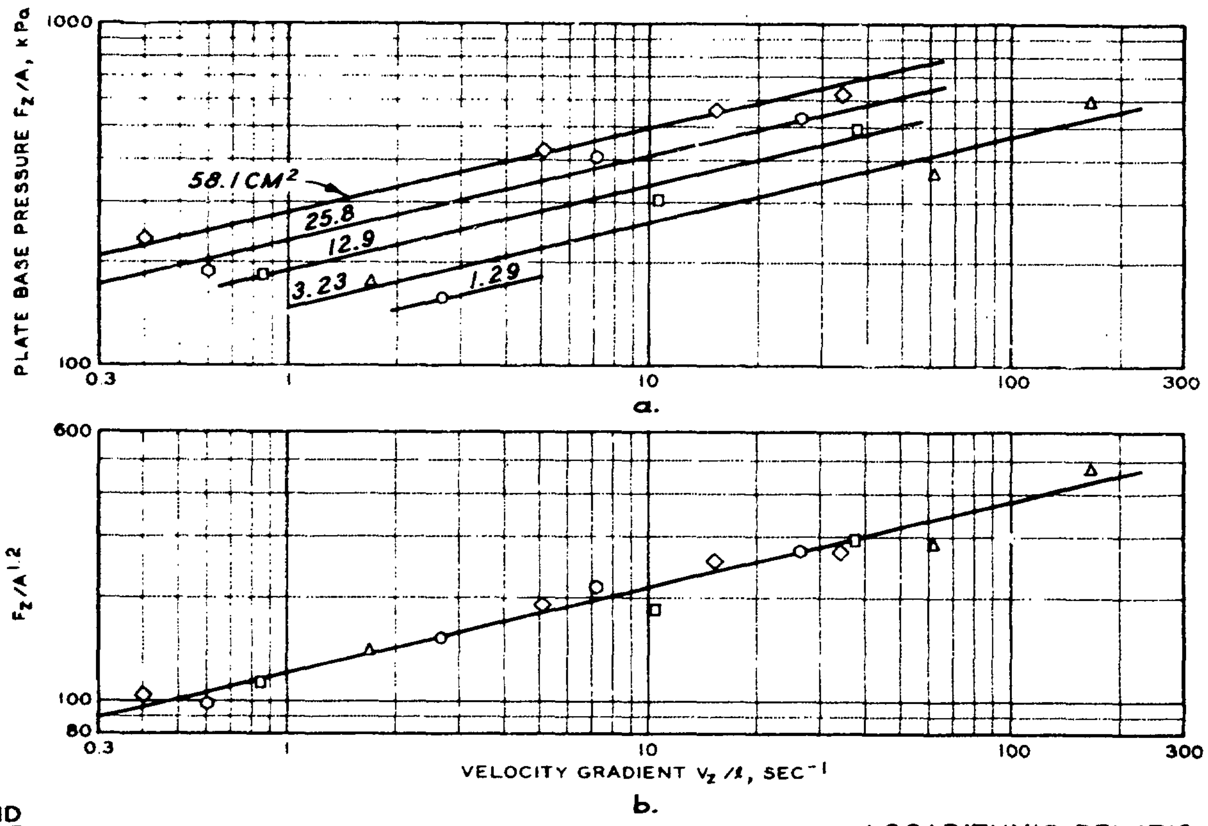

LEGEND

SYMBOL	A, CM²
○	1.29
△	3.23
□	12.9
○	25.8
◇	58.1

LOGARITHMIC RELATIONS OF F_Z/A AND OF $F_Z/A^{1.2}$ TO VELOCITY GRADIENT FOR CIRCULAR-BASE-AREA PLATES IN SAND OF G VALUES NEAR 6.2 MN/m^3

VERTICAL PENETRATIONS

V_Z VALUES ≤ 3 m/SEC

AIR-DRY YUMA SAND

79<

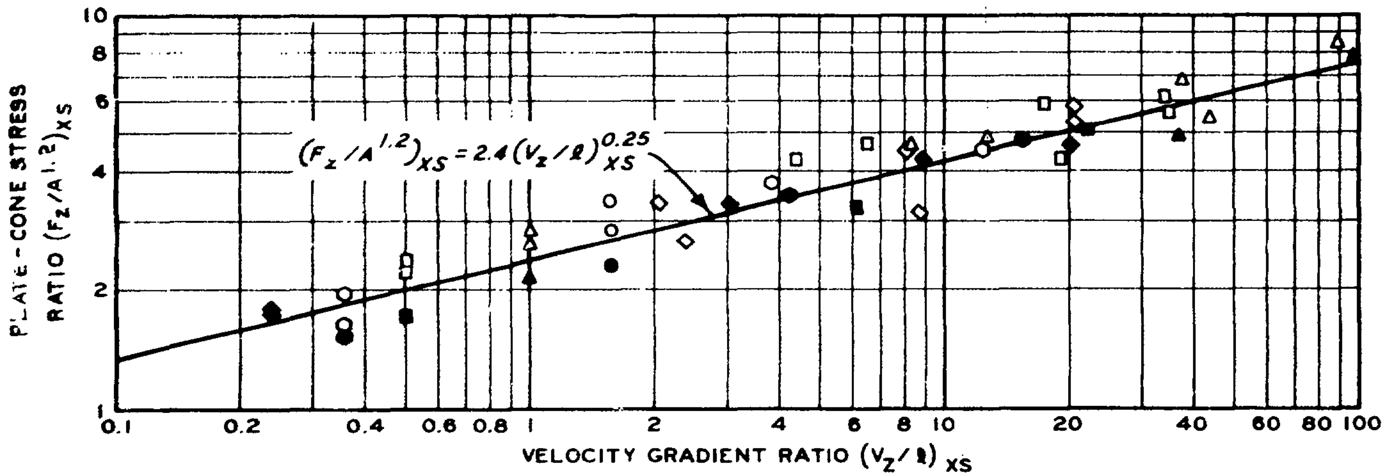

80<

LEGEND

SYMBOL	A, CM^2
○	1.29
△	3.23
□	12.9
◯	25.8
◇	58.1

NOTE: CLOSED SYMBOLS: G NEAR 6.2 MN/m^3
OPEN SYMBOLS: G NEAR EITHER 1.3 OR 2.9 MN/m^3

LOGARITHMIC RELATION OF PLATE-CONE STRESS RATIO TO VELOCITY GRADIENT RATIO FOR CIRCULAR-BASE-AREA PLATES

VERTICAL PENETRATIONS
V_z VALUES $\leq$ 3 m/SEC
G VALUES FROM 1.08 TO 6.91 MN/m^3
AIR-DRY YUMA SAND

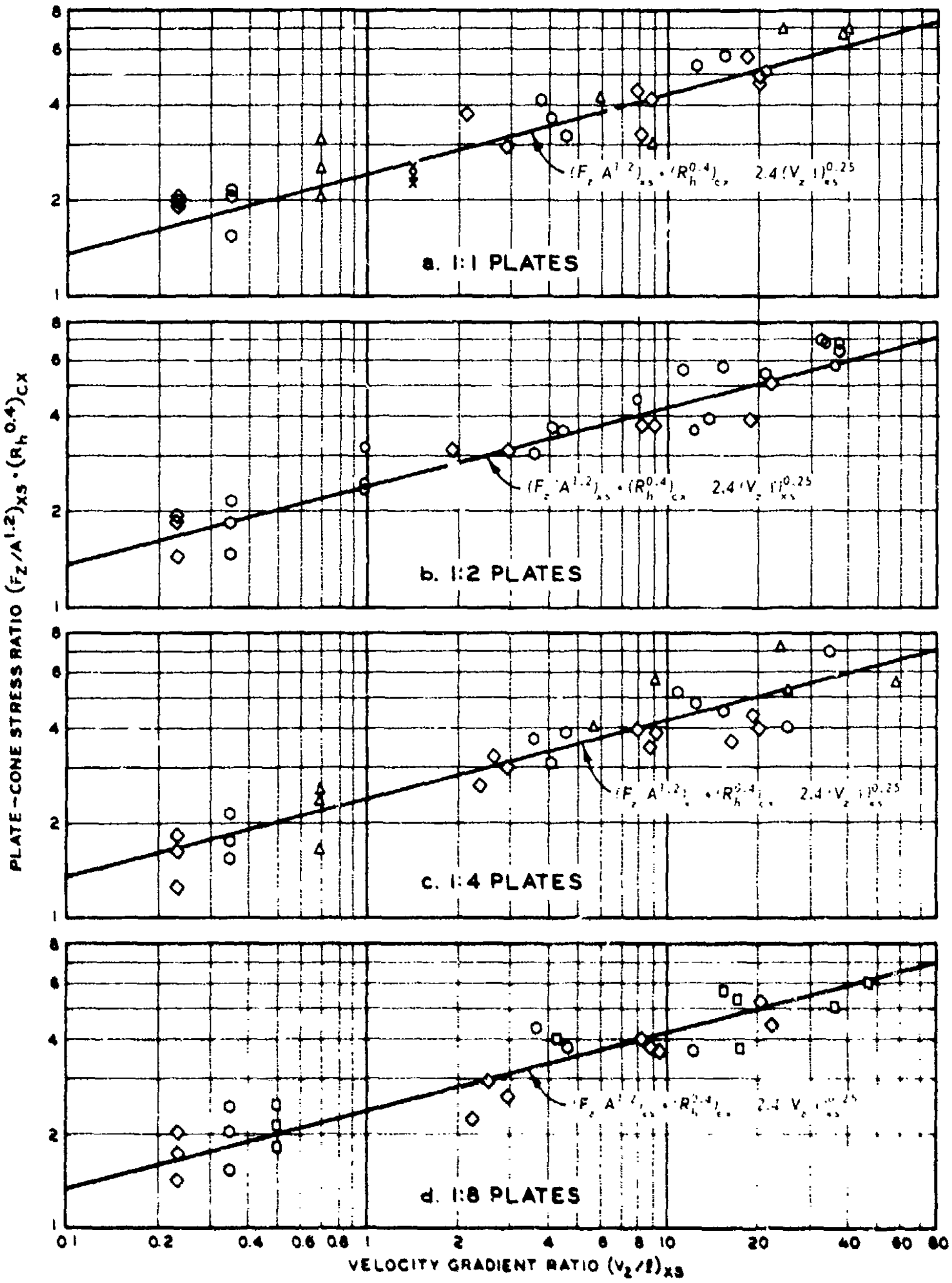

LEGEND	
SYMBOL	A, CM²
x	1.61
o	3.23
△	6.45
□	12.9
O	25.8
◇	58.1

LOGARITHMIC RELATION OF PLATE-CONE STRESS RATIO TO VELOCITY GRADIENT RATIO FOR FIVE SHAPES OF PLATES

VERTICAL PENETRATIONS

V_z VALUES ≤ 3 m/SEC

G VALUES FROM 1.08 TO 6.91 MN/m³

AIR-DRY YUMA SAND

PLATE 8

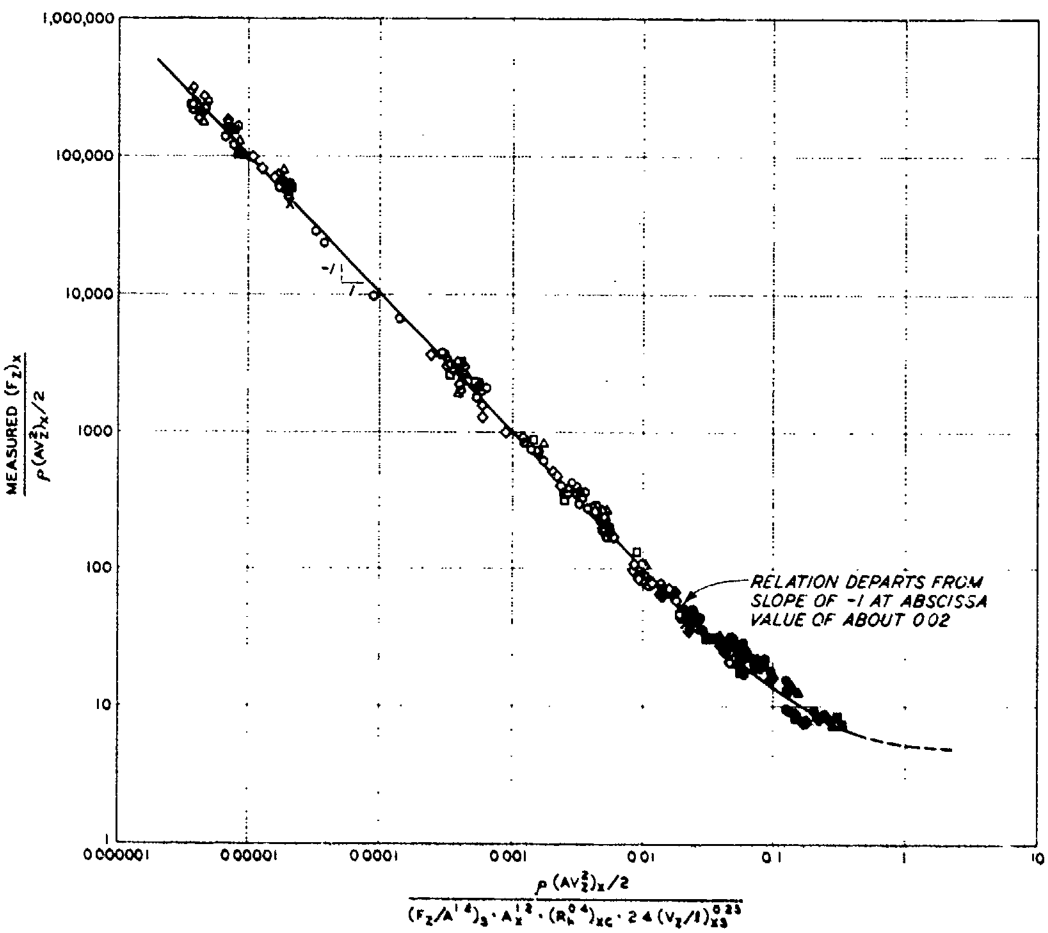

LEGEND

SYMBOL	A_X, CM^2
+	1.29
x	1.61
○	3.23
△	6.45
□	12.9
○	25.8
◇	58.1

NOTE: OPEN SYMBOLS $(V_Z)_X \leq 3m/SEC$
CLOSED SYMBOLS $(V_Z)_X > 3m/SEC$

DATA ARE PLOTTED FOR FLAT PLATES WITH FIVE SHAPES OF BASE AREAS (CIRCULAR AND RECTANGULAR 1:1, 1:2, 1:4, AND 1:8)

MODIFIED C_D VERSUS N_R RELATION FOR DESCRIBING $(F_Z)_X$ FOR FLAT PLATES

VERTICAL PENETRATIONS
V_Z VALUES FROM 305 TO 725 CM/SEC
G VALUES FROM 1.08 TO 6.91 MN/m^3
FIVE SHAPES OF FLAT PLATES
AIR-DRY YUMA SAND

82

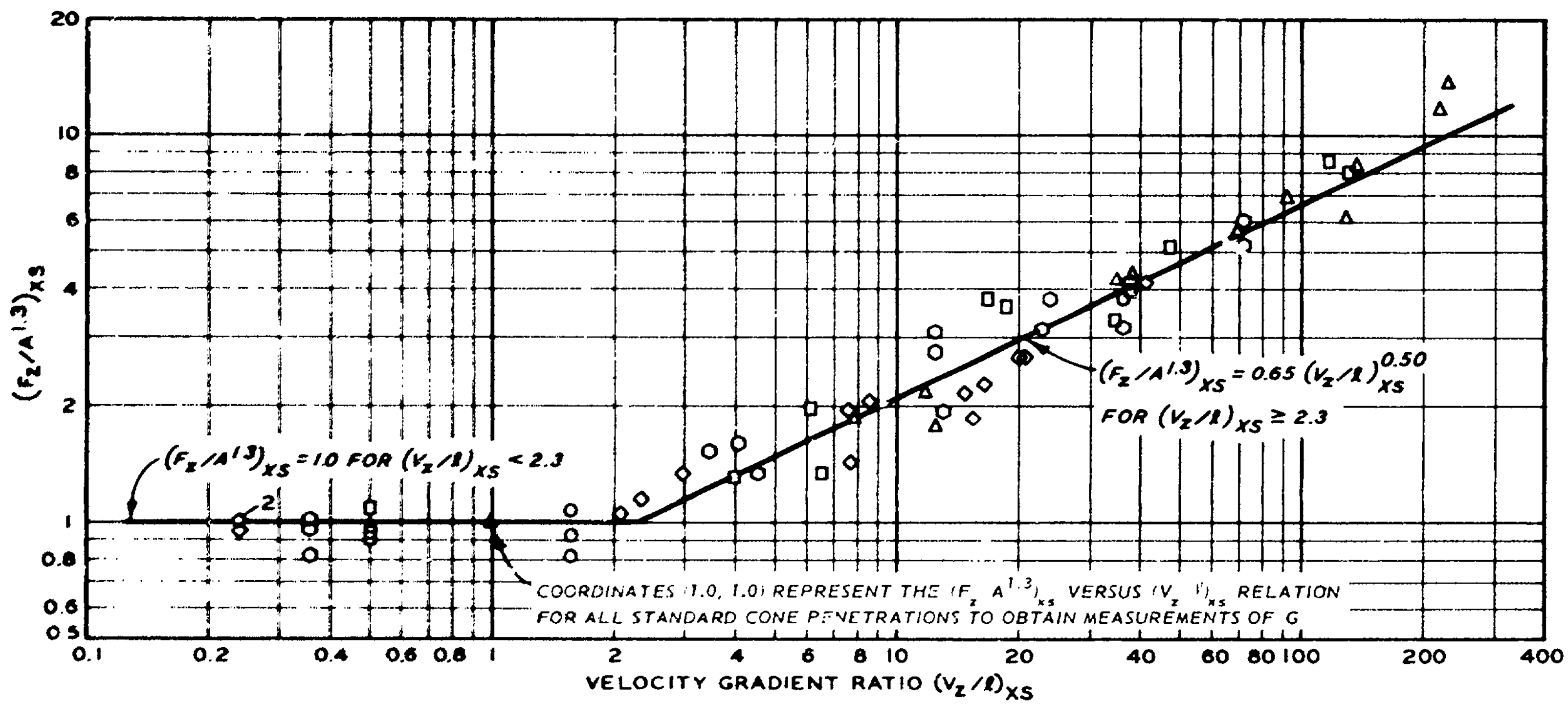

83<

LEGEND

SYMBOL	A, CM²
O	1.29
Δ	3.23
□	12.9
O	25.8
◇	58.1

LOGARITHMIC RELATION OF $(F_Z/A^{1.3})_{XS}$ TO VELOCITY GRADIENT RATIO FOR 30-DEG-APEX-ANGLE CONES

VERTICAL PENETRATIONS
V_Z VALUES ≤ 3 m/SEC
G VALUES FROM 1.08 TO 6.91 MN/m³
AIR-DRY YUMA SAND

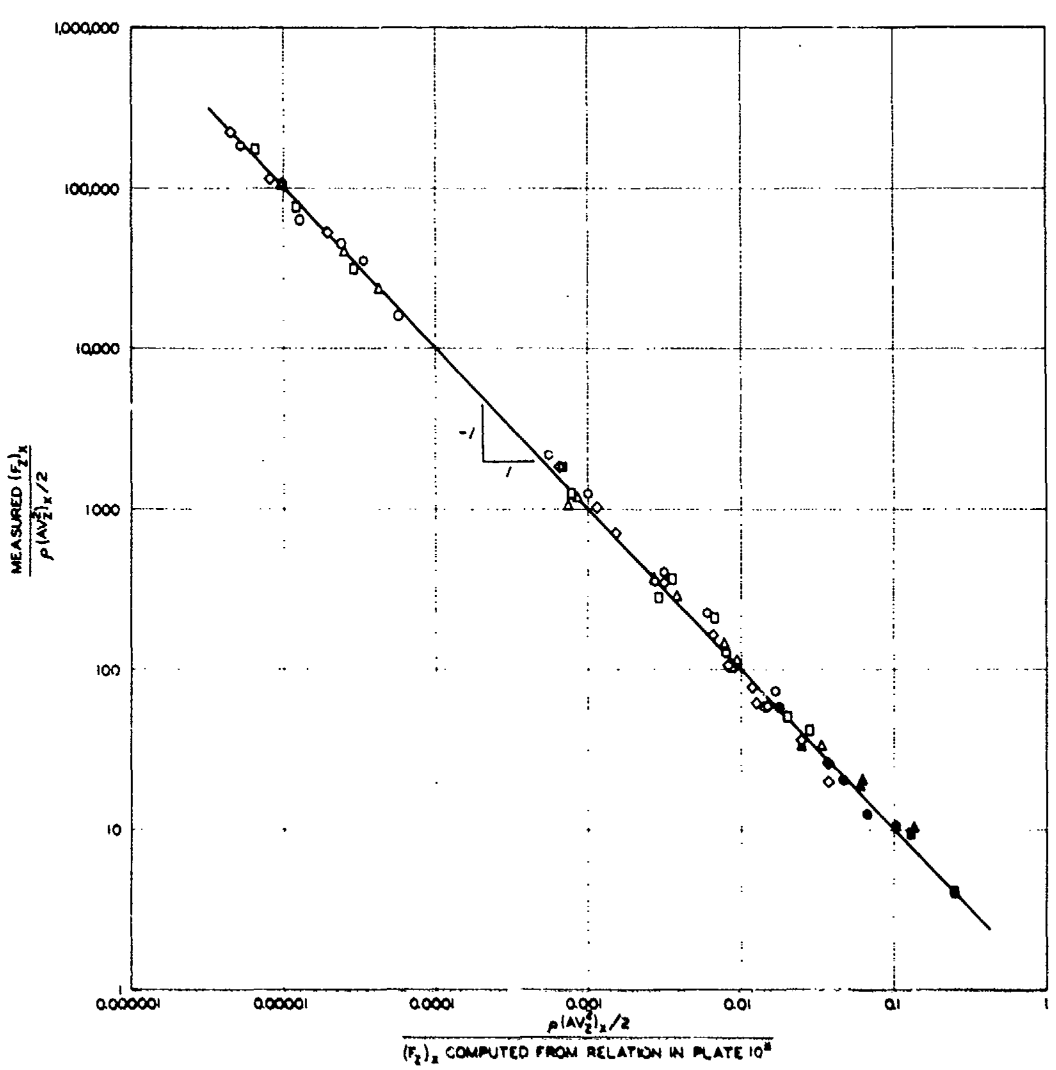

LEGEND

SYMBOL	A, CM²
○	1.29
△	3.23
□	12.9
○	25.8
◇	58.1

NOTE: OPEN SYMBOLS $(V_z)_s \le 3$ m/SEC
CLOSED SYMBOLS $(V_z)_s > 3$ m/SEC

* $(F_z)_s = (F_z/A^{1.3})_b \, A_s^{1.3}$, FOR $(V_z/f)_{ss} < 2.3$
$(F_z)_s = (F_z/A^{1.3})_b \, A_s^{1.3} \cdot 0.65 (V_z/f)_{ss}^{0.30}$,
FOR $(V_z/f)_{ss} \ge 2.3$

MODIFIED C_D VERSUS N_R RELATION FOR DESCRIBING $(F_z)_x$ FOR 30-DEG-APEX-ANGLE CONES

VERTICAL PENETRATIONS
V_z VALUES FROM 3.05 TO 694 CM/SEC
G VALUES FROM 1.08 TO 6.91 MN/m³
FIVE SIZES OF CONES
AIR-DRY YUMA SAND

84<

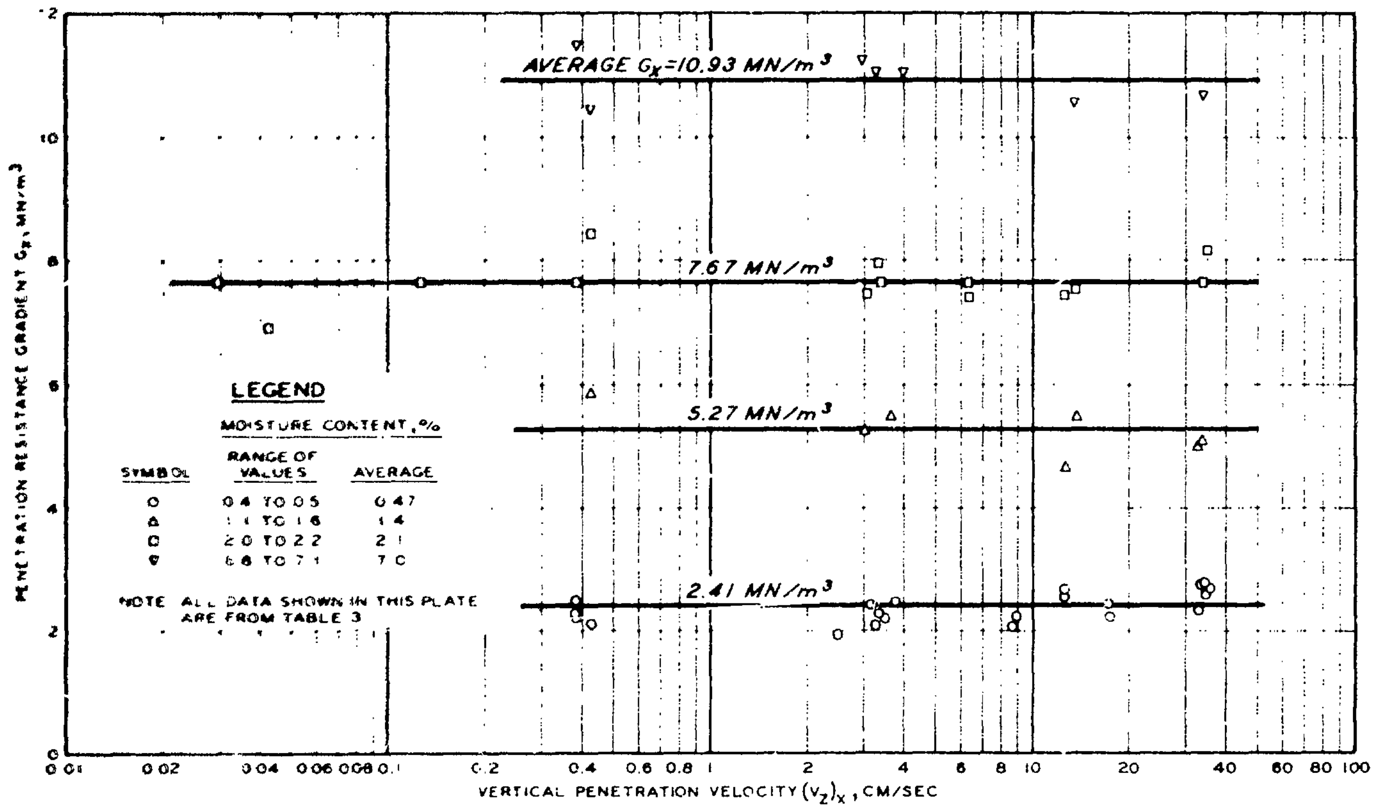

EFFECT OF VELOCITY ON
PENETRATION RESISTANCE GRADIENT AT
FOUR LEVELS OF MOISTURE CONTENT

VERTICAL PENETRATIONS
3.23-CM²-BASE-AREA CONE
UNIT DRY WEIGHT = 15.4 ± 0.1 kN/m³
YUMA SAND

PLATE 12

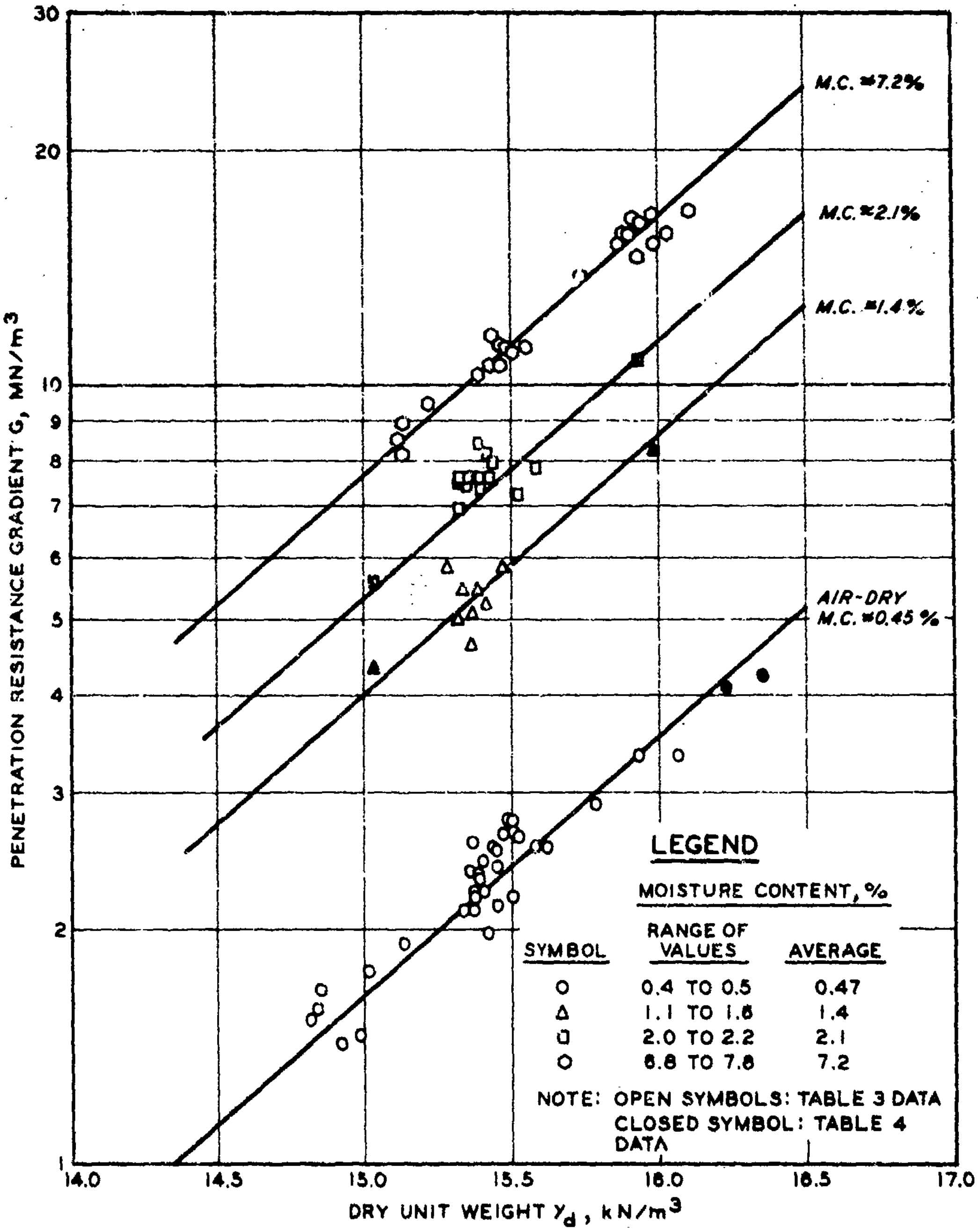

RELATION OF PENETRATION RESISTANCE GRADIENT TO UNIT DRY WEIGHT

FOUR MOISTURE CONTENT LEVELS
3.23-CM^2-BASE-AREA CONE
LOW-SPEED VERTICAL PENETRATIONS
YUMA SAND

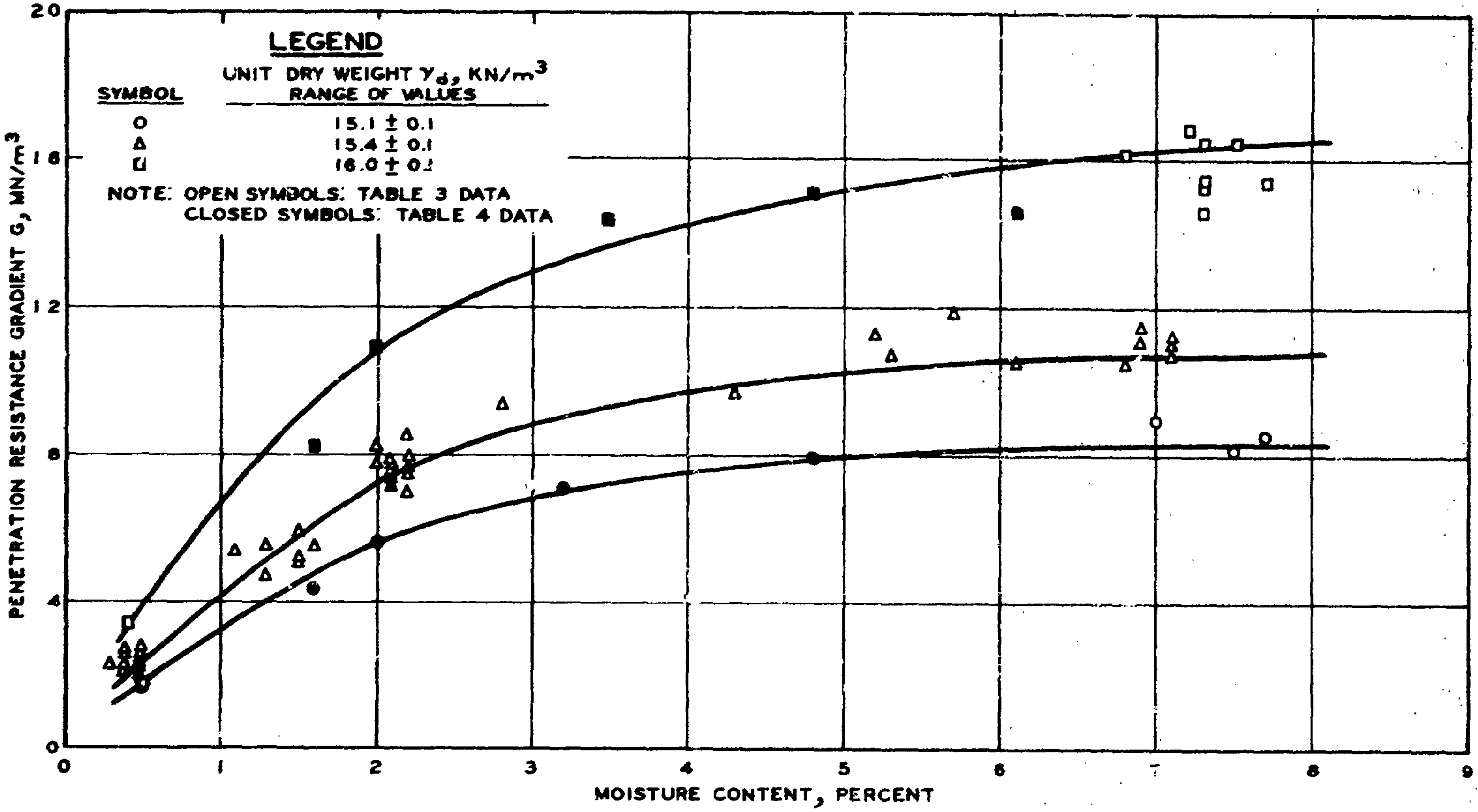

RELATION OF PENETRATION RESISTANCE GRADIENT TO MOISTURE CONTENT

YUMA SAND
THREE LEVELS OF SAND UNIT DRY WEIGHT
3.23-CM^2-BASE-AREA CONE
LOW-SPEED VERTICAL PENETRATIONS

87

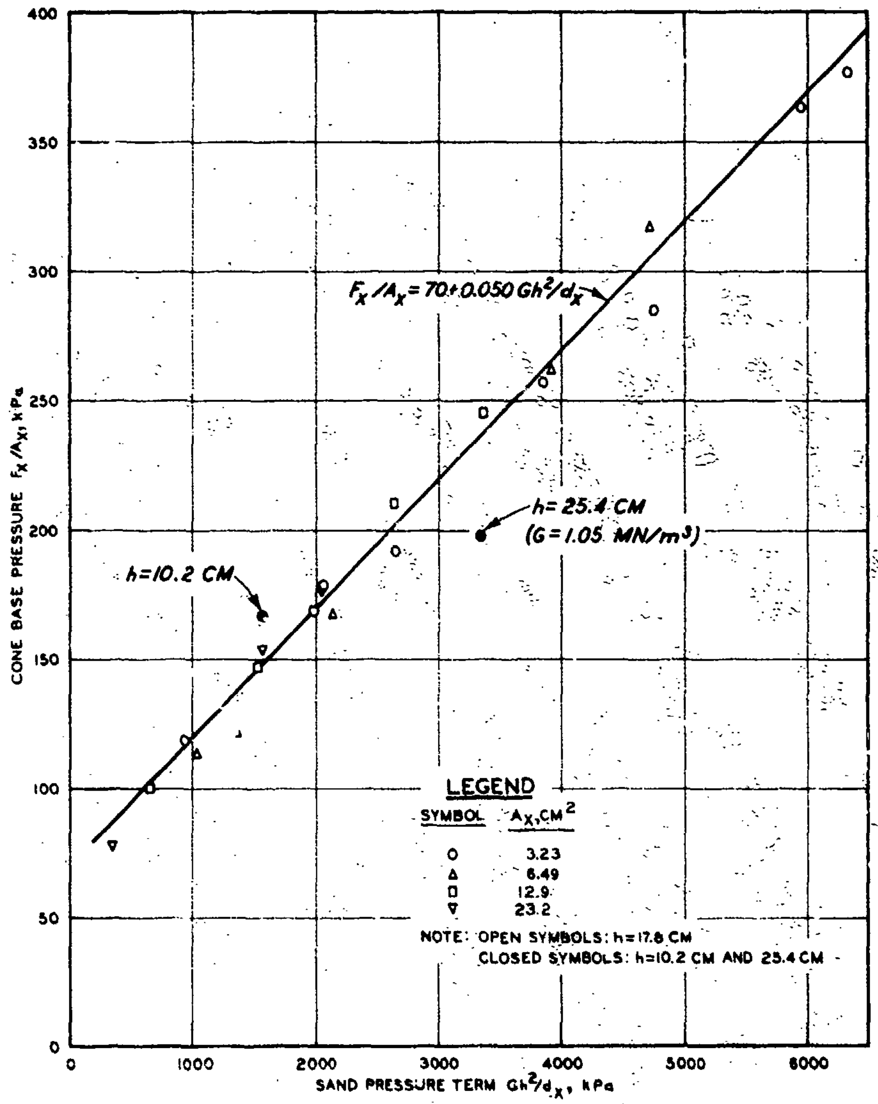

RELATION OF NUMERATOR TO DENOMINATOR OF SAND-CONE PRESSURE RATIO $\frac{F_X/A_X}{Gh^2/d_X}$

HORIZONTAL PENETRATIONS

V_X = 30 CM/SEC

G VALUES FROM 0.58 TO 4.33 MN/m³

FOUR SIZES OF 30-DEG-APEX-ANGLE CONES

CONE TIP DEPTHS OF 10.2, 17.8, AND 25.4 CM

AIR-DRY YUMA SAND

88<

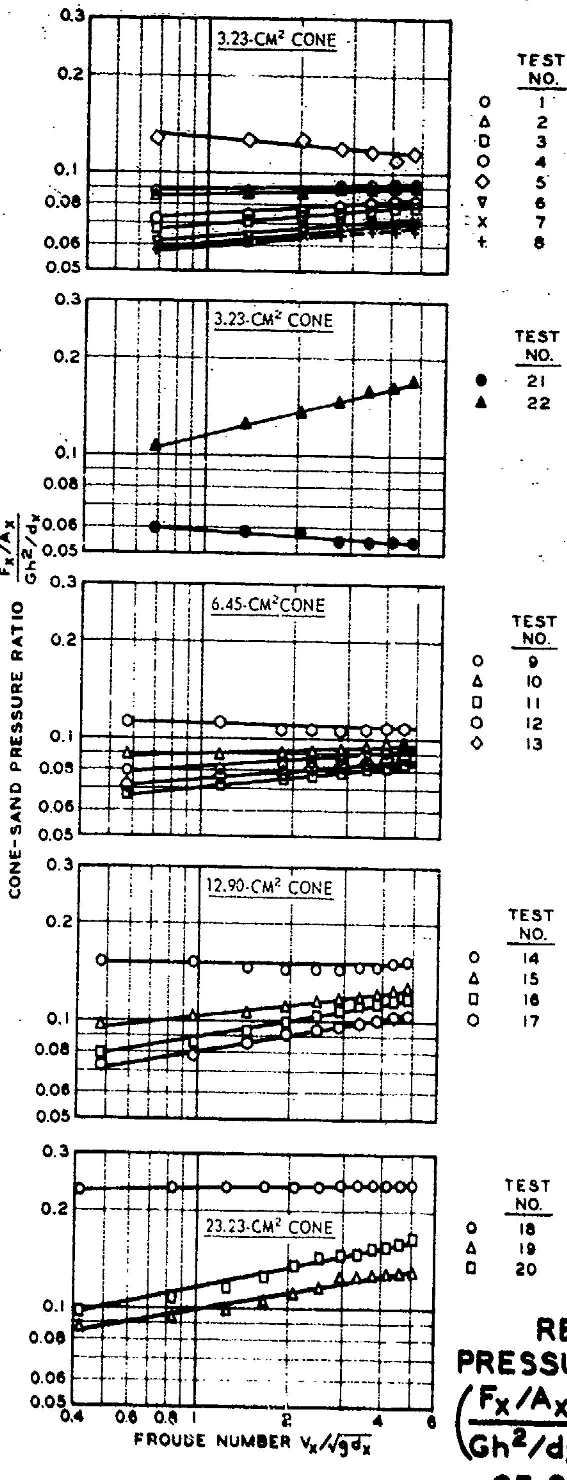

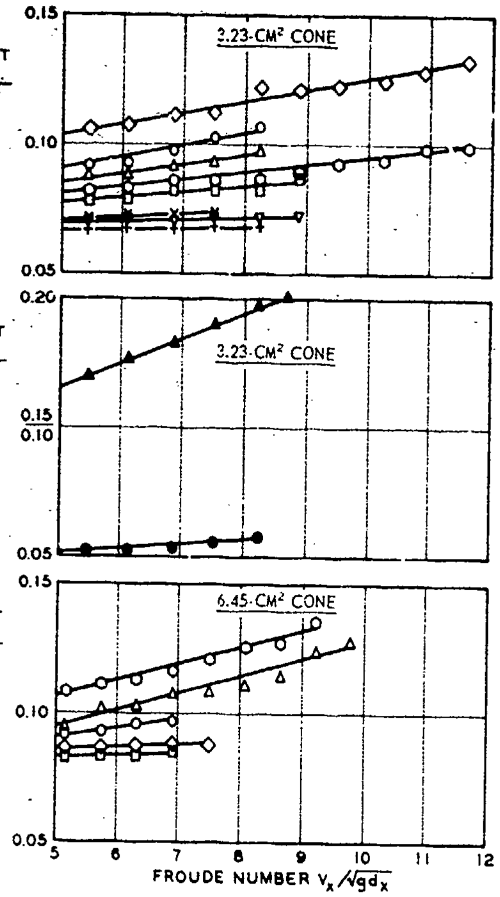

NOTE: ARITHMETIC PLOTS OF THE $\frac{F_x/A_x}{Gh^2/d_x}$ VERSUS $V_x/\sqrt{gd_x}$ RELATION ARE NOT SHOWN FOR THE 12.90- AND 23.23-CM² CONES, SINCE MAXIMUM VALUES OF $V_x/\sqrt{gd_x}$ FOR THEIR TESTS WERE ONLY 6.2o AND 5.42, RESPECTIVELY.

DEPTH OF CONE TIP h = 25.4 CM FOR TEST 21, 10.2 CM FOR TEST 22, AND 17.8 CM FOR ALL OTHER TESTS.

RELATIONS OF CONE-SAND PRESSURE RATIO TO FROUDE NUMBER $\left(\frac{F_x/A_x}{Gh^2/d_x}\text{ TO } V_x/\sqrt{gd_x}\right)$ FOR FOUR SIZES OF 30-DEG-APEX-ANGLE CONES

LOGARITHMIC RELATIONS FOR $V_x/\sqrt{gd_x} \leq 5$

ARITHMETIC RELATIONS FOR $V_x/\sqrt{gd_x} > 5$

G VALUES FROM 0.58 TO 4.33 MN/m³

CONE TIP DEPTHS OF 10.2, 17.8, AND 25.4 CM

AIR-DRY YUMA SAND

89<

PLATE 16

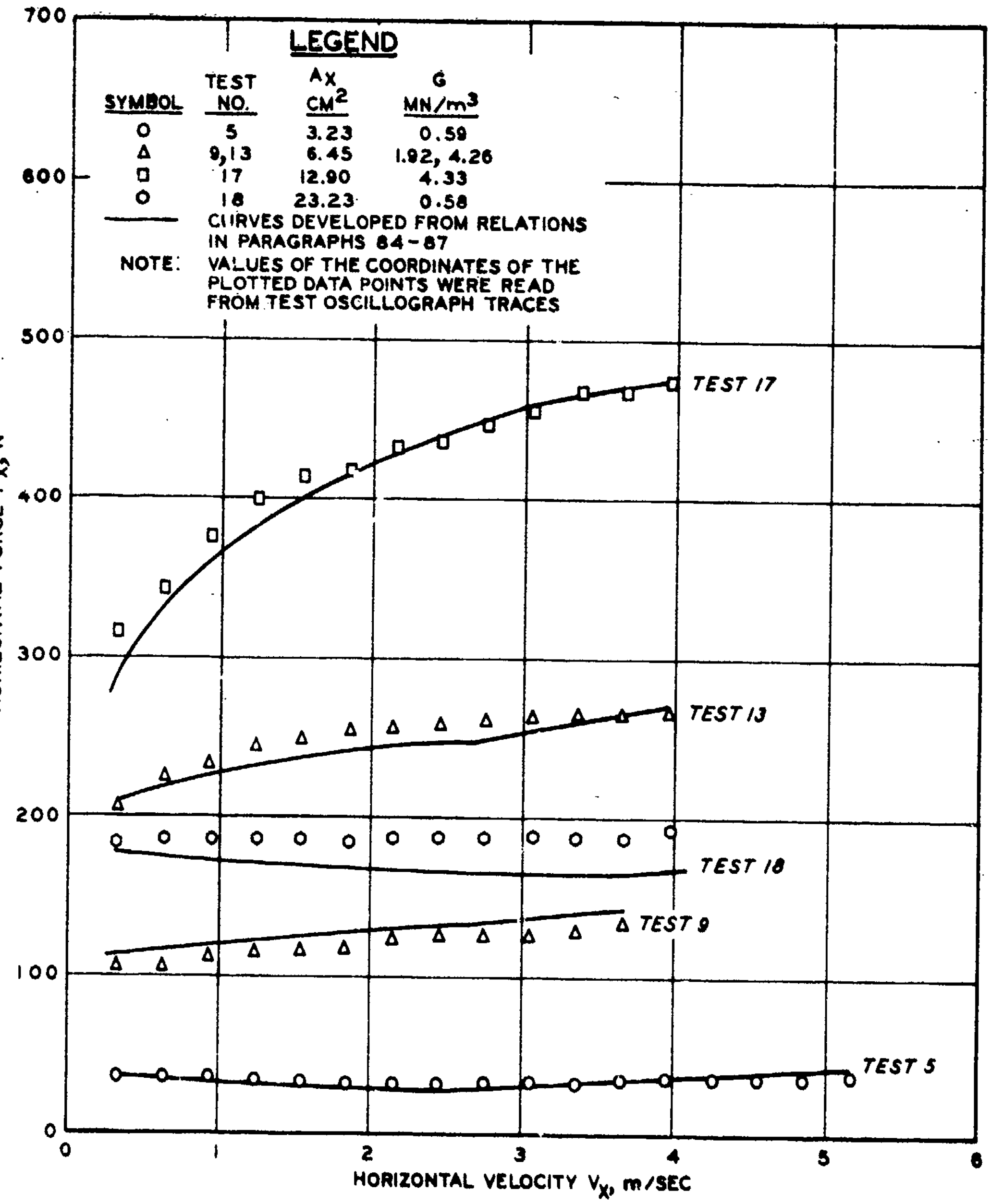

RELATION OF
HORIZONTAL FORCE TO VELOCITY

FOUR SIZES OF 30-DEG-APEX-ANGLE CONES
G VALUES FROM 0.58 TO 4.33 MN/m^3
17.8-CM CONE TIP DEPTH
AIR-DRY YUMA SAND

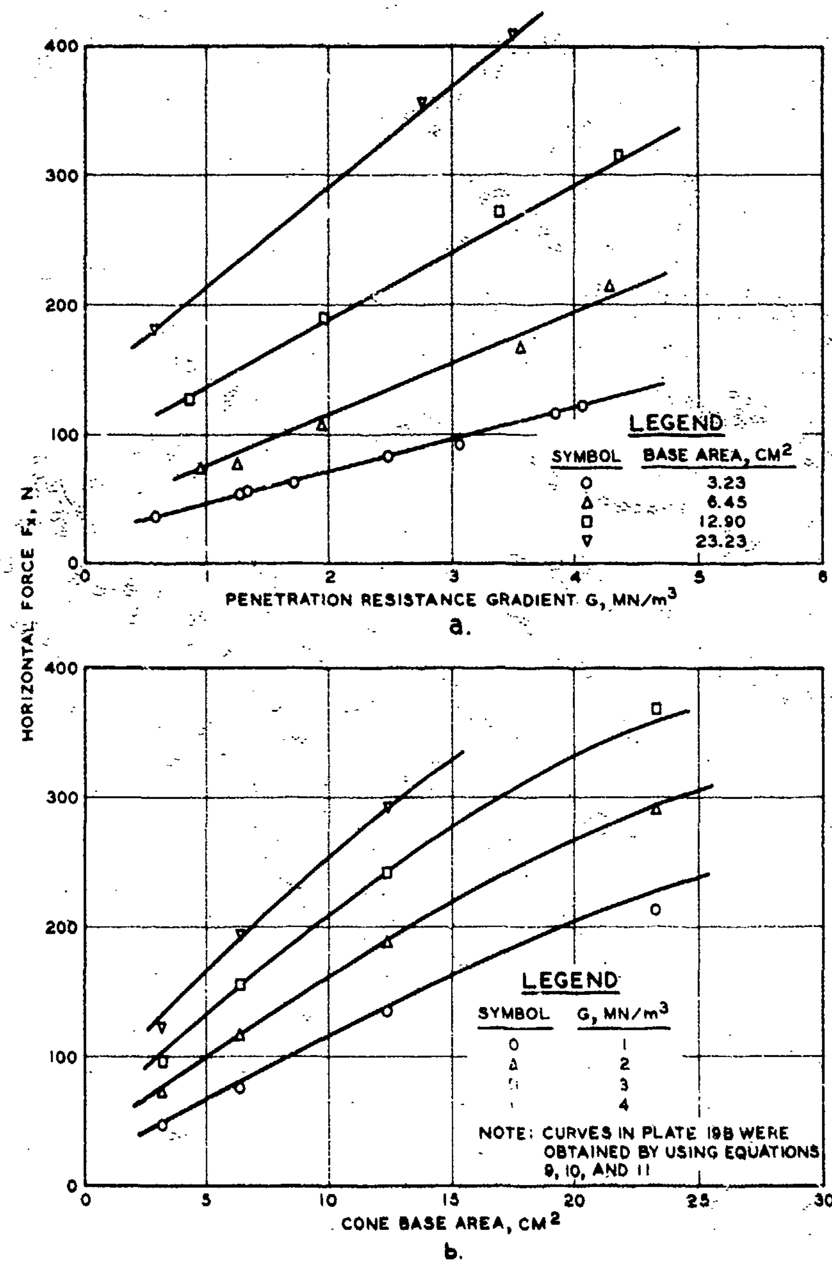

RELATIONS OF HORIZONTAL FORCE TO PENETRATION RESISTANCE GRADIENT AND TO CONE BASE AREA

FORCE MEASURED IN
HORIZONTAL PENETRATION TESTS

17.8 CM DEPTH

30.5 CM/SEC PENETRATION SPEED

AIR-DRY YUMA SAND

In accordance with ER 70-2-3, paragraph 6c(1)(b), dated 15 February 1973, a facsimile catalog card in Library of Congress format is reproduced below.

Turnage, Gerald W

Measuring soil properties in vehicle mobility research; Report 6: Resistance of coarse-grained soils to high-speed penetration, by G. W. Turnage. Vicksburg, U. S. Army Engineer Waterways Experiment Station, 1974.

1 v. (various pagings) illus. 27 cm. (U. S. Waterways Experiment Station. Technical report 3-652, Report 6)

Sponsored by Assistant Secretary of the Army (R&D), Department of the Army Project 4A061101A91D.

Includes bibliography.

1. Coarse grained soils. 2. Mobility. 3. Penetration. 4. Probes. 5. Soil penetration. 6. Soil properties. 7. Vehicles. I. U. S. Office of the Chief of Research and Development. (Series: U. S. Waterways Experiment Station, Vicksburg, Miss. Technical report 3-652, Report 6)

TA7.W34 no.3-652 Report 6